Structure, substrate selectivity, and catalytic mechanism of the fosfomycin resistance enzyme, FosB, from Gram-positive pathogens

By

Mary Elizabeth Keithly

Dissertation
Submitted to the Faculty of the
Graduate School of Vanderbilt University
in partial fulfillment of the requirements
for the degree of

DOCTOR OF PHILOSOPHY
in

Chemistry
August, 2016
Nashville, Tennessee

Approved:

Walter J. Chazin, Ph.D.

Brian O. Bachmann, Ph.D.

Gary A. Sulikowski, Ph.D.

John A. McLean, Ph.D.

Charles R. Sanders, Ph.D.

To my amazing husband, Brad,

your support and love always make my dreams possible.

To my two beautiful daughters, Lillian and Violet,

you fill my heart with love and make my life complete.

In loving memory of my Grandpa Charlie,

he will always be my guiding light and true inspiration in life.

ACKNOWLEDGEMENTS

I would like to express my gratitude to the following people:

My husband, Brad, for all of your love, patience, and support. I could not have made this journey without you and your belief in me. You pushed me to continue to pursue my career and dreams even when I would have given up. I love you and thank you for all you continue to do for me and our family.

My two daughters, Lillian and Violet, who arrived during my time at Vanderbilt and helped inspire me to finish. My sister, Katie, and my mom and dad for all of the encouragement and support. Thank you for listening to all of the times I needed to vent and for encouraging me to keep at it. My in-laws, Denny and Sherri Keithly, you have welcomed me to the family like I am your own daughter and I thank you for all of the love and support you have shown me over the years.

My advisor, Dr. Richard Armstrong, for providing support, scientific advice, and support for my graduate research. He always fostered my development as both a scientist and a teacher by allowing me to participate in extracurricular programs that would take me away from my research. I am grateful for the opportunity to be a part of his lab. Even though Dr. Armstrong passed away in June 2015, his influence will always be a part of myself and all of the students he supported and trained.

Dr. Walter Chazin for becoming my research advisor and committee chair after Dr. Armstrong passed. Your support and advice and were extremely helpful and I know I would not have been able to finish the last year without you. Dr. Charles Sanders for providing support and

guidance to the lab after Dr. Armstrong passed. You took on the challenge of supporting our lab and have done an excellent job in guiding all of us down the right path. To the other members of my committee, Dr. Brian Bachmann, Dr. Gary Sulikowski, and Dr. John McLean, thank you for your guidance and support throughout the years. I would also like to thank Dr. Carmelo Rizzo for his guidance and support during the difficult time after Dr. Armstrong passed.

Dr. Donald Stec and Markus Voehler of the NMR facilities, Dr. Wade Calcutt and Julie Coleman of the mass spectrometry research center, and Dr. Joel Harp of the crystallography facility for all of their expertise and assistance with various experiments throughout the years. Dr. Laura Busenlehner, for her training and scientific advice on HDX-MS experiments.

I would like to specially thank the current and former lab members in the Armstrong lab. In particular, Dr. Matt Thompson for invaluable support, advice, encouragement, and friendship. Much of the work presented in this dissertation could not have been completed without his help. Dr. Paul Cook, Dr. Edward Prage, and Dr. Megan Branch all helped make my initial transition into the lab and my project smooth and successful and I am eternally grateful for their continued support. To my friends and fellow graduate students, Kristin Droege, Kevin Jagessar, Michael Goodman, Dr. Merced Malabanan and Dr. Nicholas Rightmire, your support and friendship helped make my time at Vanderbilt a true joy.

Finally, I would like to thank Sandra Ford in the Chemistry department for always being there to listen and find the answers to any problem I came up with. You truly are the Chemistry graduate student's "Vandy Mom".

These studies were supported by the National Institutes of Health (R01 GM030910) and the Vanderbilt Training Program in Environmental Toxicology (T32 ES007028).

TABLE OF CONTENTS

LIST OF TABLES

LIST OF FIGURES

LIST OF ABBREVIATIONS

ADP	adenosine diphosphate
ATP	adenosine triphosphate
BSH	bacillithiol
BSSB	bacillithiol disulfide
CDC	Center for Disease Control
Fos	fosfomycin
$FosB^{Ba}$	FosB from *Bacillus anthracis*
$FosB^{Bc}$	FosB from *Bacillus cereus*
$FosB^{Bs}$	FosB from *Bacillus subtilis*
$FosB^{Sa}$	FosB from *Staphylococcus aureus*
$FosB^{Ss}$	FosB from *Staphylococcus saprophyticus*
GlcNAc-Mal	N-acetylglucosamine-malate
GlcN-Mal	glucosamine-malate
GSH	glutathione
HDX-MS	Hydrogen/Deuterium exchange mass spectrometry
HPLC	high performance liquid chromatography
LMW	low molecular weight
m/z	mass to charge ratio
MAR	microbial antibiotic resistance
MRSA	methicillin resistant *Staphylococcus aureus*
MS/MS	tandem mass spectrometry

MSH	mycothiol
MurA	diphospho-N-acetylglucosamine transferase
NMR	nuclear magnetic resonance
PCR	polymerase chain reaction
SAD	single wavelength anomalous diffraction
UDP-Glc-NAc	UDP-N-acetylglucosamine
VICB	Vanderbilt Institute of Chemical Biology
V_{max}	maximum velocity of the enzyme reaction
VOC	Vicinal Oxygen Chelate

CHAPTER I

INTRODUCTION

A History of Antibiotics

In the early 1940's, antibiotics were introduced clinically for the treatment of bacterial infections.[1-2] Antibiotics function by targeting essential physiological or metabolic functions of the bacterial cell, such as the biosynthesis of the cell wall, proteins, and DNA.[1] Over the next 20 years, more than 20 classes of antibiotics were discovered. Each antibiotic class is distinguished by a shared common core structure or scaffold, but only four new classes have been introduced since the 1960s (Figure 1).[2] Three of these classes, mutilins, lipopeptides, and oxazolidinones, are still currently in clinical trials.[2] Therefore, they are not yet available for the clinical treatment of bacterial infection. Furthermore, there is the possibility that these classes will not make it out of clinical trials for approval as a treatment by the FDA.

Except for the discovery of the carbapenems class in 1985, the 40 year innovation gap in the identification of new classes of antibiotics was filled by developing synthetic modifications of existing antibiotic scaffolds.[2] Furthermore, there has been a significant decrease in the number of new antibiotics approved by the FDA each year.[4] The identification of new classes of antibiotics is a costly process and yields little profit for pharmaceutical companies, which explains the innovation gap in discovery.[2, 4-5] Altogether, this is a cause for concern given the increasing problem of microbial antibiotic resistance.

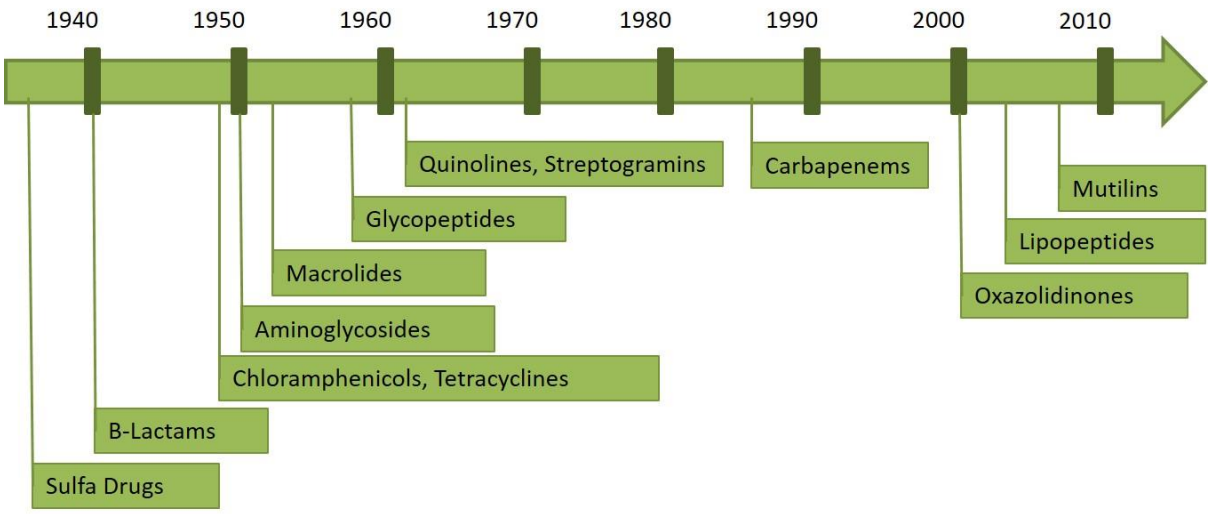

Figure 1. Timeline of discovery of new classes of antibiotics with a 40 year innovation gap.[2]

Microbial Antibiotic Resistance

Shortly after the introduction of antibiotics to the clinical setting, evidence of microbial antibiotic resistance (MAR) emerged. By the late 1950's, resistance to multiple antibiotics was reported.[2] MAR continues to spread rapidly and has become an increasing problem because of the dwindling availability of new antibiotic treatments.

MAR is typically first caused through sequential mutations in chromosomes. This is followed by resistance arising from mobile genetic elements, such as plasmids and bacteriophages. These mobile genetic elements can be transferred from one bacteria to another, but what is most concerning is that they can transfer across bacterial species.[1]

There are three major mechanisms of resistance: (1) enzymatic inactivation of antibiotics through modification or destruction of the drug; (2) alteration of drug transportation; and (3) alteration of the intracellular drug target (Figure 2).[1] Chromosomal mutations typically lead to

alteration of the drug target and plasmid encoded proteins are responsible for the other two mechanisms of resistance.

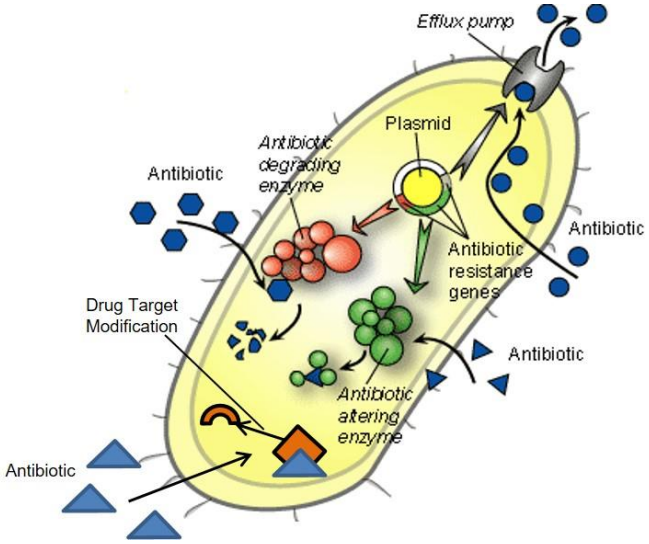

Figure 2. Mechanisms of microbial antibiotic resistance.[1] The three major mechanisms of resistance are shown above. This include alteration of the intracellular drug target, which is typically encoded by sequential chromosomal mutations. Mechanisms of resistance that are typically transferred through mobile genetic elements, such as plasmids, include enzymatic inactivation of antibiotics through modification or destruction of the drug and alteration of drug transportation. Reprinted with permission from Levy, S. B., and Marshall, B. (2004) Antibacterial resistance worldwide: causes, challenges and responses., *Nat Med 10*, S122-129. Copyright 2004 Nature Publishing Group.

In 2013, the Center for Disease Control (CDC) released a report describing the rising antibiotic resistance threat in the United States. According to this report, one of the major culprits for the rapid spread of MAR across the world are the over prescription and improper use of antibiotics.[6] This includes the use of antibiotics in food-producing animals to prevent, control, and treat disease and promote growth, which contributes to MAR strains of bacteria in the food we eat. Additionally, the CDC states that almost 50% of administered antibiotics are unnecessary or ineffective as prescribed, resulting in an increase in MAR strains of healthy bacteria in the patient's

gut.[6] Since plasmid encoded resistance can be passed between bacterial species, these two extraneous uses of antibiotics can increase the spread of MAR infections.

The spread of MAR infections is reported to cause over 2 million illnesses and 23,000 deaths per year in the United States.[6] Combating MAR infections leads to prolonged treatment and extended hospitalization for patients. This often results in increased healthcare costs and loss of productivity in society that is estimated to require up to 35 billion dollars per year.[6]

Incremental improvements to existing classes of antibiotics has proven to be an effective short-term method to combat MAR infections.[2] As MAR strains continue to spread, more long-term strategies for treatment are needed. The most promising strategies that have emerged are the discovery of new antibiotics and combination therapies.[1-2, 4] Combinations of multiple antibiotics, including antibiotics no longer used for traditional treatments, have been used to successfully treat MAR infections.[1-2, 4-5, 6-7] Furthermore, the combination of an antibiotic with an inhibitor to the enzymatic resistance mechanism for MAR infections has also been successful. A notable example of this type of therapy is the drug Augmentin, which has been used to successfully treat infections resistant to penicillin. This demonstrates the need for a clear understanding of the enzymatic resistance mechanisms for various antibiotics. Knowledge of such mechanisms would allow for drug design of inhibitors to be used as part of combination therapies for MAR infections.

Fosfomycin

Fosfomycin (Fos), or cis-1,2-epoxy-propyl phosphonic acid, is a broad spectrum antibiotic isolated in 1969 from various strains of *Streptomyces* by Merck Research Laboratories.[8] Fos is effective against both Gram-positive and Gram-negative bacteria.[8] Fos inhibits cell wall biosynthesis by covalent inactivation of the enzyme pyruvate-uridine diphospho-N-

acetylglucosamine transferase (MurA). Mur A catalyzes the ligation of a phosphoenolpyruvate to the 3'-hydroxyl group of UDP-N-acetylglucosamine (UDP-GlcNAc).[9] The MurA reaction represents the first committed step in peptidoglycan synthesis, which is a necessary component for of the bacterial cell wall. Fos is a phosphoenolpyruvate analogue that covalently binds to MurA at an active site cysteine residue (Cys115 in *E. coli*) in the presence of UDP-GlcNAc (Figure 3).[10]

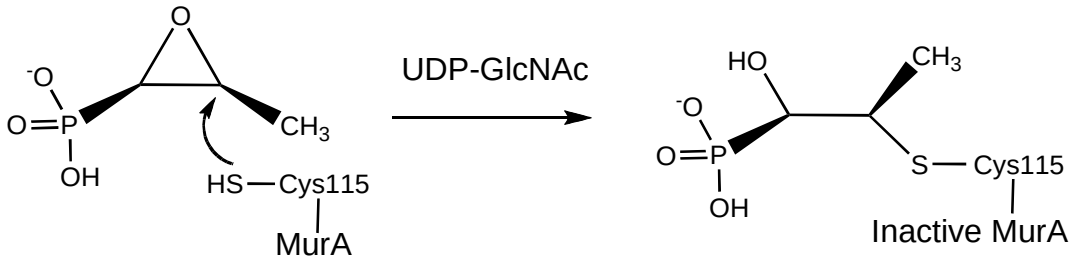

Figure 3. Fos reaction mechanism. Fos functions as a phosphoenolpyruvate analogue that can covalently bind to an active site cysteine residue (Cy115 in *E. coli*) of MurA when UDP-GlcNAc is present.

Fos is currently used in the United States under the trade name Monurol® and has low toxicity in humans. It is typically prescribed in a single three gram oral dose for the treatment of urinary tract infections, but has also been used in the treatment of gastrointestinal infections and multi-drug resistant infections.[11] Treatment with a large dose results in high concentrations of the active drug, which circumvents the primary MAR mechanism of alteration to drug transportation in cells. Shortly after the discovery of Fos, resistance to the antibiotic was reported. Chromosomal mutations leading to modification of the transportation of Fos and modification of MurA were the first types of resistance reported.[12] Almost a decade later, plasmid encoded resistance to fosfomycin was observed after isolation of the transposon Tn2921 from *Serratia marcescens*.[13]

The gene Tn2921 was determined to encode a 16 kDa protein, FosA, which catalyzes the inactivation of fosfomycin by addition of glutathione (GSH).[12, 14]

Fosfomycin Resistance Enzymes

Based on sequence similarity and reactions catalyzed, there are three known classes of genomically encoded fosfomycin resistance enzymes: FosA, FosX, and FosB (Figure 4). FosA, found in Gram-negative organisms, is a manganese- and potassium-dependent GSH transferase. The enzyme catalyzes the nucleophilic addition of GSH to carbon-1 of Fos, which opens the epoxide ring producing a compound with no bactericidal properties.[15] FosX is a manganese-dependent epoxide hydrolase that catalyzes the hydration of Fos at carbon-1 resulting in inactive Fos.[16] FosB, present in Gram-positive organisms, has been shown to catalyze a similar to the reaction to FosA.[17] Since Gram-positive organisms do not contain GSH, a different low molecular weight (LMW) thiol is added to carbon-1 of Fos by FosB. Figure 6 shows the reactions catalyzed by the three classes of Fos resistance enzymes.

In addition to similarity in sequence and reactions catalyzed, the Fos resistance enzymes also share structural similarities. These enzymes are members of the Vicinal Oxygen Chelate (VOC) superfamily that all contain a paired βαβββ motif (Figure 5).[18] In Fos resistance enzymes this motif is found at the N-terminus of each subunit. The enzymes exist as homodimers in which both monomers participate in coordination of the metal ion and formation of the enzyme active sites.[3]

```
FosA      MLTGLNHLTLAVADLPASIAFYRDLLGFRLE-------ARWDQGAYLELGSLWLCLSREP  53
FosX      MISGLSHITLIVKDLNKTTTFLREIFNAEEIYSSGDQTFSLSKEKFFLIAGLWICIMEGD  60
FosB      MLKSINHICFSVRNLNDSIHFYRDILLGKLL-------LTGKKTAYFELAGLWIALNEEK  53
          *:..:.*: : * :*  :  * *:::  .           .:  :: :..**:.: .

FosA      QYGG--PAADYTHYAFGIAAADFARFAAQLRAHGVREW---KQNRSEGDSFYFLDPDGHR  108
FosX      SLQE----RTYNHIAFQIQSEEVDEYIERIKALGVEIKPERPRVEGEGRWIYFYDFDNHL  116
FosB      DIPRNEIHFSYTHIAFTIDDSEFKYWHQRLKDNNVNILEGRVRDIRDRQSIYFTDPDGHK  113
          .        *.* ** *   :.  :  :::   *.      :   :   :** * * *

FosA      LEAHVGDLRSRLAACRQAPYAGMRFAD   135
FosX      FELHAGTLEERLKRYHE----------   133
FosB      LELHTGTLENRLNYYKEAKPHM-TFYK   139
          :* *.* *..**   ::
```

Figure 4. Sequence alignment of the three known classes of Fos resistance enzymes. The sequence of FosA is from *Pseudomonas aeruginosa*, FosX is from *Listeria monocytogenes*, and FosB is from *Staphylococcus aureus*.

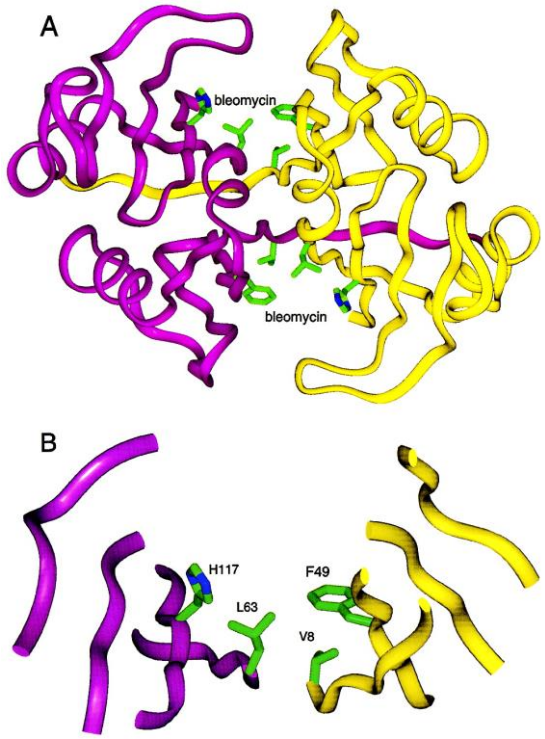

Figure 5. Ribbon representation of the structure of the Vicinal Oxygen Chelate superfamily's βαβββ motif: (A) view of the bleomycin resistance protein's homodimer and (B) close-up view of the cavity formed by the paired βαβββ motifs. The side chains shown are at the positions occupied by the metal ligands of other VOC superfamily members. The representations were constructed with PDB 1BYL.[3] Reprinted with permission from Armstrong, R. N. (2000) Mechanistic diversity in a metalloenzyme superfamily., *Biochemistry 39*, 13625-13632.. Copyright 2000 American Chemical Society.

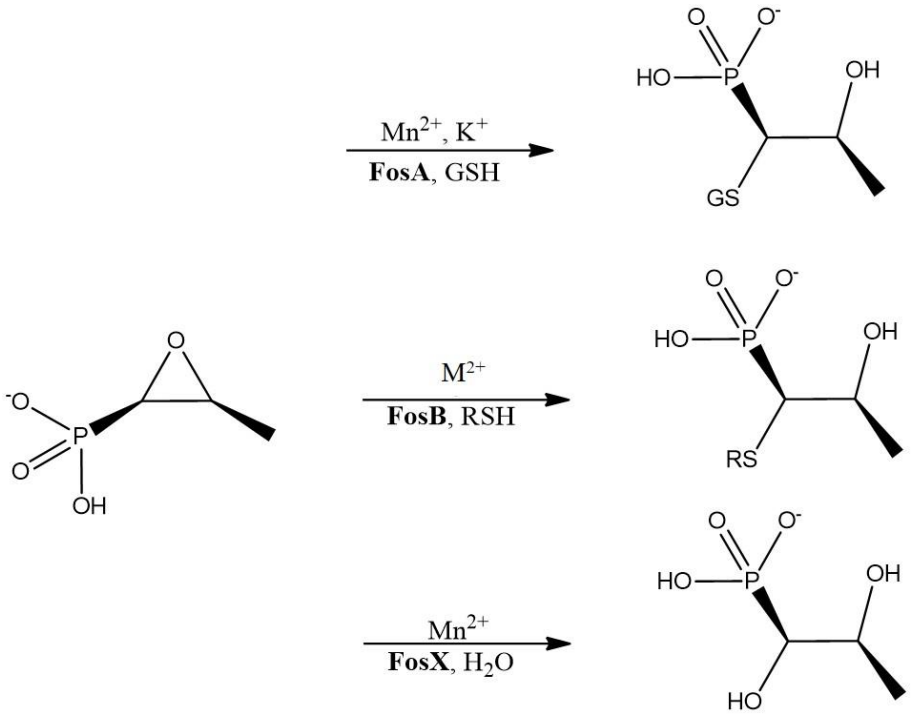

Figure 6. Reactions catalyzed by Fos resistance enzymes. FosA, a manganese- and potassium-dependent GSH transferase, catalyzes the nucleophilic addition of GSH to carbon-1 of Fos opening the epoxide ring producing an inactive compound. FosB, a divalent-dependent thiol-transferases, catalyzes the nucleophilic addition of a LMW thiol, such as cysteine, to carbon-1 of Fos producing an inactive compound similar to that created by FosA. FosX is a manganese-dependent epoxide hydrolase that catalyzes the hydration of Fos at carbon-1 resulting in inactive Fos.

FosB

FosB was initially described as a magnesium-dependent cysteine transferase.[17] These early studies indicate that overexpression of FosB in *Escherichia coli* cells, confers high resistance to Fos with a minimum inhibitory concentration (MIC) > 20 mg/mL), similar to the overexpression of FosA (MIC > 30 mg/mL).[17] Based on this similarity, it is expected that the catalytic efficiency of FosB with the appropriate thiol substrate and divalent metal activator would also be comparable to that of FosA activity with GSH, manganese, and potassium. However, the *in vitro* catalytic activity of cysteine transferase function with magnesium as the metal activator is low (k_{cat}/K_m^{thiol}

= 180 ± 20 $M^{-1}s^{-1}$) compared to the manganese and potassium dependent FosA GSH transferase function (k_{cat}/K_m^{thiol} = 1.7 ± 0.3 X 10^5 $M^{-1}s^{-1}$).[17] These data indicate that FosB may utilize a different thiol substrate and/or divalent metal activator for optimal FosB activity.

At the time the work presented in this dissertation began, the structure of FosB was unknown. The kinetic analyses presented here reveal the catalytic selectivity and mechanism of FosB activity. Additionally, several high resolution crystal structures determined as a part of this work will be discussed to further support the kinetic data. A better understanding of the catalytic mechanism, substrate selectivity, and structure of FosB could allow for the design of drugs used to inhibit FosB and increase the efficacy of Fos in the clinical setting.

Bacillithiol

In 2009, bacillithiol (BSH) was isolated from *Bacillus anthracis*, *Bacillus subtilis*, and *Deinococcus radiodurans* (Figure 7).[19] BSH is a LMW thiol found in Gram-positive organisms in concentrations similar to that of cysteine in these organisms. The structure of BSH is similar to that of mycothiol (MSH), a LMW thiol that is found in *mycobacteria* and functions similarly to GSH.[19-20] Incidentally, the biosynthetic pathway for BSH was discovered based on similarities with the MSH biosynthetic pathway. [20]

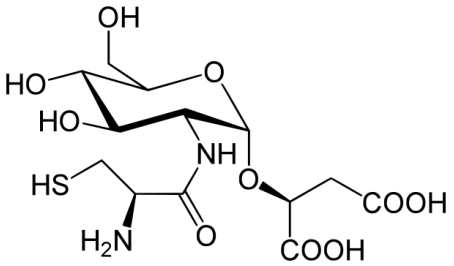

Figure 7. Structure of bacillithiol.

Bioinformatic analysis revealed a three step enzymatic process for the biosynthesis of BSH (Figure 8). The enzyme BshA is a glycosyltransferase that catalyzes the formation of N-acetylglucosamine malate (GlcNAc-Mal) using UDP-GlcNAc and L-malate, the first step in BSH biosynthesis. BshB, a deacetylase, hydrolyzes the acetyl group from GlcNAc-Mal to generate the second intermediate, glucosamine-malate (GlcN-Mal). The final step is the addition of cysteine to form BSH and is proposed to be catalyzed by BshC, a putative cysteine ligase.

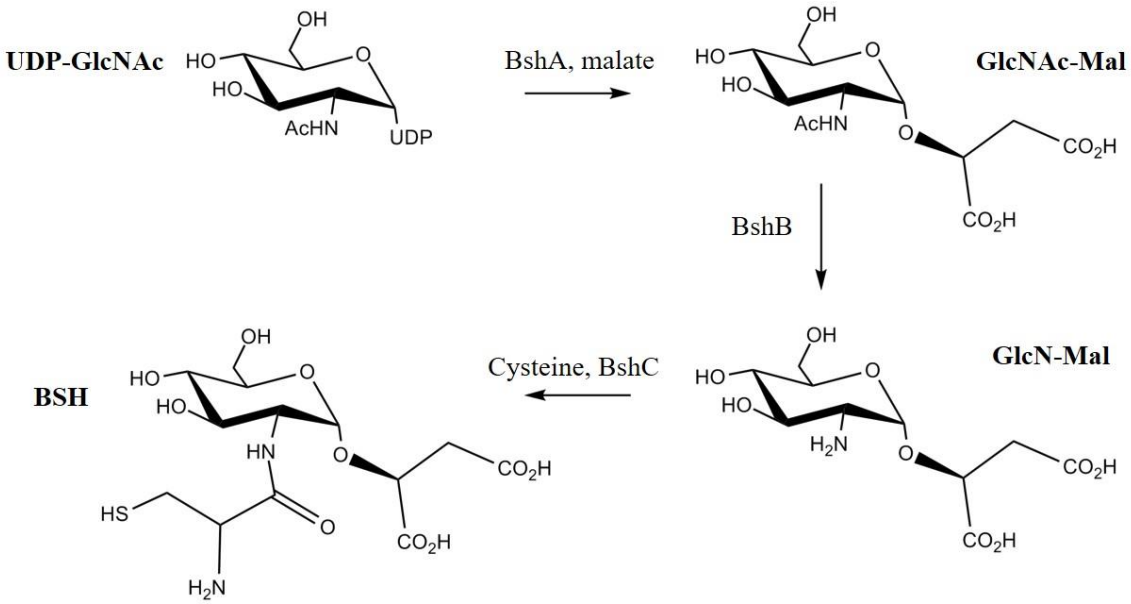

Figure 8. Proposed biosynthesis pathway for BSH. The glycosyltransferase, BshA, catalyzes the first step in BSH biosynthesis, which is the formation of GlcNAc-Mal using UDP-GlcNAc and L-malate. BshB, a deacetylase, hydrolyzes the acetyl group from GlcNAc-Mal to generate the second intermediate, GlcN-Mal. The final step is the addition of cysteine to form BSH and is proposed to be catalyzed by BshC, a putative cysteine ligase.

The enzymatic activities of BshA and BshB have been confirmed *in vitro*, but confirmation of *in vitro* BshC activity still remains elusive.[20] However, HPLC analysis of BshC null mutant strains revealed a complete absence of BSH leading to a 5-fold increase in the accumulation of

GlcN-mal compared to wild type strains.[20] This indicates BshC is the likely candidate to catalyze the final step of BSH biosynthesis.

A study of BSH activity in wild type strains compared to BSH null mutant strains revealed reduced sporulation efficiency and an increased sensitivity to high salt, acid stress, thiol alkylating agents, thiol-reactive electrophiles, and Fos in cells lacking BSH (Table 1).[20] This suggests BSH, like GSH and MSH, plays a role in detoxification of electrophiles and antibiotics.

Table 1. Phenotypes of BSH null cells

Compound	Wild type*	*bshA**
mBBr 1.5 mmol	2.15 ± 0.07	2.55 ± 0.06
Diamide 15 mmol	2.13 ± 0.1	2.4
H_2O_2 150 µmol	2.8 ± 0.14	2.9
Methylglyoxal 27.5 mmol	3.45 ± 0.07	3.95 ± 0.06
N-ethylmaleimide 0.5 mmol	2.87 ±0.15	3.37 ±0.06
Iodoacetamide 0.25 mmol	1.97 ±0.06	2.5 ± 0.1
Fosfomycin 500 mg	2.0 ± 0.1	4.3 ±0.06
Penicilllin G 2mg	3.0 ± 0.1	3.4 ± 0.2
Rifampin 1mg	2.4	2.5
Nitrofurantoin 0.5 mmol	2.0	1.7
Bacitracin 0.75 mmol	1.15 ± 0.07	1.25 ± 0.07

*Diameter (cm) of the zone of growth inhibition around a 0.6-cm filter paper disk containing the indicated compounds. Values shown are averages ± SD ($n \geq 3$), and

Results from Newton and Fahey revealed the presence of a BSH-dependent cellular detoxification system that is analogous to the MSH- and GSH-dependent detoxification systems.[21] BSH-dependent clearance of toxins begins by cleaving the amide bond linking GlcN-Mal to cysteine in BS-toxin conjugates. The resulting GlcN-Mal is recycled to reform BSH and the cysteine-toxin conjugate is acetylated to form a mercapturic acid, which is exported out of the cell. The activity of this system was confirmed using monobromobimane, monochlorobimane, and

rifamycin detoxification assays, confirming the role of BSH in cellular detoxification of electrophiles and antibiotics.[21]

The comparison of wild type strains to BSH null mutant strains also revealed an increase in sensitivity to Fos (Table 1).[20] Additionally, Sharma et al. completed a chemical synthesis of BSH and reported initial time course data comparing FosB L-cysteine transferase activity and BSH transferase activity (Figure 9).[22] Together these results indicate that BSH is the preferred LMW thiol substrate for FosB. Work presented in this dissertation will reveal that FosB is a manganese-dependent BSH-transferase.

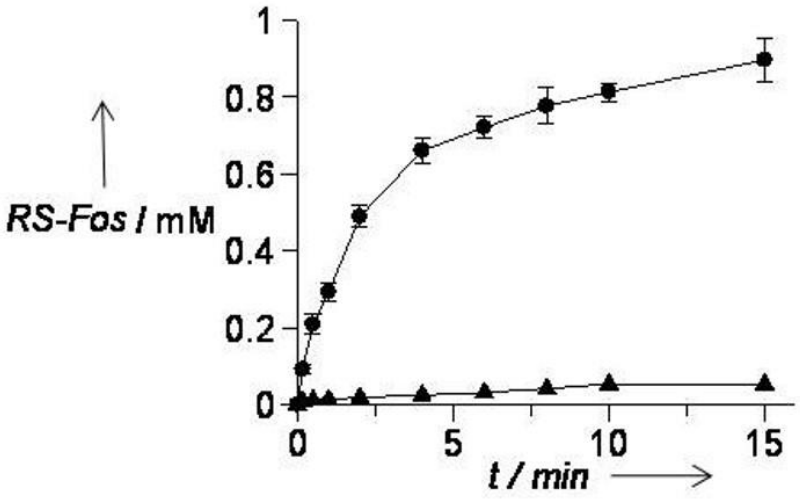

Figure 9. Time course kinetic analysis of FosB catalyzed addition of (●) 1 mM BSH or (▲) 1 mM L-Cys to fosfomycin. Reactions were carried in 20 mM HEPES, pH 7.0 with 2 mM fosfomycin, 1 mM $MgCl_2$, and 0.5 µM FosB from *S. aureus*. Reprinted with permission from Sharma, S. V.; Jothivasan, V. K.; Newton, G. L.; Upton, H.; Wakabayashi, J. I.; Kane, M. G.; Roberts, A. A.; Rawat, M.; La Clair, J. J.; Hamilton, C. J., Chemical and Chemoenzymatic syntheses of bacillithiol: a unique low-molecular-weight thiol amongst low G + C Gram-positive bacteria. *Angew Chem Int Ed Engl* **2011,** *50* (31), 7101-4. Copyright 2011 JOHN/WILEY & SONS, INC.

Methods for Determining Protein Structure

The determination of a protein's three-dimensional structure can provide insight into the protein's function and mechanism of action. Two techniques commonly employed in the determination of protein structure include nuclear magnetic resonance (NMR) spectroscopy and X-ray crystallography. Both methods are well-recognized techniques to provide high-resolution structural determination of proteins, protein-protein interactions, and protein-ligand interactions.[23] However, both methods suffer from obstacles that hinder their utility for investigating structural dynamics of proteins and their interactions. A major challenge in X-ray crystallography is that analyses can only be made in the non-native solid-state, making it difficult to elucidate dynamic movement and interactions in proteins.[24] NMR spectroscopy is solution based and can provide structural dynamic information, but it requires high concentrations of sample and is only suitable for certain proteins.[25] Backbone amide Hydrogen/Deuterium exchange mass spectrometry (HDX-MS) has emerged as a complementary technique to X-ray crystallography and NMR spectroscopy to study protein structure and dynamics.

X-ray Crystallography

X-ray crystallography requires the protein to be arranged into a uniform pattern forming a crystal lattice.[26] Once the protein crystal is large enough, it can then be analyzed by a high-resolution X-ray diffraction experiment. When the crystal is exposed to incident X-rays of known wavelength, a diffraction pattern is obtained. This diffraction pattern can be used to determine a three-dimensional picture of the electron density for the crystal. The electron density reveals the position of atoms in the crystals and ultimately the three-dimensional structure of the protein can be determined.[26]

There are a variety of limitations to this technique. The first hurdle is obtaining a large, uniform crystal. Finding the best diffracting, uniform crystal requires screening of multiple crystal conditions with a variety of changes, such as precipitants, buffers, pH ranges, and protein concentrations.[26] This process of screening typically requires a large amount of soluble protein, which can be problematic for certain proteins. Additionally X-rays can cause significant damage to the crystals during data collection, which can be minimized by flash-freezing the crystal before exposure to the X-rays.[26] However, this requires a cryo-protectant that will not damage the crystal and will not interfere with the diffraction.

Once a suitable diffraction data set is collected, the phases must be determined. Since the phase cannot be directly extracted from the data set, they must be analyzed using another method.[26] One method uses molecular replacement with a related protein structure if such a structure is available.[26] If no related structure is available, then multi-wavelength anomalous dispersion can be utilized.[26] This requires the presence of a heavy atom, such as selenium, which can be incorporated during protein expression and purification.

Finally, the structure determined from X-ray crystallography is for one possible state of the protein. The crystal freezes the protein into a static structure, which allows the diffraction pattern to be uniform. The addition of substrates, products, and co-factors with the sample during crystallization can result in different protein states. While multiple structures can indicate dynamic changes are occurring, this technique cannot be used to investigate active dynamic movement of protein.

Nuclear Magnetic Resonance Spectroscopy

NMR relies upon analysis of a spinning nucleus with magnetic properties in an applied magnetic field. Analysis of ^{1}H, ^{2}H, ^{13}C, and ^{15}N nuclei with a variety of experiments is used when determining protein dynamics and atomic-resolution structure by NMR.[27] The dynamic information is determined from relaxation of nuclei after excitation.[27] For these experiments, protein must be labeled with ^{2}H, ^{13}C, and ^{15}N. This is often costly and can decrease the amount of protein obtained during expression and purification. Furthermore, the protein must be soluble for the experiments, which can be a barrier for certain proteins.

Hydrogen/Deuterium Exchange Mass Spectrometry Theory and Methodology

HDX-MS is a sensitive method used to study protein interactions with ligands and other proteins. It has numerous advantages including no protein size limitations and sub-micromolar range for protein concentration. Hydrogen/Deuterium exchange was first described in the 1950s by Kaj Ulrik Linderstrøm-Lang when he calculated the extent of deuteration of D_2O-stabilized proteins via density gradient tubes.[28] In 1993, the study of horse cytochrome c incubated in D_2O as a function of time, proteolyzed by pepsin, and analyzed using fast atom bombardment mass spectrometry (MS) was the first example of HDX-MS.[29] In 1994, HDX-MS was completed utilizing electrospray ionization (ESI) MS coupled to liquid chromatography to complete the first structural dynamic studies of a whole protein in solution.[30]

While hydrogen exchange can be both acid- and based- catalyzed reactions, at physiological pH the reaction is typically base-catalyzed.[31] In a base-catalyzed exchange, the amide nitrogen proton is first abstracted by hydroxide ion and subsequently protonated by a solvent proton. HDX kinetics are effected by factors including pH, polypeptide conformation, solvent

exposure, and structural dynamics that alter the chemical environment of reactive sites on the protein.[32] Rapid kinetics, having an intrinsic exchange rate of about 10 s^{-1}, is indicative of solvent exposure, while slow kinetics indicate either solvent protection or possible hydrogen bonding (Figure 10).[33] The exchange of hydrogen for deuterium on the amide backbone is dependent upon the rate of structure unfolding (k_o) and refolding (k_c), which is mediated by structural fluctuations that disrupt the hydrogen bonds and result in temporary solvent access. Therefore, measuring the rate of deuterium incorporation as a function of time provides information on protein conformation and conformational changes due to structural perturbations.

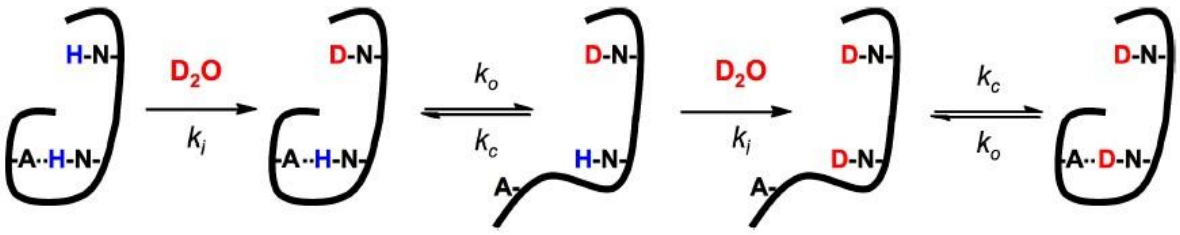

Figure 10. The Linderstrøm-Lang model of HDX. Amide protons that are solvent exposed exchange with deuterons in the solvent with a half-life on the order of milliseconds. Amide protons that are buried in the structure or involved in hydrogen bonding exchange with a half-life on the order of seconds to years and are dependent upon the rate of structure unfolding (k_o) and refolding (k_c). This allows kinetic analysis of HDX to reveal aspects of structural conformation and conformational dynamics.

HDX-MS relies on the base-catalyzed mechanism occurring at neutral pH, with the most common analysis techniques involving continuous labeling (Figure 11).[34] In this method, purified protein in a buffered solution made with H_2O is diluted in deuterated solvent and incubated at room temperature and neutral pH over a series of time points ranging from seconds to hours or days. The exchange is quenched by acidification to pH 2.5 through dilution with ice-cold buffer in H_2O, decreasing the temperature to 0 °C. The quench reduces HDX on the backbone amides

by 10^5, but other exchangeable groups will exhibit rapid back exchange.[35] Therefore, the exchanged deuteriums are trapped and label only the backbone amides. The sample is digested by an acidic protease, such as pepsin, and analyzed by reverse-phase liquid chromatography coupled to ESI-MS in positive mode. The MS data is analyzed for the change of m/z (mass to charge ratio) for individual peptides over time. Due to the relative lack of cleavage specificity of pepsin, all analyzed peptides are sequenced by tandem mass spectrometry (MS/MS) prior to HDX-MS analyses.

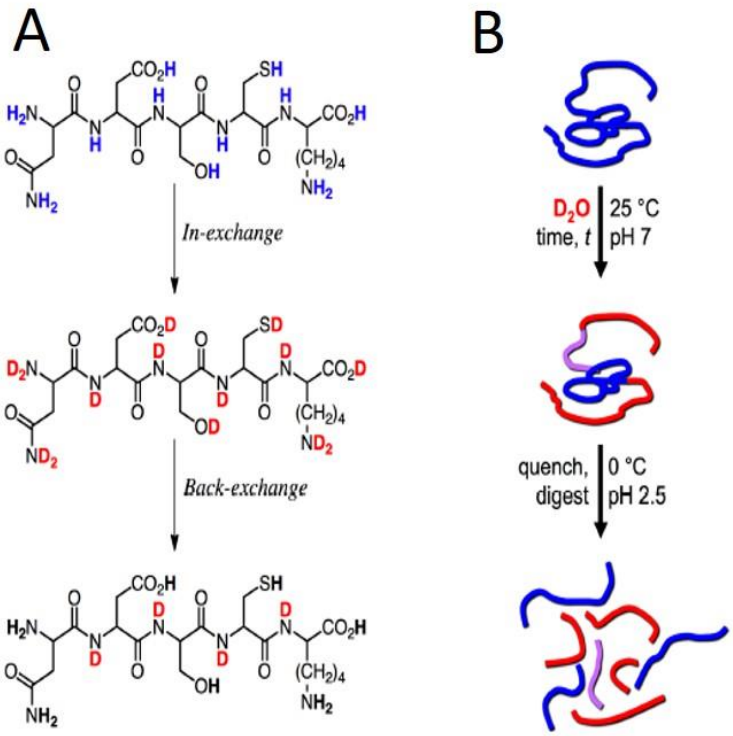

Figure 11. HDX- MS experimental method. (A) Incubation of a protein in deuterated solvent results in the incorporation, or in-exchange, of deuterium at multiple sites. Quenching the incorporation and diluting the protein in solvent lacking deuterium results in the loss, or back-exchange, of deuterium at all sites except for those of backbone amide nitrogens. This results in deuterium labeling exclusive to the backbone of the protein and can be utilized to make structural analyses. (B) The HDX assay involves a range of D2O incubation times followed by quenching and proteolysis. Each resulting peptide is subsequently analyzed for deuterium incorporation as a function of time by LC-MS.

For each time point, the number of deuterons incorporated onto the backbone amide nitrogens of each peptide is calculated from the MS data using the centroid of the resulting isotopic envelope (Figure 12). The number of incorporated deuterons is plotted as a function of time and fit to a sum of first-order exponential rate terms. HDX kinetic rates are generally divided into three phases including fast, intermediate, and slow. These three phases of exchange can be utilized to analyze structural perturbations of a protein as a result of experimental conditions that cause conformational changes.

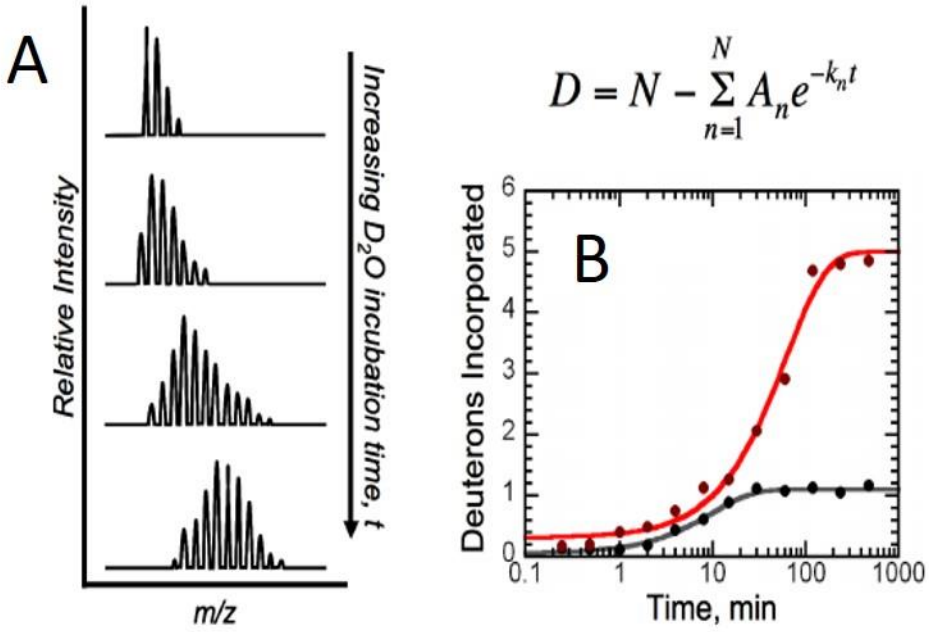

Figure 12. HDX kinetic analyses. (A) Incorporation of deuterium for each peptide is observed in a series of mass spectra as an increase in m/z (mass to charge ratio), which can be used to determine the average mass. (B) The number of deuterons incorporated onto each peptide is plotted as a function of time and fit to a sum of first order exponential rate terms. Perturbation of protein structure results in significant changes in HDX kinetics, illustrated by the red and black traces representing two different experimental conditions. These kinetic changes are used to make conformational determinations.

Purpose of These Studies

Multi-drug resistant bacterial infections have emerged as a serious global health threat according to both the CDC and World Health Organization.[6] Developing novel treatments to combat these serious diseases is necessary to fight the outbreak of infections. One method of treatment currently used combines multiple antibiotics to combat these infections and it has been suggested to include the use of older antibiotics, such as Fos.[1-2, 5a, 7] Additionally, the combination of antibiotics with inhibitors to combat resistance have proven effective as a treatment. The purpose of this study is to utilize kinetic analyses and structural studies to determine the catalytic mechanism and substrate selectivity of FosB. As FosB confers enzymatic resistance to Fos in Gram-positive organisms, furthering the understanding of the function of FosB will aid in the discovery of possible FosB inhibitors to increase the efficacy of Fos in the clinical setting.

At the initiation of this project, FosB was believed to be a magnesium-dependent cysteine-transferase, but the discovery of a new LMW thiol, BSH, led to the suggestion that BSH might be a better thiol substrate for FosB.[19-20, 22] Additionally, there were no known crystal structures of FosB. It is the aim of this study to determine the *in vitro* substrate selectivity of FosB and to investigate divalent metal activation of FosB BSH-transferase activity. We also set out to determine the crystal structure of FosB in an effort to determine the catalytic mechanism. Based on multiple crystal structures determined during this project, we initiated HDX-MS analysis to evaluate the structural dynamics of FosB upon Fos binding.

The biosynthetic pathway for BSH has been reported, but the final step has yet to be confirmed *in vitro*.[20] Preliminary results indicate that the final step is catalyzed by the enzyme BshC, a putative cysteine ligase.[20] Understanding the full biosynthetic pathway of BSH could provide an even more cost effective method of producing BSH, which would be beneficial for

studying FosB activity. This information could also provide an additional pathway as a target for FosB inhibition *in* vivo. In conjunction with Dr. Paul Cook's lab at Grand Valley State University, this research also worked to determine the substrate identity of BshC as a complement to investigating FosB activity.

CHAPTER II

MATERIALS AND METHODS

Materials

Buffer salts were purchased from Research Products International Corporation. All crystallization materials were from Hampton Research. Metals were obtained as their chloride salts from J.T. Baker. L-cysteine was purchased from Sigma Life Sciences. Fosfomycin disodium salt was from MP Biomedicals, LLC. BSH was synthesized as BSSB by the Vanderbilt Institute of Chemical Biology Chemical Synthesis Core. pET28 ($FosB^{Sa}$) was from Platinum PCR Supermix and custom primers were ordered from Invitrogen (Carlsbad, CA). Restriction enzymes were from New England Biolabs (Ipswich, MA). The pET20b(+) vector was from EMB Chemicals, Inc. (Gibbstown, NJ). XL1-blue supercompetent cells and BL21-Gold (DE3) cells were from Agilent Technologies (Santa Clara, CA).

Methods

Cloning and Expression of FosB Enzymes for Kinetic Analyses

$FosB^{Bs}$. The *fosB* gene from *Bacillus subtilis* was cloned and the $FosB^{Bs}$ enzyme expressed and purified as previously described.[16]

$FosB^{Sa}$ and $FosB^{Bc}$. The *fosB* gene from *Staphylococcus aureus* was amplified from genomic DNA as previously described.[19] The *fosB* gene from *Bacillus cereus* was amplified from genomic DNA obtained from the ATCC (10987). Each gene was subcloned into the pTYB12

vector with an N-terminal intein tag (New England Biolabs). BL21(DE3) *E. coli* competent cells were transformed with the expression vector and cultured in 1 L of Terrific Broth in 2.8 L Fernbach flasks with baffles at 37 °C and 200 rpm in a New Brunswick Innova incubator shaker. When an OD_{600} of 0.5 - 0.8 was reached, the culture was cooled to 18 °C and expression was induced by the addition of 0.1 mM IPTG. The cells were further cultured at 18 °C and 200 rpm for 24-30 hours. Cells were harvested by centrifugation at 6500 x g and 4 °C for 10 min and stored at -20 °C. Frozen cell pellets were resuspended in cold Intein Buffer (20 mM HEPES (pH 8.0) containing 1 mM EDTA, 500 mM NaCl) and 2 Complete Mini Protease Cocktail Inhibitor tablets (Roche Diagnostics). Lysozyme (0.2 mg/mL) was added and the mixture was stirred at 4 °C for 30 min. Cells were further lysed by sonication (50% power, 60% duty cycle, and 2 min on, 3 min off) on ice, until they were no longer viscous. Cellular debris was cleared by centrifugation at 30000 x g and 4 °C for 30 min.

The cleared lysate was added to a 25 mL Chitin resin (New England Biolabs) gravity column equilibrated with Intein Buffer and washed with additional Intein Buffer. Intein Buffer containing 50 mM cysteine was added to the column and incubated at room temperature for 48 hours. FosB was eluted with Intein Buffer, concentrated to ~10-15 mL, and dialyzed (molecular mass cutoff of 6-8000 kDa) against 4 L of 20 mM HEPES containing 50 mM NaCl, 1 mM EDTA and 6 g Chelex Resin (pH 7.5)] at 4 °C overnight. The final sample was concentrated in an Amicon ultrafiltration system (molecular mass cutoff of 10000 kDa) to ~0.5 mM.

$FosB^{Ba}$. The *fosB* gene from *B. anthracis* was synthesized based on the known sequence as follows. Custom oligonucleotides were purchased from Sigma (St. Louis, MO) and purified via standard desalting. The PCR Supermix was purchased from Invitrogen (Carlsbad, CA). The

pGEM kit was purchased from Promega (Madison, WI). Restriction endonucleases were purchased from New England Biolabs (Ipswitch, MA). Gel extraction and miniprep kits were purchased from Qiagen (Venlo, Netherlands). XL1-blue chemically competent *E. coli* were purchased from the Molecular Cell Biology Resource Core at the Vanderbilt University Medical Center.

Gene synthesis was carried out using methods similar to those used by Bernat et al.[12] The FosB gene sequence was divided into eight sense/antisense alternating oligonucleotides (labeled sequentially as A-H) of about 70 bp with approximately 18 bp of overlapping, complementary sequence (Table 2). Oligonucleotide A incorporates a 5' Nde I site and oligonucleotide H incorporates a 3' Xho I site.

Table 2. Oligonucleotides for $FosB^{Ba}$ gene synthesis

Oligo	Sequence (5'-3')	Reaction		
A	gggggggcatatgttaaaaggaatcaatcatctttgtttttcagtatctaatttagaagattctattacattt	1	5	7
B	atgcaagttttcttcctctaactaataattctccttccaatacttttttcgtaaaatgtaatagaatcttc			
C	gaggaagaaaacttgcatattttaatatatgtggagtatggatagcgcttaatgaagaaatacatattccaa	2		
D	tctgttcaacagaaaacgcaatatgtgtataagattgatgaatctcttttcttggaatatgtatttcttc			
E	gcgttttctgttgaacagaaagactttgaacgtctactgcagcgattagaagaaaacgatgttcatattt	3	5	
F	caacaaaatatatagattcacaatcccttacatcccgttctcttccttgtaaaatatgaacatcgttttc			
G	gaatctatatattttgttgatccagacgggcataagtttgaatttcattcagggacattgcaagaaaggc	4		
H	ttttttctcgagttagtaaaacgtcatatgaggtttatcttccctatagtaattaagcctttcttgcaatgtcc			

Four polymerase chain reactions (PCR) (labeled as 1-4) were set up using PCR Supermix (10 µL total each reaction). The reactions contained the mixture of oligonucleotides (750 nM each) indicated in Table 2. The reactions were cycled in accordance with the manufacturer's thermocycling parameters for 3 cycles. 5 µL from these reactions were combined to make reactions 5 and 6 as indicated in Table 2. Reactions 5 and 6 were then cycled for 3 cycles. 5 µL of reactions 5 and 6 were combined to make reaction 7, which was cycled for 3 cycles. Finally,

the FosB gene was PCR-amplified from reaction 7 with oligonucleotides A and H using the PCR Supermix.

The final PCR reaction was run on a 1.6% agarose gel, and a band of approximately 420 bp was excised from the gel. The DNA was extracted, A-tailed, and ligated into the pGEM-T vector. The resulting plasmid was used to transform XL1-blue chemically competent cells, which were plated onto LB/agar/amp/IPTG/Xgal plates for blue/white screening. White colonies were selected for growth in LB media, and plasmids were extracted. The plasmids were digested with Nde I and Xho I and analyzed via gel electrophoresis. Plasmids containing a gene of the appropriate size were sequenced at the Vanderbilt DNA Sequencing Core Facility. The FosB gene from a pGEM-FosB clone with the appropriate sequence was digested with NdeI and XhoI and ligated into expression vectors.

The synthetic gene was then subcloned into a pET-28b vector (Novagen) with an N-terminal hexahistadine tag. BL21(DE3) *E. coli* competent cells were transformed with the expression vector and cultured in Terrific Broth as described above at 37 °C and 200 rpm. When an OD_{600} of between 0.5 and 0.8 was reached, the culture was cooled to 20 °C and expression was induced by the addition of 0.1 mM IPTG. The cells were further cultured at 20 °C and 200 rpm for 15-20 hours. Cells were harvested by centrifugation at 6500 x g and 4 °C for 10 min and stored at -20 °C. Frozen cell pellets were resuspended in cold Lysis Buffer (20 mM HEPES, pH8.0; 300 mM NaCl; 10 mM Imidazole) with 2 protease inhibitor tablets. Lysozyme (0.2 mg/mL) was added and the mixture was stirred at 4 °C for 1 hour. Cells were further lysed by sonication (50% power, 60% duty cycle, and 2 min on, 3 min off) on ice, until they were no longer viscous. Cellular debris was cleared by centrifugation at 30000 x g and 4 °C for 30 min.

The cleared lysate was added to a 5 mL Ni-NTA agarose (Qiagen) equilibrated with Lysis Buffer and incubated by inversion at 4 °C for 1 hour. Resin was applied to a gravity column and washed with 10 column volumes of Lysis Buffer. FosB was eluted with a similar buffer, containing 300 mM Imidazole, concentrated to ~10-15 mL, and dialyzed (molecular mass cutoff of 6-8000 kDa) against 4L cold buffer (20 mM HEPES, pH 7.5; 50 mM NaCl; 1 mM EDTA; 6 g Chelex Resin) at 4 °C overnight. The final sample was concentrated in an Amicon ultrafiltration system (molecular mass cutoff of 10000 kDa) to ~1 mM.

Preparation BSH for Enzyme Assays.

Approximately 30 mg bacillithiol disulfide (BSSB) was dissolved in 50 µL 20 mM HEPES, pH 7.0. This was adjusted to a pH of 7.0 by addition of 1 M HEPES (pH 7.0) to final volume of ~1 mL. The BSSB sample was loaded onto a Reduce-Imm™ Immobilized Reductant Column (Pierce) equilibrated with Buffer #1 (100 mM HEPES (pH 8.0) containing 1 mM EDTA) and activated per the manufacturer's directions. After incubation at room temperature for 30-60 min, bacillithiol (BSH) was eluted with 9 mL of Buffer #1 and collected in 1 mL fractions. The [thiol] in the fractions was determined using the DTNB assay.

Continuous ^{31}P-NMR Activity Assays of FosB^{Sa}, FosB^{Ba}, FosB^{Bc}, FosB^{Bs} with Mg^{2+} or Ni^{2+}.

FosB (0.5 µM) was equilibrated for 5 minutes with either 1 mM $MgCl_2$ or 10 µM $NiCl_2$ and 4 mM Fos in 20 mM HEPES (pH 7.0). The reaction was initiated by addition of 2 mM BSH or cysteine, transferred to an NMR tube, and allowed to react at room temperature. At various time points a ^{31}P with ^{1}H decoupling NMR spectra was collected using Bruker DRX-500 MHz NMR. Cys-Fos, BS-Fos, and Fos had ^{31}P chemical shifts of 18.8, 18.5, and 11.9 ppm, respectively.

Using the law of conservation of mass, the substrate and product peak heights were measured and the amount of product formed was calculated from the ratio between the peak heights and the total concentration of fosfomycin used in the reaction.

Continuous ^{31}P-NMR Activity Assays of FosB^{Bc} with Zn^{2+}.

Intein-tagged FosB^{Bc} (0.5 µM) was equilibrated for 5 min with 100 µM $ZnCl_2$ and 8 mM Fos in 20 mM HEPES, pH 7.0. The reaction was initiated by addition of 4 mM BSH or L-cysteine, transferred to an NMR tube, and allowed to react at 298 K. At various time points, a ^{31}P with ^{1}H decoupling NMR spectrum was collected using Bruker AV-400 MHz NMR. Analysis of the data was completed according to the method previously described for activity assays with Mg^{2+} or Ni^{2+}.

Continuous ^{31}P-NMR Activity Assays of FosB^{Bc} with Ni^{2+} and *Mg^{2+}*

Intein-tagged FosB^{Bc} (0.25 µM) was equilibrated for 5 min with either 1 mM $MgCl_2$ or 10 µM Ni Cl_2 and 4 mM Fos in 20 mM HEPES, pH 7.0. The reaction was initiated by addition of 2 mM BSH or L-cysteine, transferred to an NMR tube, and allowed to react at 298 K. At various time points, a ^{31}P with ^{1}H decoupling NMR spectrum was collected using Bruker DRX-500 MHz NMR. Analysis of the data was completed according to the method previously described for activity assays with Mg^{2+} or Ni^{2+}.

End Point^{31}P-NMR Activity Assays of FosB^{Bc} with Mn^{2+}

Intein-tagged FosB^{Bc} (0.25 µM) was equilibrated for 5 min with 10 µM $MnCl_2$ and 4 mM Fos in 20 mM HEPES, pH 7.0. The reaction was initiated by addition of 2 mM BSH or L-cysteine and allowed to react at 298 K. Since Mn2+ can interfere with the NMR analysis, the reactions

were quenched at various time points by vortexing with 20 µL of chloroform followed by freezing on dry ice for 10 minutes. After thawing and centrifugation, the aqueous layer was incubated with chelex resin for 1 hour to remove any metals. The resin was removed via centrifugation and the supernatant was transferred to an NMR tube to collect a ^{31}P with ^{1}H decoupling NMR spectrum for each time point using Bruker DRX-500 MHz NMR. Analysis of the data was completed according to the method previously described for activity assays with Mg^{2+} or Ni^{2+}.

Steady State Kinetic Assays of $FosB^{Bc}$ with Mn^{2+}

Mn^{2+}-dependent inactivation of Fos by $FosB^{Bc}$ was measured for both BSH transferase and L-cysteine transferase activity. Intein-tagged $FosB^{Bc}$ (0.25 µM) was equilibrated for 5 min with 10 µM $MnCl_2$ and 4 mM Fos in 20 mM HEPES, pH 7.0. The reaction was initiated by addition of 0.1 to 15 mM BSH or 1 to 100 mM L-cysteine and the mixture allowed to react at room temperature. After 15 and 30 seconds, a 20 µL aliquot of the reaction mixture was quenched by addition of 40 µL of 5% (w/v) trichloroacetic acid followed by vortexing. Addition of 15 µL of 0.8 M NaOH returned the pH to 7.0. An internal standard (20 µL of 0.4 mM serine) was added and the mixture was diluted to 100 µL with 20 mM HEPES, pH 7.0. A 20 µL aliquot of the quench was added to 55 µL of borate buffer and mixed with 25 µL of the AQC reagent (Waters, Milford, MA) solubilized according to the manufacturer's directions. Derivatization reaction mixtures were incubated at 55 °C for 10 minutes followed by dilution with 400 µL of Mobile Phase A (70 mM NaOAc, pH 5.0; 7 mM trimethylamine).

Derivatized samples were analyzed on an Agilent 1260 Infinity HPLC System using fluorescence detection with excitation at 250 nm and emission at 395 nm. Samples were injected onto a 250 mm x 4.6 mm Kinetex C-18 column with a particle size of 5 µm and a pore size of 100

Å (Phenomenex, Torrance, CA) and equilibrated with 90% Mobile Phase A and 10% Mobile Phase B (80% (v/v) acetonitrile). Samples were eluted using a flow rate of 1 mL/min and the following gradient of Mobile Phase B: 10% from 0 to 6 minutes, 15 to 40% from 15 to 19 minutes, and 40 to 100% from 19 to 22 minutes. BS-Fos, L-cys-Fos, and serine had retention times of 4.0, 4.7, and 7.5 minutes, respectively. The amount of product formed was quantified as previously described. Initial rate measurements for the production of BS-Fos or L-cys-Fos were calculated using the slope of amount of product formed vs. time. All measurements were made in triplicate and averaged. The data were fit to the Michaelis Menten equation (Equation 1) where X is the substrate concentration and Y is the enzyme velocity. Values of V_{max} and K_M were determined using Equation 1 and GraphPad Prism software (La Jolla, CA). The k_{cat} value was determined using Equation 2.

Equation 1: $Y = \frac{V_{max} \cdot X}{K_M + X}$ Equation 2: $V_{max} = k_{cat}[E]$

Expression of FosB^{Bc} for Crystallography

A pET-20b expression plasmid containing the gene encoding non-tagged WT FosB^{Bc} was transformed into *E. coli* BL21 (DE3) cells. The plasmid was prepared as previously described. The cells were plated on LB agar containing 100 µg/mL of ampicillin and incubated with 37 °C for approximately 16 h. Single colonies were isolated from the LB-agar plates and used to inoculate 2 mL of LB (Gibco) starter cultures (3 cultures for a total of 6 mL) containing 80 µg/mL of ampicillin. After approximately 8 hours of incubation at 37 °C with shaking, 1 mL of starter growth was used to inoculate 1 L of Terrific Broth containing 80 µg/mL of ampicillin (6 L total). The 1 L cultures were grown at 37 °C with shaking for approximately 12 hours (or until the OD_{600}

reached ~1) and then induced with 0.5 mM IPTG. Upon induction with IPTG, the temperature was reduced to 25 °C, and the cells were allowed to grow for an additional 4 to 5 hours. The cells were harvested via centrifugation at 5000g for 15 minutes.

The *E. coli* cell pellet was resuspended in 2 mL of lysis buffer (20 mM Tris HCL, pH 7.5) per gram of cell pellet. Lysozyme was added to the slurry at 1 mg/mL and the mixture was stirred at 4 °C for 1 hour. After 1 hour of stirring, 5 mg of DNase and RNase were added and the slurry was stirred at 4 °C for another hour. The slurry was sonicated to ensure complete lysing of cells and the lysate was cleared via centrifugation at 35000g for 30 min.

An ammonium sulfate precipitation was performed on the cleared lysate solution prior to any column purification. Fractions were precipitated at 5, 20, 40, 60, 80, and 95% ammonium sulfate. The fractions were analyzed by SDS-PAGE, and fractions containing the highest ratio of FosB to other proteins were combined for further purification. The protein was dialyzed overnight in 20 mM HEPES, pH 7.0 to remove any residual lysis buffer or salt that could interfere with ion-exchange chromatography.

The collected fractions were pooled, concentrated, and loaded onto a GE Healthcare HiPrep DEAE FF 16/10 column, equilibrated with 20 mM HEPES, pH 7.0 using an Amersham Pharmacia Biotech FPLC (equipped with a 50 mL super loop). With an estimated pI of 5.22, $FosB^{Bc}$ adheres to the DEAE material, and a purple hue can be seen on the column. The protein was eluted from the column at 2 mL/min using a gradient of 0-30% NaCl in the same buffer. Fractions were analyzed for purity by SDS-PAGE. The most pure fractions were collected, combined, and dialyzed overnight into 10 mM sodium phosphate, pH 7.0.

The protein, in 10 mM sodium phosphate, pH 7.0, was subsequently loaded onto a 2.5 X 15 cm hydroxyapatite column (BioRad, Hercules, CA). $FosB^{Bc}$ adheres to the hydroxyapatite

material. The protein was eluted from the column with an increasing concentration of phosphate. The protein eluted between 100 and 400 mM phosphate according to fraction analyzed by SDS-PAGE.

Finally, the protein was dialyzed into 50 mM sodium phosphate, pH 7.5; 150 mM NaCl, 5 mM DTT. The protein was concentrated to approximately 1 mL with an Amicon 10K molecular weight cutoff membrane and loaded onto a GE Healthcare 26/60 Sephacryl column at 1 mL/min using an Amersham Pharmacia Biotech FPLC. Fractions were collected from the column at 0.5 mL each and analyzed for purity by SDS-PAGE.

The purified $FosB^{Bc}$ protein was prepared with Mn2+, Ni2+, and Co2+ by dialyzing into 50 mM Bis-Tris, pH 6.0; 5 mM EDTA; 2 mM 1,10-phenanthroline; 3 g Chelex resin. This ensured the removal of all metals. The protein was divided into fractions and dialyzed into 20 mM HEPES, pH 7.5 containing 200 µM of the respective divalent metal.

$FosB^{Bc}$ Crystallization

Initial crystals of $FosB^{Bc}$ were grown using the hanging-drop vapor-diffusion method at 298 K by mixing 3 µL of protein solution (13 mg/mL in 20 mM HEPES, pH 7.5) and 3 µL of reservoir solution (Hampton Research Index 92, 0.1 M magnesium formate and 15% polyethylene glycol (PEG) 3350 (w/v)) in a Hampton Research VDX plate. Crystallization hits were obtained in several different conditions, but those grown in HR Index 92 yielded the best diffraction. The final optimized conditions for each crystal are as follows. For $FosB^{Bc}$ with Zn^{2+} and sulfate and $FosB^{Bc}$ with Zn^{2+} and Fos, crystals used for SAD phasing were obtained after mixing equal volumes of (3 µL) of the protein solution (13 mg/mL in 20 mM HEPES, pH 7.5) and reservoir solution (0.1 M magnesium formate and 12% (w/v) PEG 3350). The $FosB^{Bc}$ with Zn^{2+} and sulfate

crystal used for molecular replacement was obtained after mixing equal volumes (3 µL) of the protein solution (13 mg/mL in 20 mM HEPES, pH 7.5; 3 mM BSH; 5 mM DTT) and reservoir solution (0.1 M magnesium formate and 9% (w/v) PEG 3350). For $FosB^{Bc}$ with Ni^{2+}, Co^{2+}, or Mn^{2+} and Fos, crystals were obtained after mixing equal volumes (3 µL) of the protein solution (13 mg/mL in 20 mM HEPES, pH 7.5; 5 mM Fos; 200 µM M^{2+}) and reservoir solution (0.1 M magnesium formate and 12% (w/v) PEG 3350, 10% (w/v) PEG 3350, or 12% (w/v) PEG 3350 for Ni^{2+}, Co^{2+}, or Mn^{2+}, respectively). For $FosB^{Bc}$ with Mn^{2+} and L-cys-Fos, crystals were obtained after mixing equal volumes (3 µL) of the protein solution (13 mg/mL in 20 mM HEPES, pH 7.5; 5 mM Fos; 5 mM L-cysteine; 5 mM DTT; incubated for ~1 hour on ice) and reservoir solution (0.1M magnesium formate and 14% (w/v) PEG 3350). For $FosB^{Bc}$ with Zn^{2+}, L-cysteine, and Fos, crystals were obtained after mixing equal volumes (3 µL) of the protein solution (13 mg/mL in 20 mM HEPES, pH7.5; 5 mM Fos; 5 mM L-cysteine; and 5 mM DTT; incubated for ~1 hour on ice) and reservoir solution (0.1 M magnesium formate and 8% (w/v) PEG 3350). For $FosB^{Bc}$ with Mn^{2+} and BS-Fos, crystals were obtained after mixing equal volumes (3 µL) of the protein solution (13 mg/mL in 20 mM HEPES, pH 7.5; 8 mM Fos; 8 mM BSH; 5 mM DTT; incubated for ~1 hour on ice) and reservoir solution (0.1 M magnesium formate and 14% (w/v) PEG 3350). All crystals were cryo-protected in the mother solution and 15% glycerol prior to freezing in liquid nitrogen and data collection.

$FosB^{Bc}$ Crystal Data Collection and Refinement

Screening for the diffraction of crystals was performed at the Biomolecular Crystallography Facility in the Vanderbilt University Center for Structural Biology using a Bruker-Nonius Microstar rotating anode X-ray generator equipped with a Proteum PT 135 CCD area

detector mounted on an X8 kappa goniometer with Montel confocal multilayer optics. Crystals were maintained at 100 K using a Bruker KryoFlex cryostat.

Diffraction data for all crystals were collected at 100 K on the LS-CAT 21-ID beamline at the APS synchrotron facility. The collected diffraction data sets were processed with HKL2000.[36] Phasing of diffraction data was done either by molecular replacement using PHASER or by SAD phasing using SHELXD/E.[37] For SAD phasing, the presence of the anomalous scatterer was confirmed and the peak wavelength determined by X-ray fluorescence. Two anomalous scatterers were located in the asymmetric unit corresponding to two active sites in the enzyme. In the case of SAD phasing, initial models were constructed using ARPwARP.[38] For molecular replacement, the first model output and refined from ARPwRP was used as the initial search model. All crystals belong to the $P2_12_12_1$ space group and contain 276 amino acids in the asymmetric unit, which represents the complete $FosB^{Bc}$ enzyme. Manual model building for each structure was performed using Coot model building software.[39] Water molecules were placed with the Coot routine, Find Waters. The final models were obtained by iterative cycles of model building in Coot and structure refinement using Refmac5 in the CCP4 suite of programs (Collaborative Computational Project, 1994).[40] All protein figures were prepared with Chimera.[41] Data collection and refinement statistics are given in Table A1 in the Appendix.

$FosB^{Bc}$ X-ray Fluorescence Spectroscopy

All X-ray fluorescence spectra of the crystals were collected at 100 K on the LS-CAT21-ID beamline at the APS synchrotron facility and used without further processing.

Table 3. Data collection and refinement statistics for $FosB^{Bc}$.

	FosB/Zn/Sulf SAD	FosB/Zn/Sulf MR	FosB/Zn/Fos SAD	FosB/Ni/Fos SAD	FosB/Co/Fos SAD	FosB/Mn/Fos MR	FosB/Mn/Cys-Fos MR	FosB/Zn/Cys-Fos MR	FosBMn/BSH-Fos MR
PDB code	4JH1	4JH2	4JH3	4JH4	4JH5	4JH6	4JH7	4JH8	4JH9
Space group	$P\,2_12_12_1$	$P\,2_12_12_1$	$P\,2_12_12_1$	$P\,2_12_12_1$	$P\,2_12_12_1$	$P\,2_12_12_1$	$P\,2_12_12_1$	$P\,2_12_12_1$	$P\,2_12_12_1$
Unit-cell prameters									
a (Å)	64.45	64.34	64.34	64.41	64.33	64.49	64.29	64.31	56.48
b (Å)	68.20	68.09	68.27	68.54	68.23	68.69	68.31	68.54	64.48
c (Å)	69.60	69.77	69.90	70.44	69.88	70.09	70.18	69.85	83.91
Data collection									
Temperature (K)	100	100	100	100	100	100	100	100	100
Wavelength (Å)	1.2823	1.0781	1.2823	1.4847	1.6046	1.1272	1.0781	1.0781	1.1272
Resolution (Å)[a]	48.71-1.55 (1.61-1.55)	48.73-1.27 (1.29-1.27)	48.84-1.50 (1.55-1.50)	49.12-1.89 (1.93-1.89)	48.82-1.77 (1.80-1.77)	49.06-1.32 (1.34-1.32)	48.95-1.55 (1.58-1.55)	48.92-1.41 (1.43-1.41)	51.13-1.77 (1.83-1.77)
Unique reflections	44556	81296	49820	25035	30425	72030	44593	59747	30311
Completeness (%)[a]	98.3 (85.2)	99.8 (99.2)	98.8 (94.2)	98.4 (97.0)	98.8 (95.6)	97.8 (99.9)	97.9 (95.6)	99.1 (97.6)	99.2 (92.7)
R_{merge} (%)[b]	9.3 (52.9)	7.6 (36.1)	9.5 (60.3)	12.6 (79.2)	9.5 (39.8)	5.1 (54.8)	6.6 (45.3)	4.8 (56.2)	8.4 (60.1)
I/σ	27.5 (2.8)	46.0 (5.8)	23 (3.3)	36.6 (5.4)	64.2 (9.0)	32.19 (2.0)	30.1 (3.6)	43.5 (3.0)	12.0 (2.1)
Redundancy	8.5 (4.7)	7.1 (7.0)	9.3 (7.1)	14.2 (14.1)	13.3 (13.0)	4.0 (3.7)	7.4 (7.3)	7.3 (7.1)	4.7 (4.4)
Refinement									
R_{work}/ R_{free} (%)[c]	13.33/18.78	12.41/15.16	12.36/16.83	17.22/21.62	16.94/20.93	13.79/17.05	13.33/18.64	13.72/17.41	18.30/23.55
Average B factor (Å^2)									
All atoms	18.17	14.80	17.67	19.28	17.33	20.38	15.67	19.74	26.37
Protein	17.01	13.34	16.25	19.03	16.90	19.62	14.55	18.66	26.15
Water	28.59	24.20	28.25	23.53	22.77	26.82	23.11	26.83	28.67
No. of atoms									
Protein	2640	2938	2707	2484	2546	2702	2682	2751	2524
Water	258	379	315	142	185	250	259	253	135
Rmsd from ideal									
Bond length (Å)	0.021	0.023	0.021	0.020	0.023	0.023	0.021	0.023	0.019
Bond angle (deg)	1.96	2.28	1.95	2.02	2.20	2.20	2.07	2.30	1.97
Ramachandran plot (%)[d]									
Most favored	234	234	234	235	234	234	232	232	230
Allowed	16	16	16	15	16	16	18	18	20
Disallowed	2	2	2	2	2	2	2	2	2

[a]Values in parentheses are for the highest resolution shell. [b]Rmerge = $\sum(|I-\bar{I}|)/\sum I \times 100$. [c]Rwork = $\sum|Fo - Fc|/\sum Fo \times 100$, where Fo is the observed structure factor amplitude and Fc is the calculated structure factor amplitude.
[d]Values are given as number of residues.

Expression of N-Terminal Hexa-His-Tagged FosB^{Sa} for Crystallography

The hexa-His-tagged FosB^{Sa} gene was amplified from the FosBSa-pET28 plasmid previously prepared for kinetic assays using primers containing restriction sites for Nde I and EcoR I. To prepare the N-terminal hexa-His-tagged FosB^{Sa} construct, the forward primer was 5'-GC GGG GCC GGG GGT ATA **CAT ATG** CAT CAT CAT CAT CAT CAC TTA AAA TCT ATT AAT C-3' and the reverse primer was 5'- GCC GGC GCC CG**G AAT TC**G CTT ATT TGT AAA ATG-3'. The underlined parts of primer sequences are complementary to the nucleotide sequences of the FosBSa pET28 gene, whereas the 5' overhanging ends of primers contain recognition sites for restriction endonucleases (bold) and are designed to facilitate cloning.

The PCR solution consisted of 200 ng of pET28(FosB^{Sa}), each primer at 10 µM, and 45 µL of Platinum PCR SuperMix. For PCR, 35 cycles were performed with a temperature profile of 30 seconds at 95 °C, 30 seconds at 55 °C, and 1 minute at 72 °C in an Applied Biosystems (Foster City, CA) 2720 thermal cycler. The amplification products were analyzed by electrophoresis on a 0.8% agarose gel stained with ethidium bromide.

The amplification products (1 µg) and pET20b vector (1µg) were digested with Nde I and EcoR I. The digested DNA was analyzed by electrophoresis as previously described; the corresponding bands on the gel were excised and the DNA was extracted with a QIAquick Gel Extraction Kit (Qiagen). Purified hexa-His-tagged FosB^{Sa} and non-tagged FosB^{Sa} were each ligated into pET20b Nde I-EcoR I sites. *E. coli* XL1-blue supercompetent cells were transformed with the ligation mixture and four colonies were assayed for the presence of the FosB^{Sa} gene fragment by plasmid extraction and plasmid DNA sequencing.

The new pET-20b expression plasmid containing the gene encoding hexa-His-tagged FosB^{Sa} was transformed into *E. coli* BL21 (DE3) cells. The cells were plated on LB-agar

containing 100 µg/mL ampicillin and incubated at 37 °C for approximately 16 hours. Single colonies were isolated from the LB-agar plates and used to inoculate 2 mL LB (Gibco) starter cultures (3 cultures for a total of 6 mL) containing 80 µg/mL of ampicillin. After approximately 8 hours of incubation at 37 °C with shaking, 1 mL of starter growth was used to inoculate 1 L of Terrific Broth containing 80 µg/mL of ampicillin (6 L total). The 1 L cultures were grown at 37 °C with shaking for approximately 12 hours (or until the OD_{600} reached ~1) and then induced with 0.5 mM IPTG. Upon induction with IPTG, the temperature was reduced to 25 °C, and the cells were allowed to grow for an additional 4 to 5 hours. The cells were harvested via centrifugation at 5000g for 15 minutes.

The *E. coli* cell pellet was resuspended in 2 mL of His tag lysis buffer (50 mM sodium phosphate, pH 8.0; 300 mM sodium chloride; 10 mM imidazole) per gram of cell pellet. Lysozyme was added to the slurry at 1 mg/mL and the mixture was stirred at 4 °C for 1 hour. After 1 hour of stirring, 5 mg of DNase and RNase were added and the slurry was stirred at 4 °C for another hour. The slurry was sonicated to ensure complete lysing of cells and the lysate was cleared via centrifugation at 35000g for 30 min.

The cleared lysate containing the hexa-His-tagged $FosB^{Sa}$ was added to a nickel-NTA purification column. The column was washed with 50 mM sodium phosphate, pH 8.0; 300 mM sodium chloride; 20 mM imidazole to remove any protein impurities. Finally, the hexa-His-tagged $FosB^{Sa}$ protein was eluted from the nickel-NTA column with 50 mM sodium phosphate, pH 8.0; 300 mM sodium chloride; 250 mM imidazole. Following elution from the column, the $FosB^{Sa}$ protein was dialyzed against 20 mM HEPES, pH 7.5 for crystallization trials.

N-Terminal Intein-Tagged FosB^{Sa} Crystallization

FosB^{Sa} purified for kinetic analyses was dialyzed against 25 mM HEPES, pH 7.5; 50 mM NaCl for crystallization trials. Crystals of intein-tagged FosB^{Sa} with the exogenous L-Cys-Cys9 disulfide bond were grown using the hanging drop vapor diffusion method at 303 K by mixing 3 µL of protein solution (20 mg/mL in 25 mM HEPES, pH 7.5; 50 mM NaCl; 10 mM $MgCl_2$; 10 mM L-cysteine; and 10 mM Fos) and 3 µL of reservoir solution (Hampton Research Index 68, 0.1 M HEPES, pH 7.5; 200 mM ammonium sulfate; 25% (w/V) PEG 3350) in a Hampton Research VDX plate. Apo crystals of intein-tagged FosB^{Sa} were grown via the same approach with the addition of 10 mM tris(2-carboxyethyl)phosphine (TCEP) to the initial protein solution. These crystals were cryo-protected with 25% ethylene glycol in 75% mother liquor.

N-Terminal Hexa-His-Tagged FosB^{Sa} Crystallization

Initial crystals of hexa-His-tagged FosB^{Sa} were grown using the hanging drop vapor diffusion method at 303 K by mixing 3 µL of protein solution (8 mg/mL in 20 mM HEPES, pH 7.5) and 3 µL of reservoir solution (Hampton Research Index 67, 0.1 M Bis-Tris, pH 6.5; 200 mM ammonium sulfate; 25% (w/v) PEG 3350) in a Hampton Research VDX plate. The final optimized conditions for each crystal are as follows. The FosB^{Sa} crystals with Zn^{2+} and sulfate used for SAD phasing and molecular replacement were obtained after mixing equal volumes (3 µL) of protein solution (7.5 mg/mL in 20 mM HEPES, pH7.5; 5 mM Fos) and reservoir solution (0.1 M Bis-Tris, pH 6.5; 200 mM ammonium sulfate, and 16% (w/v) PEG 3350). The FosB^{Sa} crystals with BSH were obtained after mixing equal volumes (3 µL) of protein solution (7.5 mg/mL in 20 mM HEPES, pH 7.5; 5 mM Fos; 5 mM BSH) and reservoir solution (0.1 M Bis-Tris, pH 6.5; 200 mM

ammonium sulfate; 16% (w/v) PEG 3350). All crystals were cryo-protected in 30% glycerol and 70% mother liquor and frozen in liquid nitrogen prior to collection of the diffraction data.

$FosB^{Sa}$ Crystal Data Collection and Refinement

Diffraction data for all crystals were collected at 100 K on either the LS-CAT 21-ID beamline at the APS synchrotron facility or the Bruker-Nonius Microstar rotating anode X-ray generator at Vanderbilt University. The collected diffraction data sets from LS-CAT 21-ID were processed with HKL2000, whereas those collected on the Bruker instrument were processed with Bruker-AXS (2010) PROTEUM2 version 2010.11 (Bruker-AXS, Madison, WI).[36] Phasing the diffraction data was done either by SAD phasing using SHELXD/E or by molecular replacement using PHASER[37] For SAD phasing, the presence of anomalous scatterers were confirmed and the peak wavelength was determined by X-ray fluorescence. In the case of SAD phasing, the initial model was constructed using ARPwARP.[38] For molecular replacement, the first model output and refined from ARPwARP was used as the initial search model. Manual model building for each structure was performed using Coot model building software.[39] Waters were placed with the Coot routine, Find Waters. The final models were obtained by iterative cycles of model building in Coot and structure refinement using Refmac5 in the CCP4 suite of programs.[40] All protein figures were prepared with Chimera.[41] Data collection and refinement statistics are listed in Table A2 in the Appendix.

Continuous ^{31}P-NMR Activity Assays of $FosB^{Sa}$ with Zn^{2+}.

Intein-tagged $FosB^{Sa}$ (0.5 μM) was equilibrated for 5 min with 100 μM $ZnCl_2$ and 8 mM Fos in 20 mM HEPES, pH 7.0. The reaction was initiated by addition of 1.8 mM BSH or L-cysteine, transferred to an NMR tube, and allowed to react at 298 K. At various time points, a ^{31}P

with ^{1}H decoupling NMR spectrum was collected using Bruker AV-400 MHz NMR. Analysis of the data was completed according to the method previously described for activity assays with Mg^{2+} or Ni^{2+}.

Table 4. Data collection and refinement statistics for $FosB^{Sa}$.

	FosB·Zn·sulfate SAD	FosB·Zn·sulfate MR	FosB·BS-Cys9	FosB·l-Cys-Cys9	apo FosB
Protein Data Bank entry	4NAY	4NAZ	4NB0	4NB1	4NB2
space group	*C*2	*C*2	*P*1	*P*1	*P*1
unit cell parameters					
a (Å)	62.49	62.62	40.93	40.88	40.61
b (Å)	62.91	62.81	44.88	44.92	44.83
c (Å)	44.91	45.05	46.87	46.35	45.67
α (deg)	90.00	90.00	110.91	61.19	119.30
β (deg)	121.91	122.08	115.24	65.04	106.79
γ (deg)	90.00	90.00	98.27	82.5	97.92
			Data Collection		
temperature (K)	100	100	100	100	100
wavelength (Å)	1.2823	1.0781	1.1272	1.5412	1.5412
resolution (Å)[a]	40.56–1.42 (1.44–1.42)	40.53–1.15 (1.17–1.15)	39.27–1.62 (1.65–1.62)	39.19–1.80 (1.85–1.80)	38.88–1.89 (1.94–1.89)
no. of unique reflections	27859	49038	32205	23472	18192
completeness (%)[a]	99.9 (100)	93.6 (89.2)	96.3 (93.9)	97.4 (80.7)	90.0 (80.3)
R_{merge} (%)[b]	5.2 (40.2)	3.9 (29.9)	3.2 (35.3)	6.0 (22.5)	5.5 (34.3)
I/σ	50.8 (4.1)	37.1 (3.1)	24.1 (2.0)	14.4 (2.7)	25.3 (3.6)
redundancy	7.1 (6.0)	3.8 (3.1)	2.0 (2.0)	3.6 (1.3)	2.5 (1.3)
			Refinement		
R_{work}/R_{free} (%)[c]	12.95/16.64	13.44/16.22	18.87/22.44	19.47/24.35	18.56/24.08
average *B* factor (Å^2)					
all atoms	19.27	16.96	23.78	20.37	22.97
protein	18.26	15.35	23.49	20.46	22.57
water	29.50	28.76	27.60	21.36	28.36
no. of atoms					
protein	1244	1375	2204	2218	2245
water	101	136	119	99	162
root-mean-square deviation from ideal					
bond lengths (Å)	0.025	0.025	0.023	0.019	0.020
bond angles (deg)	2.28	2.28	2.22	1.96	2.03
Ramachandran plot (%)[d]					
most favored	110	110	194	202	195
allowed	7	9	22	15	21
disallowed	0	0	0	0	0

[a]Values in parentheses are for the highest-resolution shell. [b]$R_{merge} = \sum(|I - \bar{I}|)/\sum I \times 100$. [c]$R_{work} = \sum|F_o - F_c|/\sum F_o \times 100$, where F_o is the observed structure factor amplitude and F_c is the calculated structure factor amplitude. [d]Values are numbers of residues.

Time Point High Performance Liquid Chromatography (HPLC) Activity Assays of FosB^{Sa} with Mn^{2+} and Mn^{2+} with Zn^{2+}.

Intein-tagged FosB^{Sa} (0.5 µM) was equilibrated for 5 min with either 10 µM $MnCl_2$ or 10 µM $MnCl_2$ and 100 µM $ZnCl_2$ and 4 mM Fos in 20 mM HEPES, pH 7.0. The reaction was initiated by addition of 1.5 mM BSH or 1.8 mM L-cysteine and the mixture allowed to react at room temperature. At various time points, a 20 µL aliquot of the reaction mixture was quenched by addition of 40 µL of 5% (w/v) trichloroacetic acid followed by vortexing. Addition of 15 µL of 0.8 M NaOH returned the pH to 7.0. An internal standard (20 µL of 0.4 mM serine) was added and the mixture was diluted to 100 µL with 20 mM HEPES, pH 7.0. A 20 µL aliquot of the quench was added to 55 µL of borate buffer and mixed with 25 µL of the AQC reagent (Waters, Milford, MA) solubilized according to the manufacturer's directions. Derivatization reaction mixtures were incubated at 55 °C for 10 minutes followed by dilution with 400 µL of Mobile Phase A (70 mM NaOAc, pH 5.0; 7 mM trimethylamine).

Derivatized samples were analyzed on an Agilent 1260 Infinity HPLC System using fluorescence detection with excitation at 250 nm and emission at 395 nm. Samples were injected onto a 250 mm x 4.6 mm Kinetex C-18 column with a particle size of 5 µm and a pore size of 100 Å (Phenomenex, Torrance, CA) and equilibrated with 90% Mobile Phase A and 10% Mobile Phase B (80% (v/v) acetonitrile). Samples were eluted using a flow rate of 1 mL/min and the following gradient of Mobile Phase B: 10% from 0 to 6 minutes, 15 to 40% from 15 to 19 minutes, and 40 to 100% from 19 to 22 minutes. BS-Fos, L-cys-Fos, and serine had retention times of 4.0, 4.7, and 7.5 minutes, respectively. The amount of product formed was quantified as previously described.[16]

Disk Diffusion Assay

[The work described in this section was performed by Dr. Neal Hammer from Dr. Eric Skaar's lab.]

Soft agar was inoculated with an overnight culture of Newman or USA300 JE2 methicillin-resistant *S. aureus* isolate and poured over a tryptic soy agar plate. Four sterile Whatman paper discs were placed on top of the cooled soft agar. The indicated amounts of Fos were added to each disk from a 50 mg/mL stock. The plates were incubated overnight at 37 °C.

Expression of Native FosB^{Sa} for HDX-MS Analyses

The new pET-20b expression plasmid containing the gene encoding non-tagged FosB^{Sa} was transformed into *E. coli* BL21 (DE3) cells. The cells were plated on LB-agar containing 100 µg/mL ampicillin and incubated at 37 °C for approximately 16 hours. Single colonies were isolated from the LB-agar plates and used to inoculate 6 mL LB (Gibco) starter cultures (6 cultures for a total of 36 mL) containing 100 µg/mL of ampicillin. After approximately 16 hours of incubation at 37 °C with shaking, one starter culture was used to inoculate 1 L of Terrific Broth containing 100 µg/mL of ampicillin (for a total of 6 L of large cultures). The 1 L cultures were grown at 37 °C with shaking for approximately 3 hours (or until the OD_{600} reached 0.5-0.8) and then induced with 0.1 mM IPTG. Upon induction with IPTG, the temperature was reduced to 18 °C, and the cells were allowed to grow for an additional 16 to 20 hours. The cells were harvested via centrifugation at 6500 X g and 4 °C for 10 min.

Cell pellets were resuspended in lysis buffer (20 mM Tris HCL, pH 8.5) and 2 Complete Mini Protease Cocktail Inhibitor tablets (Roche Diagnostics) were added. Lysozyme (0.5 mg/mL) was added and the mixture was stirred at 4 °C for 20 min. After 20 minutes, 5 mg of DNase and

RNase were added and the slurry was stirred at 4 °C for 2 hours. Cells were further lysed by sonication (50% power, 60% duty cycle, and 2 min on, 3 min off) on ice, until they were no longer viscous. Cellular debris was cleared by centrifugation at 30000 x g and 4 °C for 30 min.

An ammonium sulfate precipitation was performed on the cleared lysate solution prior to any column purification. Fractions were precipitated at 30, 70, and 90% ammonium sulfate. The fractions were analyzed by SDS-PAGE, and fractions containing the highest ratio of FosB to other proteins were combined for further purification. The collected fractions were pooled, concentrated, and dialyzed overnight in DEAE Buffer A (20 mM Tris HCL, pH 8.5; 5% glycerol) to remove any residual lysis buffer or salt that could interfere with ion-exchange chromatography.

The dialysis was loaded onto a GE Healthcare HiPrep DEAE FF 16/10 column, equilibrated with DEAE Buffer A using an Amersham Pharmacia Biotech FPLC (equipped with a 50 mL super loop). With an estimated pI of 7.9, $FosB^{Sa}$ does not adhere to the DEAE material at this pH. The protein was eluted from the column at 2 mL/min at 100% DEAE Buffer A before increasing to 50% of DEAE Buffer B (20 mM Tris HCL, pH 8.5; 1 M NaCl; 5% glycerol). Fractions were analyzed for purity by SDS-PAGE. The most pure fractions were collected, combined, and dialyzed overnight against DEAE Buffer C (20 mM Tris HCL, pH 9.0; 5% glycerol).

The dialysis was loaded onto a GE Healthcare HiPrep DEAE FF 16/10 column, equilibrated with DEAE Buffer C using an Amersham Pharmacia Biotech FPLC (equipped with a 50 mL super loop). The protein was eluted from the column at 2 mL/min at 100% DEAE Buffer C before increasing to 50% of DEAE Buffer D (20 mM Tris HCL, pH 9.0; 1 M NaCl; 5% glycerol). Fractions were analyzed for purity by SDS-PAGE. The most pure fractions were collected,

combined, and dialyzed overnight against SP Buffer (20 mM Tris HCL, pH 8.5; 150 mM NaCl; 5% glycerol).

The protein was concentrated to approximately 1 mL with an Amicon 10K molecular weight cutoff membrane and loaded onto a GE Healthcare 26/60 Sephacryl S-100 HR column at 1 mL/min using an Amersham Pharmacia Biotech FPLC. Protein was eluted from the column with SP Buffer. Fractions were collected from the column at 0.5 mL each and analyzed for purity by SDS-PAGE. The purified $FosB^{Sa}$ protein was collected, combined and concentrated with an Amicon 10K molecular weight cutoff membrane. The final sample was dialyzed against 4 liters of 20 mM Tris HCL, 8.5; 1 mM EDTA; 6 g Chelex resin. This ensured the removal of all metals before storing 1.7 mM $FosB^{Sa}$ at -80 °C.

$FosB^{Sa}$ Peptide Sequencing by Tandem Mass Spectrometry

Prior to HDX-MS analyses, non-tagged $FosB^{Sa}$ was sequenced by LC-MS/MS. The protein was brought to a final concentration of 40 µM in H_2O at a volume of 50 µL. Digestion was performed on ice for five minutes by the addition of 2 µL of 200 mg/mL Protease XVIII in H_2O. The resulting peptides were separated by reversed-phase HPLC on an ice-cold Phenomenex Aeris Peptide 3.6 µ XB-C18 50 X 21 mm column and eluted at a flow rate of 0.1 mL/min with a thirty minute gradient of 5-95% acetonitrile and 0.4% formic acid. Scans of m/z 300 to 2000 were utilized for peptide detection using positive electrospray ionization on a ThermoFinnigan LTQ linear ion trap mass spectrometer at the Mass Spectrometry Core Lab at Vanderbilt University. Peptides were sequenced by data-dependent MS/MS by CID.

The putative identity of each peptide was determined using the computational program PEAKS Client 6 (Bioinformatics Solutions Inc.), which determines the identity of peptide

fragments from raw data.[42] PEAKS predicts peptide fragmentation based on the type of protease used, the FASTA sequence for the protein, MS instrument used, and the parameters used for MS. Experimental fragmentation patterns are matched with predicted peptide fragmentation. The false discovery rate (FDR) is calculated for the match using decoy sequences and is reported as a -10log(p) value, where p is the probability that a false identification of the current search has the same or better significance.

All peptides with a -10log (p) value greater than 20 (equal to a p value of 0.01) were selected and verified using MassXpert MS analysis software.[43] This presents all possible peptides within the protein with the same parent mass as experimental data. Then the experimental fragmentation spectra will be compared to theoretical fragmentation patterns of the possible peptides generated by ProteinProspector program MS-Product.[44] Verified peptides were combined to create a peptide coverage map.

Amide HDX-MS

Analyses of backbone amide H/D exchange were performed on $FosB^{Sa}$ in the presence of Mn^{2+}, Mn^{2+} and Fos, or Mn^{2+}, Fos, and BSH. HDX-MS analyses were completed using the continuous labeling method. Prior to deuterium incorporation, 200 µM $FosB^{Sa}$ samples were combined with 200 µM $MnCl_2$, or 200 µM $MnCl_2$ and 20 mM Fos and incubated for 5 minutes at room temperature. If required, 20 mM BSH was added to the sample immediately prior to deuterium incorporation. Deuterium incorporation was initiated by a five-fold dilution of 10 µL of the pre-incubated protein solution in 99.9% atm D_2O at room temperature (final concentrations were 40 µM $FosB^{Sa}$, 40 µM $MnCl_2$, 4 mM Fos, or 4 mM BSH). The incorporation was quenched at various time points between 15 seconds to 8 hours by a two-fold dilution in ice-cold 100 mM

KH_2PO_4, pH 2.3. The protein was digested on ice for five minutes by addition of 2 µL of 200 mg/mL protease XVIII in H_2O. The resulting peptides were separated by reversed-phase HPLC on an ice-cold Phenomenex Aeris Peptide 3.6 µ XB-C18 50 X 21 mm column and eluted at a flow rate of 0.1 mL/min with a fifteen minute gradient of 5-95% acetonitrile and 0.4% formic acid. All samples were prepared individually and run on the same day. Scans of m/z 300 to 2000 were utilized for peptide detection using positive electrospray ionization on a ThermoFinnigan LTQ linear ion trap mass spectrometer at the Mass Spectrometry Core Lab at Vanderbilt University.

Deuterium incorporation was observed as a shift in the centroid ion envelope for each peptide. In order to correct for deuterium incorporation that occurs after the quenching step, a control for time point zero ($m_{0\%}$) was performed, in which 10 µL of the pre-incubated protein was solution was added to 40 µL of H_2O at room temperature followed by quenching and digestion with protease XVIII as described above.

The spectra from each HDX-MS sample were analyzed using the program HDExaminer (Sierra Analytics).[42] The program determines the centroids of the isotope envelope for each peptide at each HDX time point using a program-specific algorithm and a list of known peptide fragments with their respective retention times. After analysis, each peptide centroid was manually optimized for the best fit of the known peptide. HDExaminer determines the number of deuterons incorporated onto each peptide using Equation 3, correcting for the loss and gain of deuterium during the analysis, where D is the number of deuterons incorporated, N is the total number of exchangeable backbone amides, m_t is the average mass of the partially deuterated peptide sample at time t, and $m_{0\%}$ and $m_{100\%}$ are the average masses of the non-deuterated and fully deuterated peptide control samples, respectively. For this analysis, the theoretical $m_{100\%}$ determined by the HDExaminer program was used.

Equation 3: $D = N(\frac{m_t - m_{0\%}}{m_{100\%} - m_{0\%}})$

Each experiment was repeated in duplicate and averaged. The percentage of deuterium incorporation for each peptide was plotted as a function of log time using Kaleida-Graph (Synergy Software). The resulting plot was fit to the sum of first-order rate expressions using Equation 4, where N is the total number of exchangeable hydrogens and A_i is the number of amide protons that exchange at the rate k_i for the exchange time t.

Equation 4: $D = N - \sum_{i-1}^{n} A_i \times e^{-k_i t}$

Mass spectrometric analysis of purified BshC.

The native BshC enzyme was analyzed for the presence of tightly-bound ligands utilizing liquid chromatography-mass spectrometry prior to cleavage with rTEV protease. The BshC preparation (approximately 1 nmol of protein in 50 mM ammonium bicarbonate, pH 7.5) was separated by HPLC on a 50 mm x 2.1 mm Phenomenex Aeris Peptide C18 column with 3.6 µm particle size. Protein with bound substrate was eluted with a 10 minute gradient from 5-95% acetonitrile with 0.4% formic acid. The spectra were obtained in negative mode at various voltages (5-15 V) utilizing a ThermoFinnigan LTQ linear ion trap mass spectrometer at the Mass Spectrometry Core Lab at Vanderbilt University. Peaks of 112.7 m/z, 158.7 m/z, 262.7 m/z, and 425.7 m/z were observed, and a peak search was conducted at MassBank.[45] The 112.7 m/z, 158.7 m/z, and 425.7 m/z peaks are suggestive of adenosine nucleosides, whereas the 262.7 m/z has no match in the database. These data suggest that adenosine nucleosides are present in the sample, but their exact identity cannot be confirmed.

CHAPTER III

DETERMINATION OF THE CATALYTIC SELECTIVITY OF THE FOSFOMYCIN RESISTANCE ENZYME, FosB[1]

Results

The discovery of the new LMW thiol in Gram-positive bacteria, BSH, in 2009 implicated that BSH could be the primary substrate for FosB activity instead of the previously reported L-cysteine.[19] However, BSH was not commercially available and the biosynthetic pathway was not fully elucidated and confirmed *in vitro*. Therefore, to begin investigating the possibility that FosB is a BSH-transferase, we needed to obtain stable BSH that could be utilized to initiate both kinetic and structural studies.

The Vanderbilt Institute of Chemical Biology (VICB) Chemical Synthesis Core developed a novel 11 step synthesis of bacillithiol disulfide (BSSB) utilizing D-glucosamine as a starting point with an overall 8-9% yield.[46] While these synthetic studies were underway, Hamilton and coworkers reported the chemical synthesis of BSH starting with D-glucal. Shortly thereafter, BSH became commercially available at a cost of $225/mg. The synthesis developed by the VICB Chemical Synthesis Core provided our lab with over one gram of BSSB at a cost of approximately $15/mg, which is 15 fold cheaper than the commercially available BSH. Additionally, BSSB is

[1] Reprinted with permission from Lamers, A. P., Keithly, M. E., Kim, K., Cook, P. D., Stec, D. F., Hines, K. M., Sulikowski, G. A., and Armstrong, R. N. (2012) Synthesis of Bacillithiol and the Catalytic Selectivity of FosB-Type Fosfomycin Resistance Proteins, *Org Lett 14*, 5207-5209.

more stable than BSH for storage and use. It can also readily be reduced to BSH for use in kinetic assays and structural studies.

A New Continuous ^{31}P NMR Method

Upon receipt of BSSB, I used a commercially available thiol reduction column to develop a reduction method of BSSB to afford BSH in 45% yield. I then developed a new continuous ^{31}P NMR activity assay for FosB enzymes, which was used to begin investigating substrate and metal ion selectivity using time course kinetic analyses of FosB from four Gram-positive organism: *Staphylococcus aureus*, *Bacillus subtilis*, *Bacillus cereus*, and *Bacillus anthracis* ($FosB^{Sa}$, $FosB^{Bs}$, $FosB^{Bc}$, and $FosB^{Ba}$ respectively). While this NMR assay is quick and convenient, it cannot be utilized with paramagnetic metals or for performing detailed steady-state kinetic analyses.

The enzymatic inactivation of Fos by FosB was initiated in a 3 mM NMR tube and continuously monitored at various time points by ^{31}P with ^{1}H decoupling NMR spectroscopy. Figure 13 shows representative NMR spectra with Cys-Fos, Bs-Fos, and Fos peaks, which have the unique chemical shifts of 18.9, 18.6, and 12.1 ppm respectively. The exact chemical shifts are pH dependent, but are always distinct for the substrates and products. The NMR assays contained an excess of Fos in order to allow the use of the law of conservation of mass to calculate the amount of product formed. The spectra collected for each time point were used to calculate the peak height of Fos substrate and the BS-Fos or Cys-Fos product. The amount of product formed was calculated from the ratio between the peak heights of substrate and product and the total concentration of Fos used in the reaction.

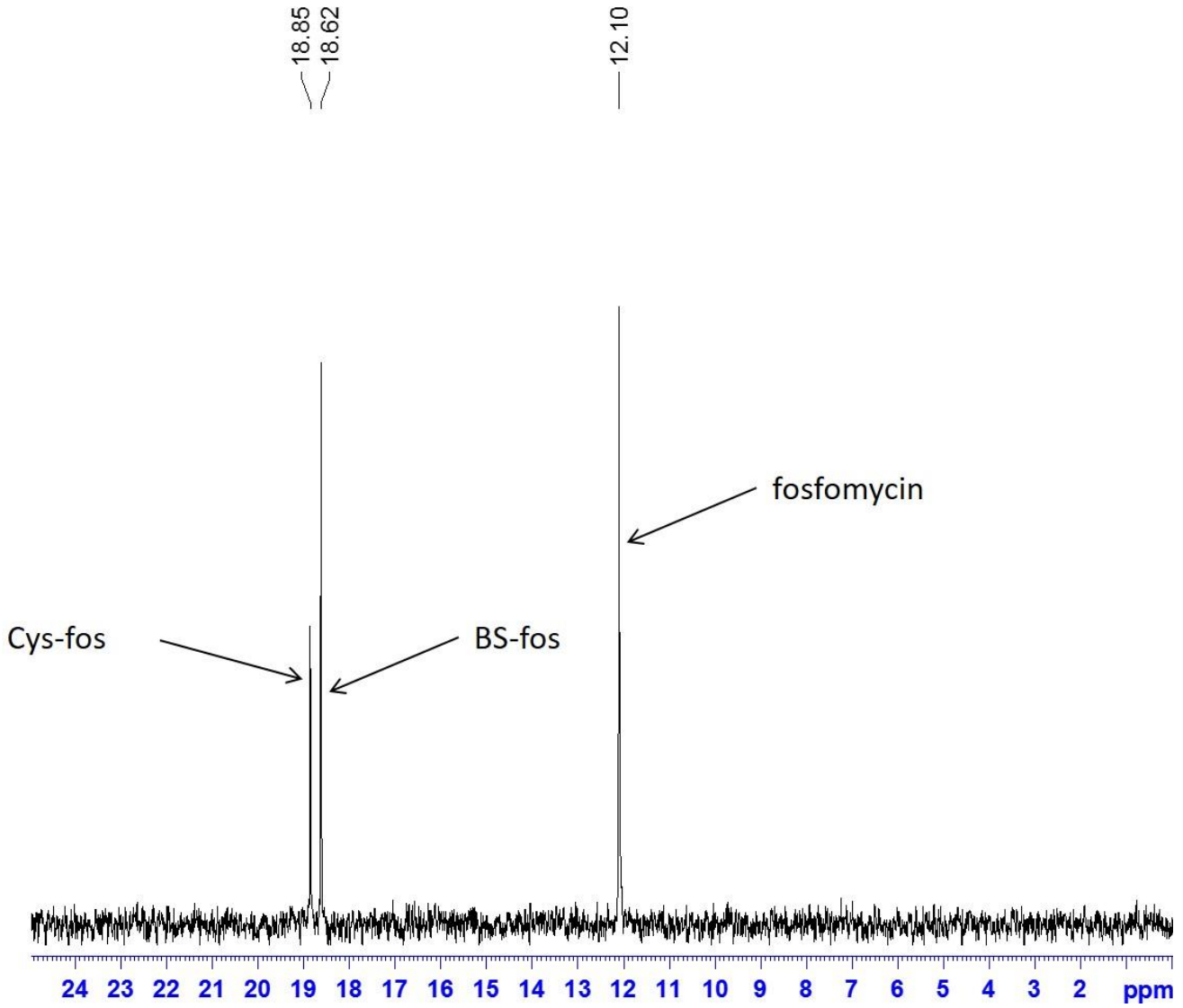

Figure 13. Representative spectra of the new continuous ^{31}P NMR assay. This is a spectra of a mixed enzymatic assay, which shows unique chemical shifts for Cys-Fos, BS-Fos, and Fos peaks of 18.9, 18.6, and 12.1 ppm respectively.

Time Course Kinetic Analyses of FosB Inactivation of Fosfomycin

Access to BSH allowed for screening of FosB enzymes from several different bacterial species. Each enzyme was analyzed using time course kinetics with the continuous ^{31}P NMR analysis previously described. The assays were completed with L-cysteine, and BSH as possible thiol substrates. Metal dependent activation of these enzymes was analyzed using the diamagnetic metals Ni^{2+} and Mg^{2+}.

Figure 14 shows results for $FosB^{Sa}$, $FosB^{Bs}$, $FosB^{Bc}$, and $FosB^{Ba}$. The results indicate a very clear preference of the $FosB^{Sa}$ enzyme for BSH and Ni^{2+}, but no activity with L-cysteine in the presence of Mg^{2+}. The $FosB^{Bs}$, $FosB^{Bc}$, and $FosB^{Ba}$ enzymes also show an increase in activity with BSH compared to L-cysteine, but it is a moderate increase in $FosB^{Bc}$ and $FosB^{Ba}$. These data also show that the unlike $FosB^{Sa}$, activation of FosB from the bacilli species with Ni^{2+} and Mg^{2+} is similar.

While the NMR assay is not suitable for analyzing detailed steady-state kinetics, the results can be used to estimate the approximate minimum turnover numbers (k_{cat}) from the initial rates of the reactions (Table 3). The apparent k_{cat} for $FosB^{Sa}$ with BSH and Ni^{2+} is ~30 s^{-1}, but with Mg^{2+} drops to ~1 s^{-1}. $FosB^{Sa}$ activity with L-cysteine and Ni^{2+} also drops to ~0.9s^{-1}. The apparent k_{cat} for $FosB^{Bs}$ with BSH and Ni^{2+} or Mg2+ are ~6 s^{-1} and ~3 s^{-1}, respectively. With L-cysteine the k_{cat} values are much lower, on the order of 0.05 to 0.2 s^{-1}.

Table 5. Apparent k_{cat} values determined from FosB time course activity assays.

Strain	Metal	Thiol	Apparent k_{cat} (s-1)
$FosB^{Sa}$	Ni^{2+}	BSH	30
$FosB^{Sa}$	Mg^{2+}	BSH	1
$FosB^{Sa}$	Ni^{2+}	L-cysteine	0.9
$FosB^{Sa}$	Mg^{2+}	L-cysteine	unable to determine
$FosB^{Bs}$	Ni^{2+}	BSH	6
$FosB^{Bs}$	Mg^{2+}	BSH	3
$FosB^{Bs}$	Ni^{2+}	L-cysteine	0.2
$FosB^{Bs}$	Mg^{2+}	L-cysteine	0.05
$FosB^{Bc}$	Ni^{2+}	BSH	1.7
$FosB^{Bc}$	Mg^{2+}	BSH	1.7
$FosB^{Bc}$	Ni^{2+}	L-cysteine	0.6
$FosB^{Bc}$	Mg^{2+}	L-cysteine	0.2
$FosB^{Ba}$	Ni^{2+}	BSH	1.7
$FosB^{Ba}$	Mg^{2+}	BSH	2.1
$FosB^{Ba}$	Ni^{2+}	L-cysteine	0.4
$FosB^{Ba}$	Mg^{2+}	L-cysteine	0.3

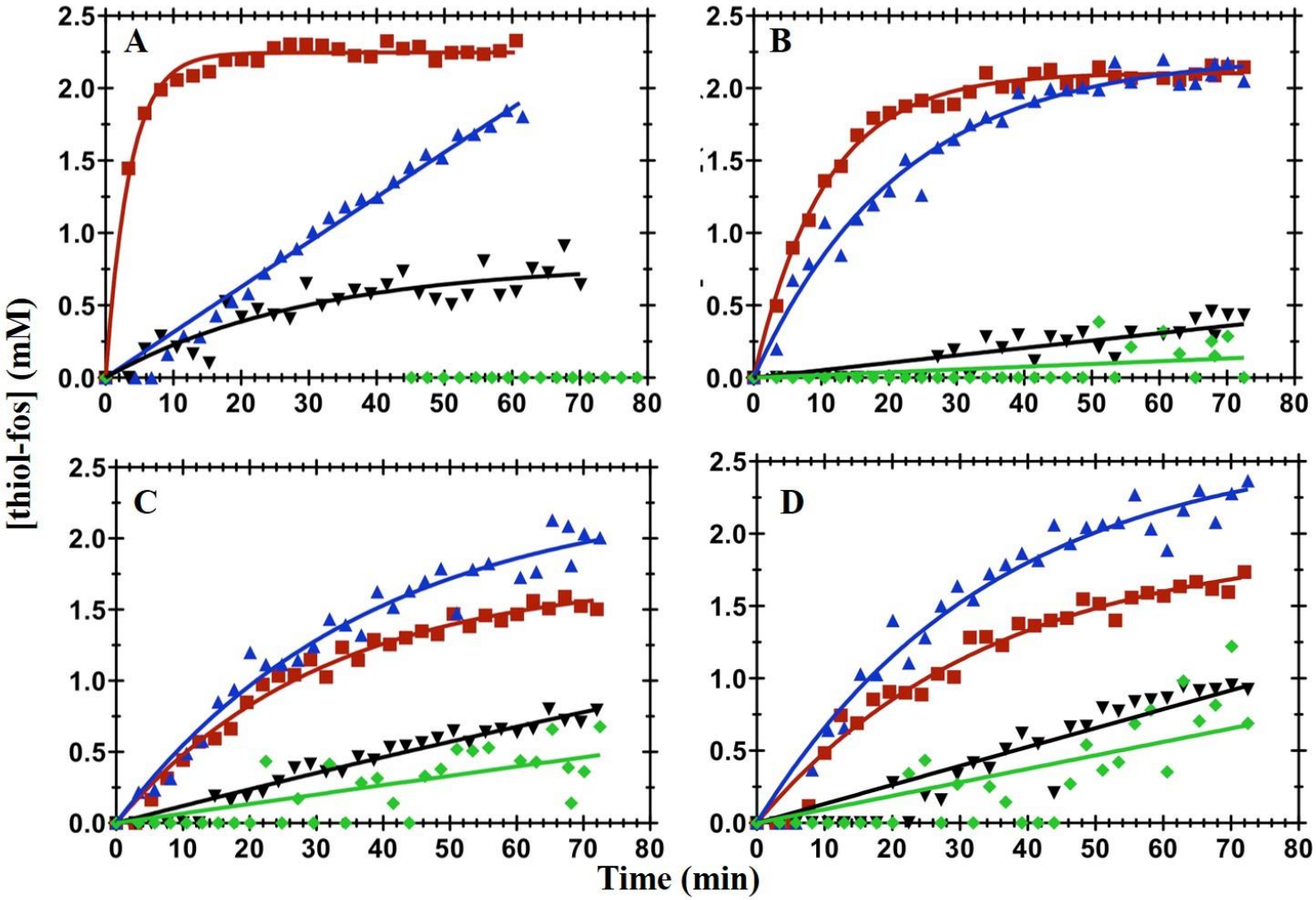

Figure 14. Time course kinetic analyses of FosB inactivation of Fos. Time course of the $FosB^{Sa}$, $FosB^{Bs}$, $FosB^{Bc}$ and $FosB^{Ba}$ catalyzed-addition of BSH or L-cysteine to fosfomycin in the presence of Mg^{2+} or Ni^{2+} shown in panels A, B, C, and D, respectively. Reactions were carried out at 25˚ C in 20 mM HEPES, pH 7.0 with 4 mM fosfomycin and 0.5 μM enzyme in the presence of (■) 2 mM BSH and 10 μM Ni^{2+}, (▲) 2 mM BSH and 1 mM Mg^{2+}, (▼) 2 mM L-cysteine and 10 μM Ni^{2+} or (◆) 2 mM L-cysteine and 1 mM Mg^{2+}.

Discussion

The new chemical synthesis of BSSB developed by the VICB chemical synthesis core provided our lab with stable BSH at an affordable cost. This allowed us to begin preliminary analysis of the substrate selectivity for the FosB enzymes from multiple bacterial species. Upon receipt of the BSSB, a commercially available reduction column was used to obtain BSH at a 45% yield. A new continuous ^{31}P NMR assay was developed to use for analysis of time course enzyme assays. This assay is quick and easy to use for time course kinetic assays. However, it is unsuitable for use with paramagnetic metals or for detailed steady state kinetics.

The NMR assay was used to complete the initial analysis of FosB enzymatic activity with L-cysteine compared to BSH. Additionally, we probed the metal dependent activation of FosB by both Ni^{2+} and Mg^{2+}. The results of the time course kinetic analyses show a clear preference for BSH over L-cysteine as the *in vitro* thiol substrate for FosB enzymes from several Gram-positive organisms. However, between the two diamagnetic metals tested, there preference for FosB activation was not as clear. While $FosB^{Sa}$ showed a significant increase in activity when Ni^{2+} was present, the FosB enzymes from bacilli species had no preference between Ni^{2+} and Mg^{2+}.

In conclusion, the newly described synthesis of BSSB opens the door for more detailed kinetic and metal-ion preference studies of the FosB enzymes as well as structural investigation of the FosB enzyme in complex with BSH and products. FosB was originally described as an Mg^{2+}-dependent L-cysteine-transferase, but the results of these initial time-course kinetic analyses indicate the FosB is actually a BSH-transferase. While we know the enzyme is dependent on a divalent metal, further investigation of multiple divalent metals was required to determine the best activating metal-ion cofactor.

CHAPTER IV

ANALYSIS OF THE STRUCTURE AND FUNCTION OF FosB FROM *Bacillus cereus* REVEALS FosB IS A MANGANESE-DEPENDENT BACILITHIOL-TRANSFERASE[2]

Results

Time Course Kinetic Analyses of FosB^{Bc} Inactivation of Fosfomycin

The metal activation of FosB^{Bc} by Mg^{2+} and Ni^{2+} were previously investigated, but the divalent activation of the FosB enzymes remained unclear.[46] It is possible that metal activation may be dependent upon the organism containing the FosB enzyme. To further probe the appropriate divalent metal activation of FosB^{Bc}, kinetic analyses for the inactivation of Fos by the nucleophilic addition of L-cysteine or BSH in the presence of Mg^{2+}, Ni^{2+}, and Zn^{2+} were conducted utilizing the continuous ^{31}P NMR method previously described in Chapter II of this work.

Additionally, kinetic analysis of FosB activation by Mn^{2+} was completed using a modified version of the continuous ^{31}P NMR assay. Since Mn^{2+} is a paramagnetic metal and will interfere with the NMR assay, the reaction was quenched and metal was removed for ten different time points ranging from 30 sec to 60 min. Each time point was analyzed by ^{31}P NMR and the spectra were processed in the same manner as those run using the continuous assay.

Initial reactions were conducted at 298 K in 20 mM HEPES, pH 7.0 with 8 mM Fos and 0.5 μM FosB^{Bc} in the presence of 4 mM BSH or L-cysteine and 10 mM Mg^{2+} or 100 μM Zn^{2+}

[2] Reprinted with permission from Thompson, M. K., Mary. E.; Harp, Joel; Cook, Paul D.; Jagessar, Kevin L.; Sulikowski, Gary A.; Armstrong, Richard N. (2013) Structural and Chemical Aspects of Resistance to the Antibiotic Fosfomycin Conferred by FosB from Bacillus cereus, *Biochemistry 52*, 7350-7362. Copyright 2012 American Chemical Society.

(Figure 15). The concentration of Mg^{2+} was selected to be significantly greater than K_{act} (~200 µM) reported for the homologous $FosB^{Bs}$ enzymatic activity with L-cysteine as the thiol substrate.[17] The results revealed that Zn^{2+} is a potent inhibitor of $FosB^{Bc}$ activity with both L-cysteine and BSH.

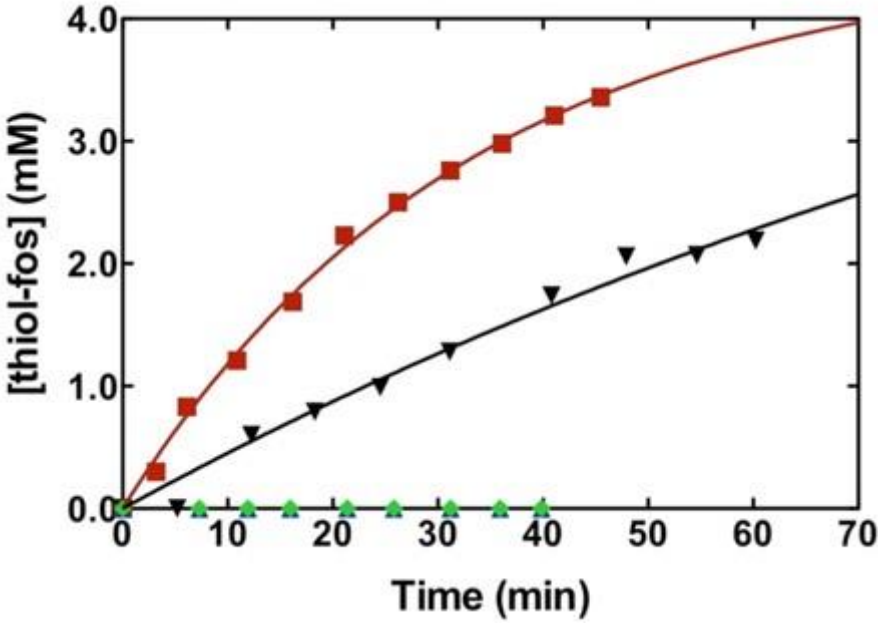

Figure 15. Time course kinetic analysis of $FosB^{Bc}$ catalyzed addition of BSH or L-cysteine to Fos in the presence of Mg^{2+} and Zn^{2+}. Reactions were carried out at 25˚ C in 20 mM HEPES, pH 7.0 with 8 mM fosfomycin and 0.5 µM enzyme in the presence of (■) 4 mM BSH and 10 mM Mg^{2+}, (▼) 4 mM L-Cys and 10 mM Mg^{2+}, (▲) 4 mM BSH and 100 µM Zn^{2+}, or (◆) 4 mM L-Cys and 100 µM Zn^{2+}.

Additional reactions to test metal activation by Mn^{2+}, Ni^{2+}, or Mg^{2+} were conducted with half the enzyme and co-substrate concentrations (Figure 16). This change was necessary because the inactivation of Fos by addition of BSH in the presence of Mn^{2+} is so efficient that the initial observable time point via the NMR method using the higher concentrations was beyond completion. The concentration of Mg^{2+} was also reduced to 1 mM to more accurately reflect the

prevailing intracellular concentrations of the metal. Reduction of the Mg^{2+} concentration had no effect on the results.

The apparent k_{cat} values for $FosB^{Bc}$ with each metal and thiol substrate were approximated from the data. The apparent k_{cat} for $FosB^{Bc}$ with BSH and Mn^{2+}, Ni^{2+}, or Mg^{2+} are 26.7 s^{-1}, 1.3 s^{-1}, and 1.0 s^{-1} respectively. The apparent k_{cat} for $FosB^{Bc}$ with L-cysteine and Mn^{2+}, Ni^{2+}, or Mg^{2+} are 2 s^{-1}, 0.6 s^{-1}, and unable to be determined respectively. The results demonstrate that $FosB^{Bc}$ has a distinct preference for BSH over L-cysteine with metal activation *in vitro* as follows: Mn^{2+}>Ni^{2+}>Mg^{2+}. Therefore, $FosB^{Bc}$ is a Mn^{2+}-dependent BSH-transferase.

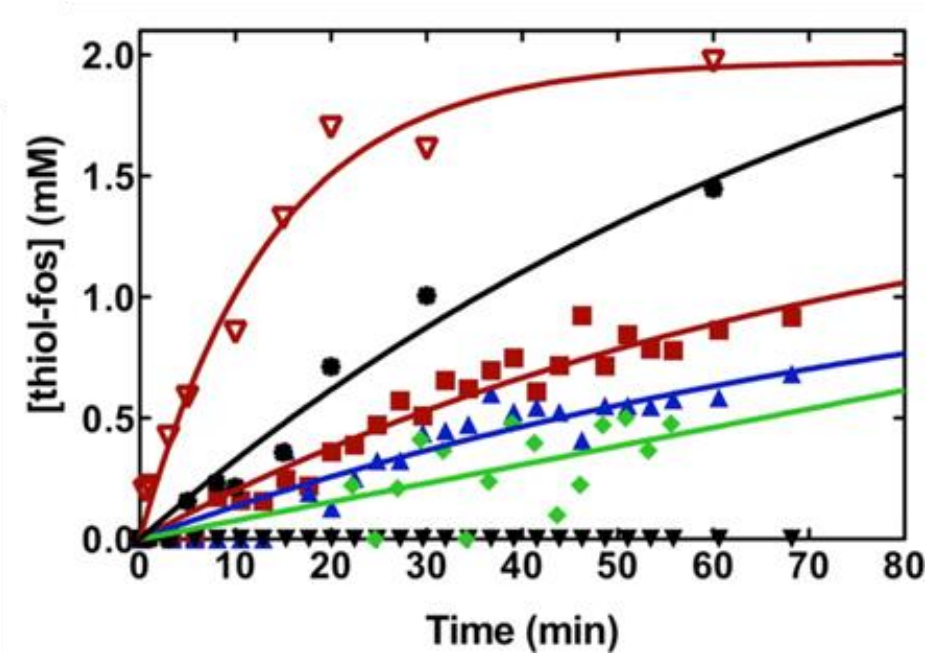

Figure 16. Time course kinetic analysis of $FosB^{Bc}$ catalyzed addition of BSH or L-cysteine to Fos in the presence of Mg^{2+}, Ni^{2+}, or Mn^{2+}. Reactions were carried out at 25° C in 20 mM HEPES, pH 7.0 with 4 mM fosfomycin and 0.25 µM enzyme in the presence of (▽) 2 mM BSH and 10 µM Mn^{2+}, (■) 2 mM BSH and 10 µM Ni^{2+}, (▲) 2 mM BSH and 1 mM Mg^{2+}, (●) 2 mM L-cysteine and 10 µM Mn^{2+} (▼) 2 mM L-cysteine and 10 µM Ni^{2+}, or (◆) 2 mM L-cysteine and 1 mM Mg^{2+}.

Steady State Kinetic Analyses of FosB Inactivation of Fosfomycin

In order to compare the catalytic efficiency of $FosB^{Bc}$ inactivation of Fos by nucleophilic addition of BSH in the presence of Mn^{2+}, steady state kinetic analyses were completed. An endpoint high performance liquid chromatography (HPLC) assay with fluorescence detection of ACCQ-Fluor derivatized samples was used to complete the analysis using both L-cysteine and BSH as substrates and Mn^{2+} for metal activation. Figure 17 shows the Michaelis Menten plots of this analysis and the calculated steady state kinetic constants can be found in Table 4.

Table 6. Steady state kinetic constants for the $FosB^{Bc}$ catalyzed addition of BSH or L-cysteine to Fos in the presence of Mn^{2+}.

Thiol	**V_{max} (M/s)**	**k_{cat} (s^{-1})**	**k_{cat}/K_M^{thiol} ($M^{-1}s^{-1}$)**	**K_M^{thiol} (mM)**
L-cysteine	3.39×10^{-5}	135.6	1.3×10^{3}	104
BSH	2.12×10^{-5}	84.8	1.0×10^{4}	8.4

The increase in activity with BSH compared to L-cysteine correlates with the similar increase in activity seen during the time course analyses previously described. There is also a 10-fold increase in activity with L-cysteine with Mn^{2+} compared to published data for $FosB^{Bs}$ activity with L-cysteine and Mg^{2+} (k_{cat}/K_m^{thiol} is 180 $M^{-1}s^{-1}$).[17] The results for $FosB^{Bc}$ show that the catalytic efficiency of FosB activity with BSH and Mn^{2+} is an order of magnitude lower than would be expected to account for *in vivo* activity. While this work was in progress, Roberts et al. published mechanistic studies of $FosB^{Sa}$. Our results correlate with the data published for $FosB^{Sa}$ (k_{cat}/K_m^{thiol} is 4×10^{3} $M^{-1}s^{-1}$).[47]

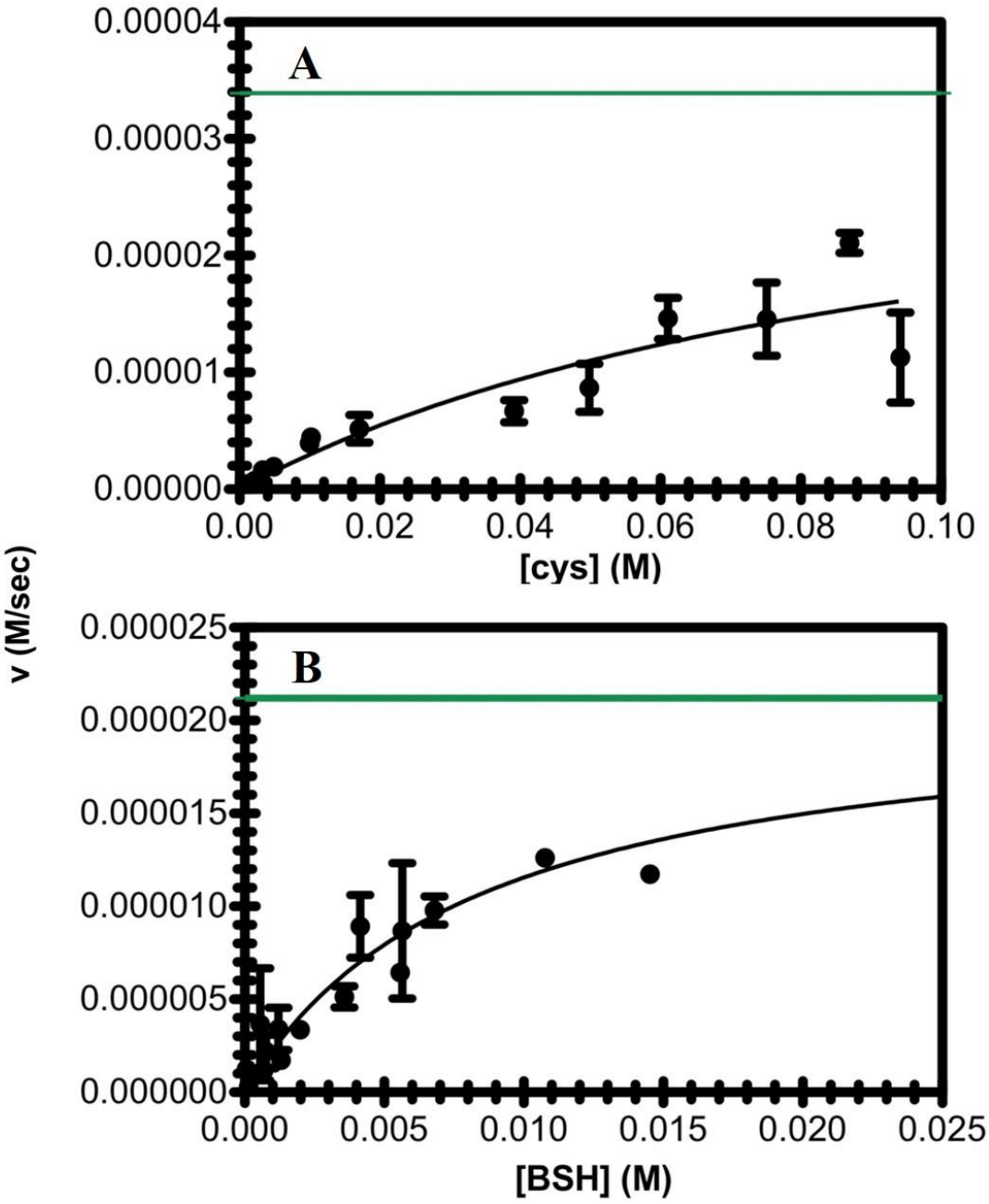

Figure 17. Steady state kinetic analysis of $FosB^{Bc}$ catalyzed addition of BSH or L-cysteine to Fos in the presence of Mn^{2+}. Reactions were carried out at 25˚ C in 20 mM HEPES, pH 7.0 with 4 mM Fos and 0.25 μM enzyme in the presence of 10 μM Mn^{2+} and (A) 1-100 mM L-cysteine or (B) 0.1-15 mM BSH. The green line represents V_{max} for each analysis.

Crystal Structure Determination of FosB^{Bc}

Nine high resolution crystal structures of FosB^{Bc} in complex with various combinations of divalent metals, substrates, or products were determined. The crystal structure of FosB^{Bc}•Zn^{2+} (PDB 4JH1) was refined to 1.55 Å resolutions. An X-ray fluorescence scan of the crystal prior to diffraction data collection confirmed the presence of a high concentration of Zn^{2+} (Figure 18). Diffraction data was then collected at the K_α absorption edge of Zn^{2+}, which is a wavelength of 1.28 Å. Phases were determined by single wavelength anomalous diffraction (SAD) from the Zn^{2+} k_α edge and Zn^{2+} was used to model the observed density.

Using a similar method of data collection, structures of FosB^{Bc}•Zn^{2+}•Fos (PDB 4JH3), FosB^{Bc}•Ni^{2+}•Fos (PDB 4JH4), and FosB^{Bc}•Co^{2+}•Fos (PDB 4JH5) were determined to 1.49 Å, 1.89 Å, and 1.77 Å resolutions respectively. Each diffraction data set was collected at the K_α absorption edge of Zn^{2+}, Ni^{2+}, or Co^{2+} (1.28 Å, 1.48 Å, or 1.61 Å respectively) and initial phases were determined by SAD phasing of the corresponding divalent metal for each structure (Figures 19-21) . X-ray fluorescence scans of each crystal prior to diffraction data collection was used to confirm the presence of each metal (Figures 18, 22-23).

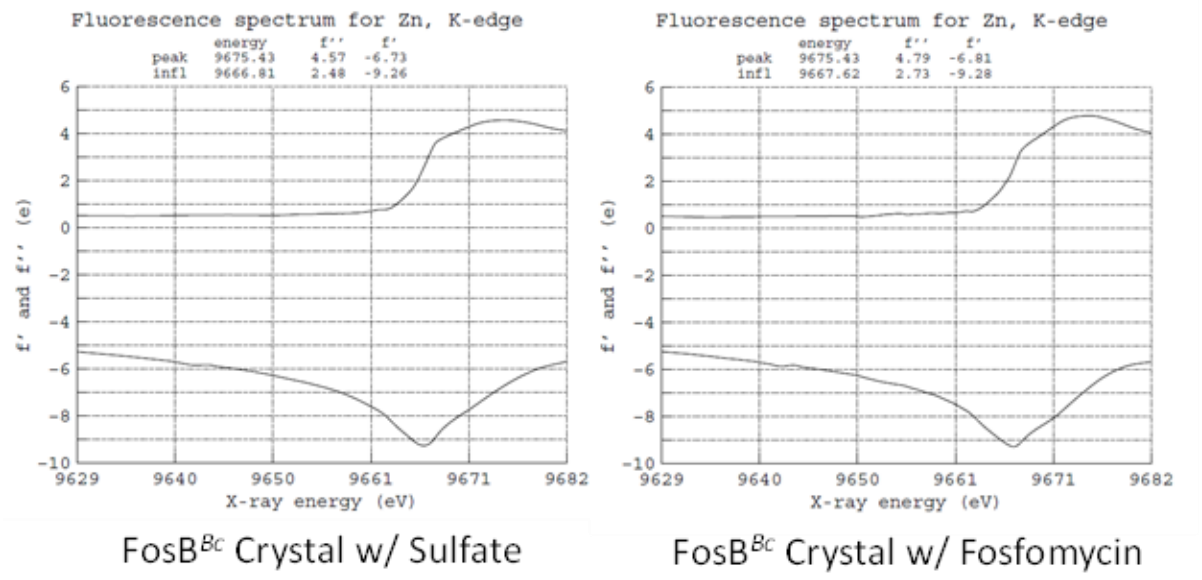

Figure 18. X-ray fluorescence scans of the $FosB^{Bc}$•Zn^{2+} crystals.

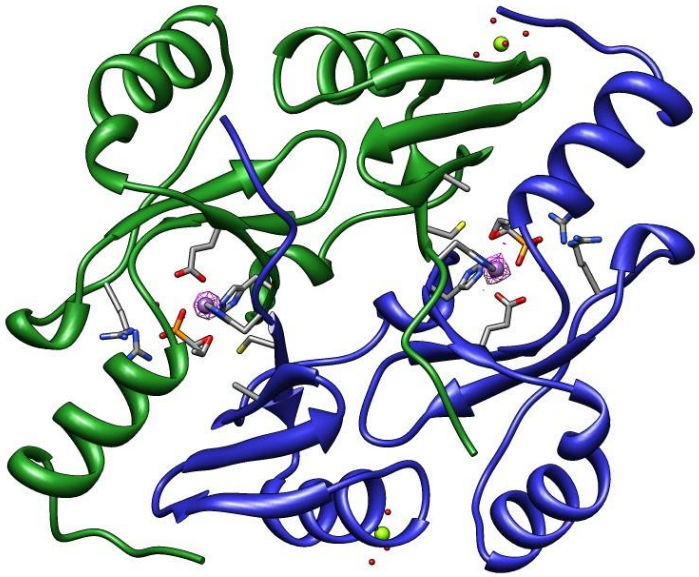

Figure 19. Overall X-ray crystal structure of $FosB^{Bc}$•Zn^{2+}•Fos at 1.50 Å resolution (PDB 4JH3). The anomalous density map from the SAD experiment shown around the Zn^{2+} metal ions is contoured at 5 σ. R_{work} = 12.36% and R_{free} = 16.83%.

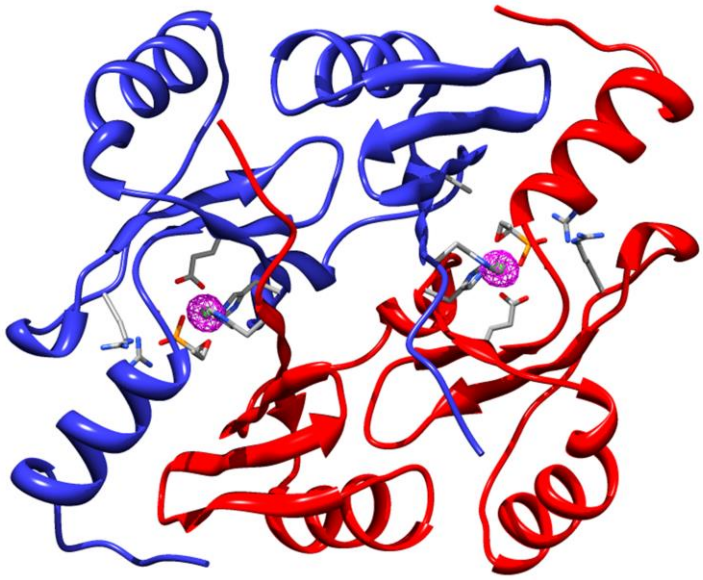

Figure 20. Overall X-ray crystal structure of $FosB^{Bc}$•Ni^{2+}•Fos at 1.89 Å resolution (PDB 4JH4). The anomalous density map from the SAD experiment shown around the Ni^{2+} metal ions is contoured at 5 σ. R_{work} = 17.22% and R_{free} = 21.22%.

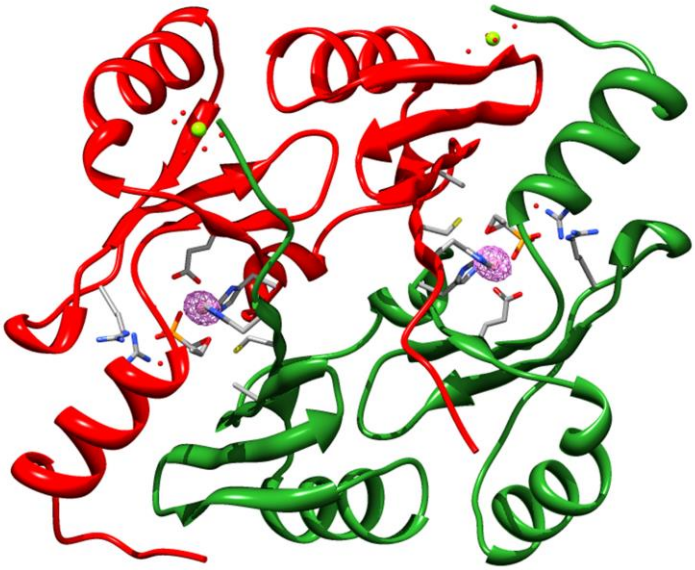

Figure 21. Overall X-ray crystal structure of $FosB^{Bc}$•Co^{2+}•Fos at 1.77 Å resolution (PDB 4JHH). The anomalous density map from the SAD experiment shown around the Co^{2+} metal ions is contoured at 5 σ. R_{work} = 16.94% and R_{free} = 20.93%.

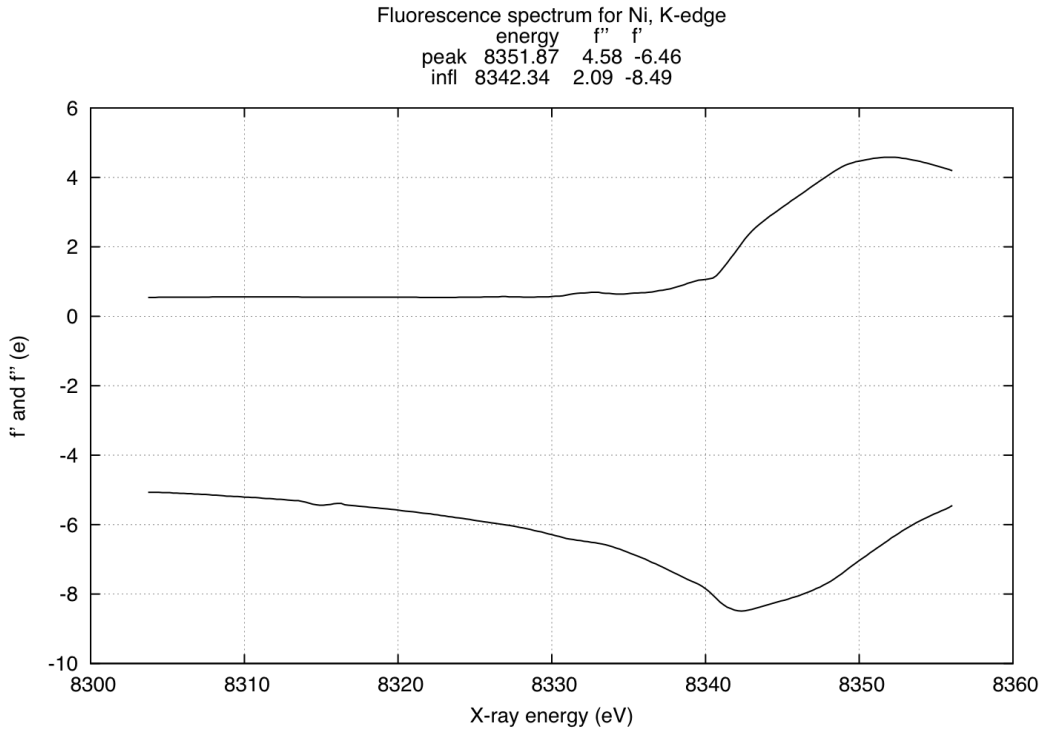

Figure 22. X-ray fluorescence scans of the $FosB^{Bc}$•Ni^{2+}•Fos crystal.

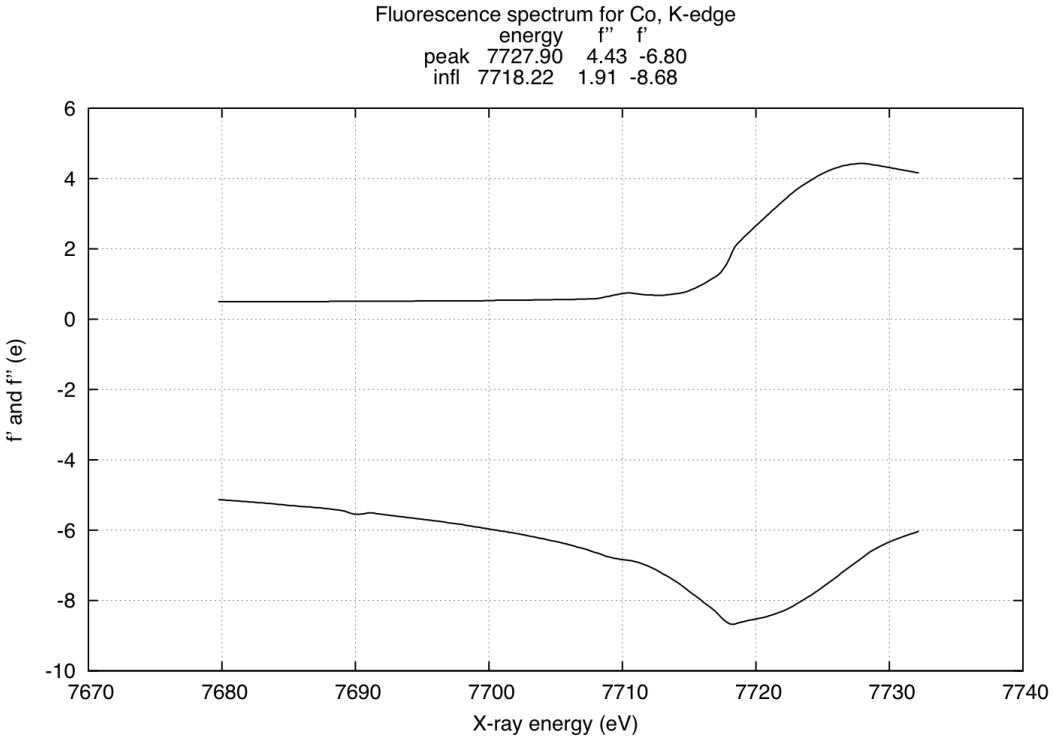

Figure 23. X-ray fluorescence scans of the $FosB^{Bc}$•Co^{2+}•Fos crystal.

Co-crystallization of $FosB^{Bc}$ in the presence of BSH resulted in higher quality crystals, but the BSH molecule was never observed in the structure. This resulted in a 1.27 Å structure of $FosB^{Bc}$•Zn^{2+}•SO_4^{2-} (PDB 4JH2) determined by molecular replacement. Crystals of $FosB^{Bc}$ grown in the presence of Zn^{2+}, Fos, and L-cysteine produced electron density that is not clearly the product or the Fos and L-cysteine cosubstrates. The structure of $FosB^{Bc}$•Zn^{2+}•Fos•L-cysteine (PDB 4JH8) was determined to 1.41 Å resolution and solved by molecular replacement. The electron density of carbon-1 of Fos appears more substrate-like in character and the strong electron density above carbon-1 is most certainly that of sulfur. The ambiguity of the remaining electron density for L-cysteine is likely caused by a combination of occupancy and multiple conformations in the solvent channel.

Structures of $FosB^{Bc}$•Mn^{2+}•Fos (PDB 4JH6), $FosB^{Bc}$•Mn^{2+}•L-cysteine-Fos (PDB 4JH7), and $FosB^{Bc}$•Mn^{2+}•Bs-Fos (PDB 4JH9) were determined to 1.32 Å, 1.55 Å, and 1.55 Å resolutions respectively using molecular replacement. Crystals were analyzed by X-ray fluorescence prior to diffraction data collection to confirm the presence of Mn^{2+} (Figure 24). However, due to the longer wavelength of the K_α absorption edge of Mn^{2+} (1.89 Å), which can damage protein crystals during data collection, these structures were solved by molecular replacement instead of SAD phasing. The B factors for each of the metal sites in the crystal indicate Mn^{2+} ions are a good fit for the observed electron density. A library file in CIF format for (1R,2S)-1-(S-L-cysteinyl)-2-hydroxypropylphosphonate product was created using the online PRODRG Server and inserted into the model for $FosB^{Bc}$•Mn^{2+}•L-cysteine-Fos.[48] The same product was used to model the observed density in the active site of $FosB^{Bc}$•Mn^{2+}•Bs-Fos because the glucosamine-malate domain of BSH was not observed (Figure 25). It is likely that this is not observed because the glucosamine-malate moiety is simply not homogenous in the crystal. Protein flexibility is critical

for proper enzyme function and the rigidity of the crystal may prevent proper seating of the BSH molecule in the enzyme.

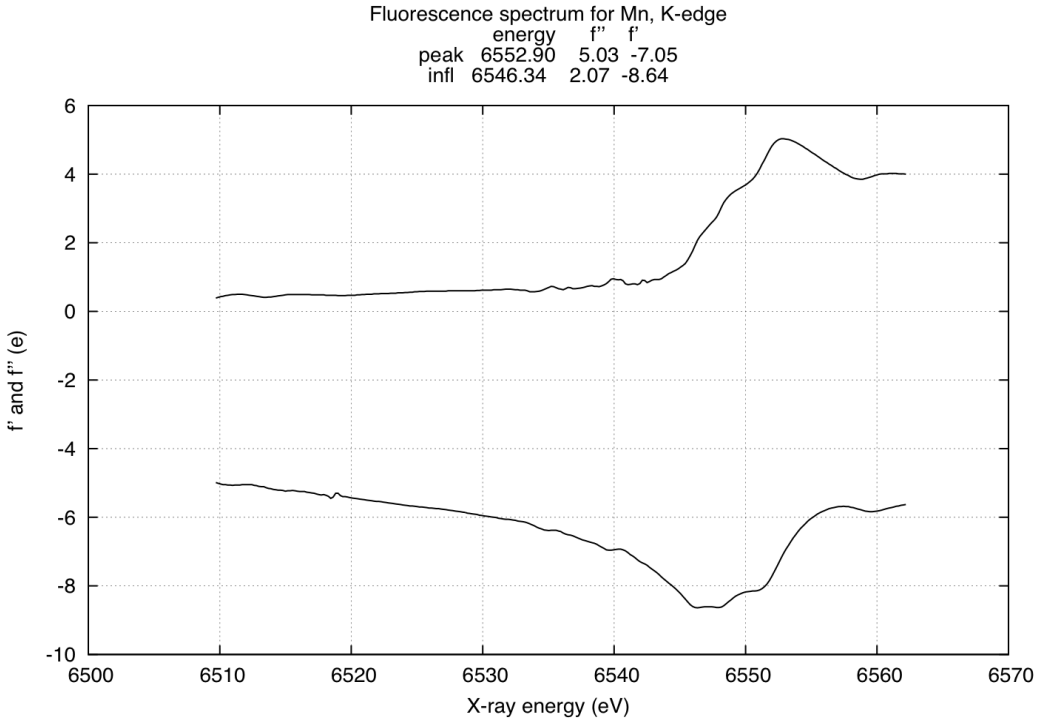

Figure 24. X-ray fluorescence scans of the $FosB^{Bc}$•Mn^{2+}•Fos crystal.

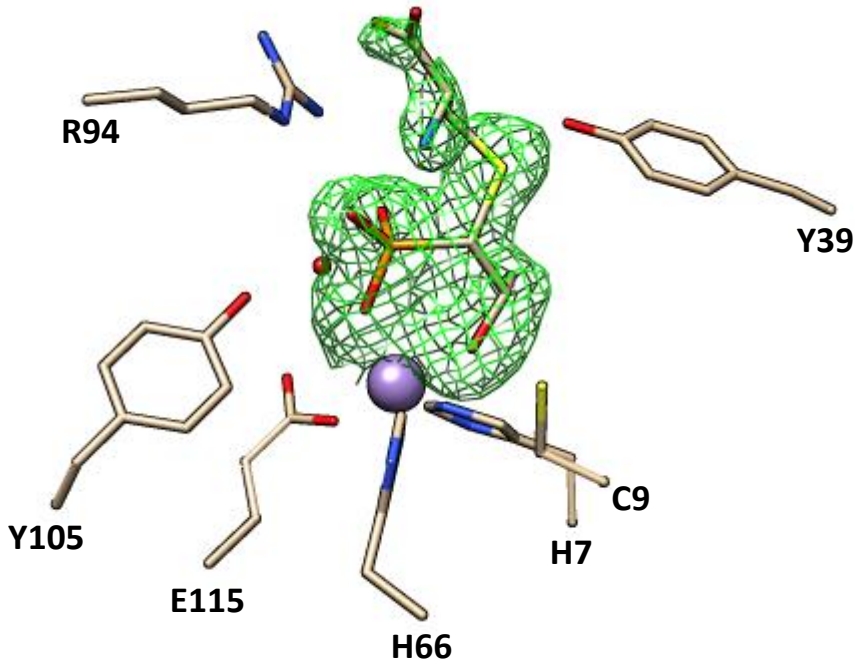

Figure 25. The active site of FosB^{Bc} in complex with Mn^{2+} in the presence of BS-Fos at 1.77 Å resolution (PDB 4JH9). The model was refined with L-cys-Fos since the complete density for BS-Fos is missing. Final refinement had a R_{work} = 18.30% and R_{free} = 23.55%. The difference electron density shown for product is contoured 3σ. The unit cell dimensions for this crystal are different than the others reported (Table 1) indicating a significant difference in crystal packing. That product has been formed is evidenced by opening of the epoxide ring of the antibiotic and a C1-S bond length of 1.85 Å. Unlike what is observed in the FosB^{Bc}•Mn^{2+}•L-cys-Fos structure, the electron density in this structure weakens near the C_α end of the L-cysteinyl domain. Thus, what is observed in this structure is the phosphonate end of Bs-Fos tethered to the Mn^{2+} metal within the enzyme while the glucosamine-malate moiety of BS-Fos solvent exposed and disordered on the surface of the enzyme within the crystal.

Structural Characterization of FosB^{Bc}

As anticipated, the overall structure reveals that FosB is a homodimer belonging to the VOC superfamily of metalloenzymes similar to the other Fos resistance enzymes, FosA and FosX (Figure 26).[18] The structures contain a 3D domain-swapped arrangement of tandem βαβββ motifs in which both subunits of the homodimer participate in formation of the active site, which is a characteristic feature of the VOC superfamily.[3] Like the FosA and FosX enzymes, FosB also

utilizes two histidines and a glutamic acid to coordinate the metal ion. Additionally, the structure in complex with Fos and various divalent metals establishes the presence of Fos coordinated to Zn^{2+}, Ni^{2+}, Co^{2+}, or Mn^{2+} (PDBs 4JH1, 4JH4, 4JH5, and 4JH6; Figure 27A). Similar to the FosA structure in complex with Fos, the geometry of metal coordination for $FosB^{Bc}$ with bound Fos is a highly distorted, five-coordinate trigonal bipyramidal configuration with His7, His66, and the phosphonate oxygen of Fos in the equatorial sites and Glu115 and the oxirane oxygen of Fos in the axial sites.

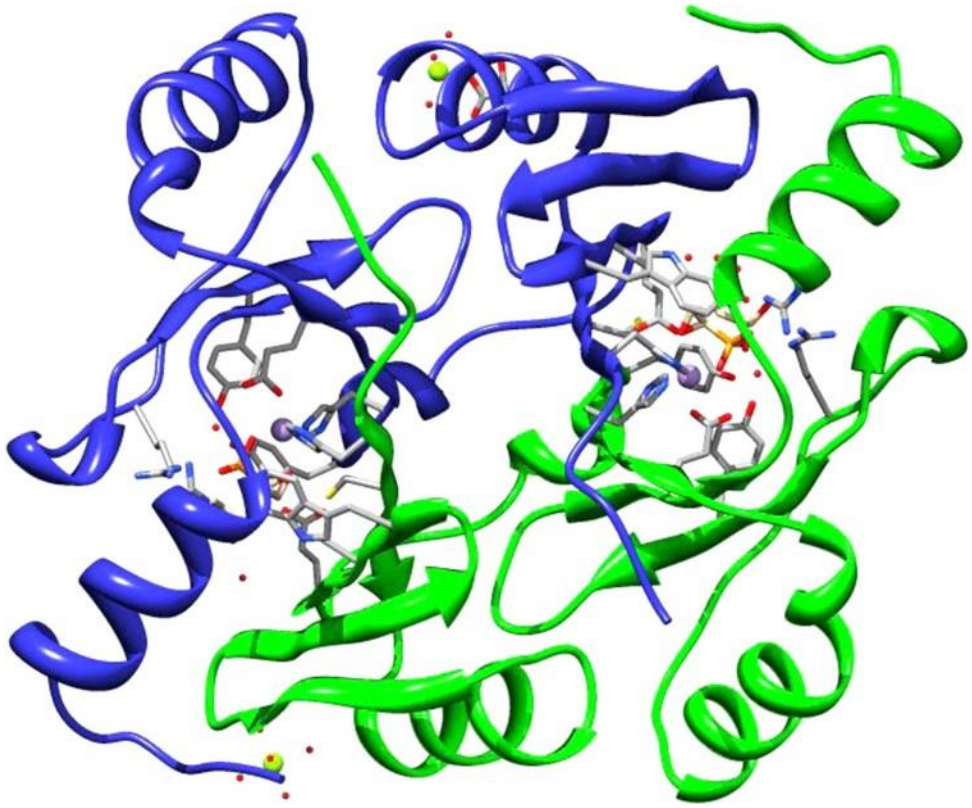

Figure 26. Overall X-ray crystal structure of $FosB^{Bc}$ in complex with Mn^{2+} and Fos at 1.32 Å resolution (PDB 4JH6). R_{work} = 13.79% and R_{free} = 17.05%

$FosB^{Bc}$ in complex with Mn^{2+} and the L-cysteine-Fos product was determined at 1.55 Å. In this structure, the epoxide ring of Fos is opened via nucleophilic addition of L-cysteine to

carbon-1 of Fos. Carbon-1 is sp^3 hybridized and strong electron density is observed for the sulfur. The L-cysteine-Fos product (constructed in PRODRG according to the stereochemistry reported by Bernat et al.) is identified as (1R,2S)-1-(S-L-cysteinyl)-2-hyrdoxypropylphosphonate, the same product as that reported for FosA (Figure 27B).[15a, 48] Inversion of the configuration at carbon-1 indicates that the reaction proceeds via direct S_N2 addition of the thiol to the oxirane carbon.

The crystals of $FosB^{Bc}$ grown in the presence of Zn^{2+}, Fos, and L-cysteine produced electron density that most closely resembles the Fos and L-cysteine cosubstrates (Figure 27C). The density of the Fos carbon-1 is more substrate-like in geometry than that of the product complex seen in Figure 27B. Additionally, the electron density above carbon-1 of Fos has a peak of 17.30σ, which is too intense for even the most well-ordered water molecules. When refined with L-cysteine, the sulfur atom has a B factor of 27.1 $Å^2$ averaged over the two sites, which compares quite well with the overall B factor for the structure of 19.7 $Å^2$. Furthermore, the oxygen of Tyr39 is 3.25 Å from the sulfur and the location of the sulfur superimposes that of the thioether of L-cysteine-Fos in the $FosB^{Bc}$•Zn^{2+}•Fos•L-cysteine structure. Finally, the distance between carbon-1 of Fos and the sulfur is 2.79 Å, which is significantly shorter than the theoretical van der Waals interaction of 3.50 Å and much longer than a typical carbon-sulfur single bond (1.83 Å). This likely represents the location of the sulfur when it is poised for nucleophilic attack of Fos. This structure represents a ternary structure with both substrates in the active site, which is an anticipated result because Zn^{2+} is a potent inhibitor of $FosB^{Bc}$ activity.

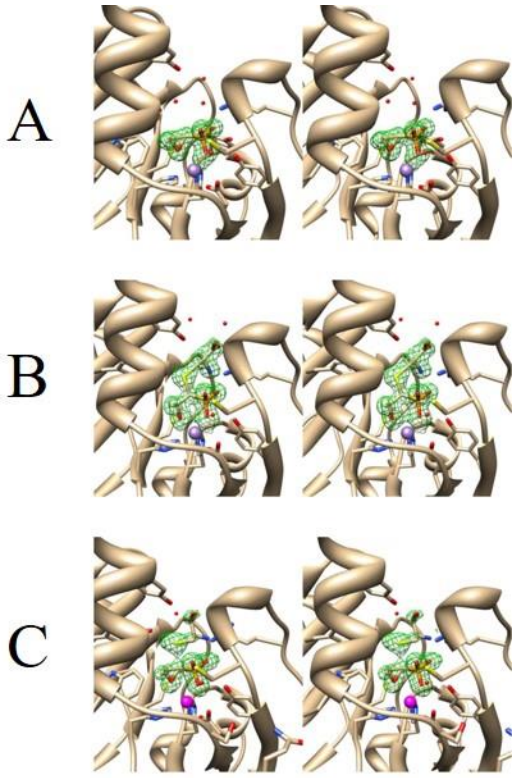

Figure 27. Stereo views of (A) $FosB^{Bc}$•Mn^{2+}•Fos (PDB 4JH6), (B) $FosB^{Bc}$•Mn^{2+}•L-cysteine-Fos (PDB 4JH7), and (C) $FosB^{Bc}$•Zn^{2+}•Fos•L-cysteine (PDB 4JH8). Difference densities are the 2*F*o–*F*c maps calculated before addition of the ligands to the coordinate files and are contoured at 3σ. The electron density in (A) shows the position of Fos coordinated to Mn^{2+}. The electron density in (B) shows L-cysteine-Fos coordinated to Mn^{2+}. The carbon-1 density of L-cysteine-Fos is sp3 hybridized following nucleophilic attack by the thiol. The electron density in (C) shows Fos coordinated to Zn^{2+} and the density for carbon-1 of Fos is more substrate-like in geometry than that of (B), indicating no product formation. The strong electron density above carbon-1 likely belongs to sulfur. The ambiguity in the rest of the density for the L-cysteine is probably due to a combination of occupancy and multiple conformations in the crystal.

Superposition of the $FosB^{Bc}$•Zn^{2+}•Fos•L-cysteine ternary structure and the $FosB^{Bc}$•Mn^{2+}•L-cysteine-Fos product structure shows that Asn50 is the only residue that changes position in the active site. In the ternary structure, Asn50 is oriented approximately 90° relative to the product structure. This positions the O_δ of Asn50 4.13 Å from the Fos carbon-1 and N_δ of Asn50 4.20 Å from the sulfur of L-cysteine.

Surface analysis of the $FosB^{Bc}$ structures revealed a well-defined pocket and access channel to carbon-1 of Fos (Figure 28). The pocket and access channel are appropriate in size and shape to accommodate L-cysteine or BSH. The positioning of Fos in the active site is oriented to place the backside of carbon-1 directly in the center at the end of the solvent access channel. This is necessary for nucleophilic addition of the thiol to Fos.

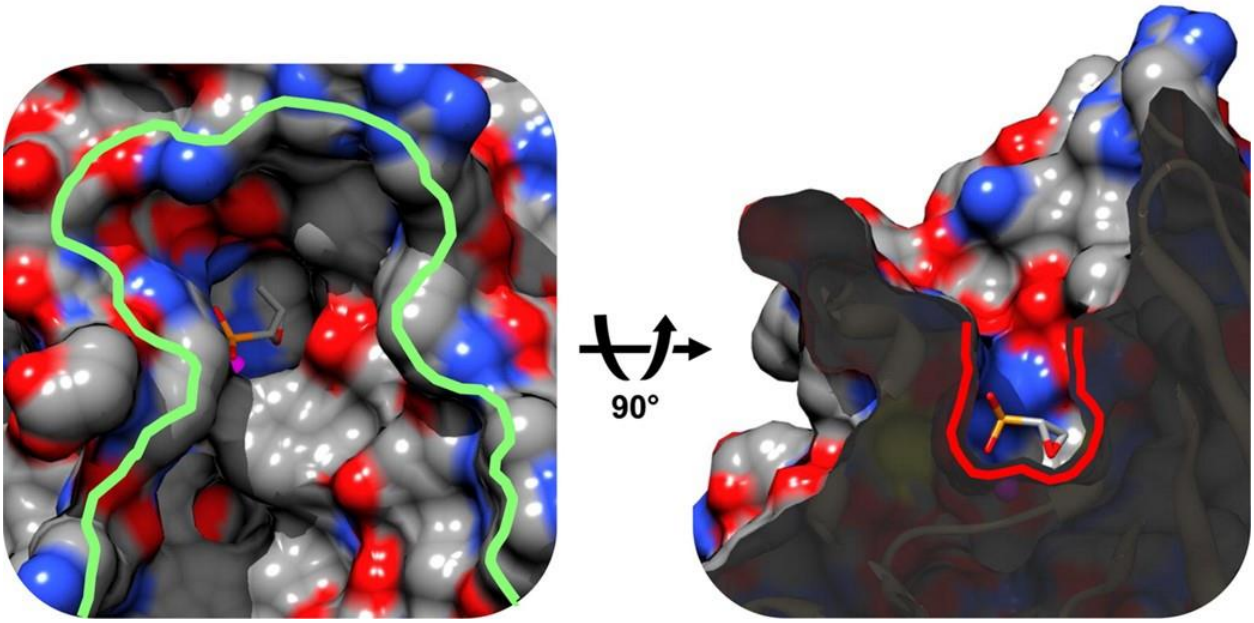

Figure 28. Surface analysis of $FosB^{Bc}$ in complex with Fos (PDB 4JH3). (**left**) Top-view of the channel from the surface of the protein into the active site. The green line contours a depression in the surface of the protein large enough to accommodate BSH. (**right**) Narrowing of the channel near Fos (shown in stick representation). The narrow section (outlined in red) is large enough to accommodate either L-cysteine or the cysteinyl moiety of BSH.

Discussion

Initial crystallization of $FosB^{Bc}$ contained Zn^{2+} in the active site (PDBs 4JH1 4JH2, and 4JH3), which is similar to a structure deposited in the PDB for $FosB^{Ba}$ (PDB 4IR0). The presence of the metal was confirmed using X-ray fluorescence and SAD phasing from the K_α edge of Zn^{2+}. These crystals were grown from purified $FosB^{Bc}$ grown in terrific broth media without further

manipulation to add or remove specific metals. Therefore, Zn^{2+} was the divalent metal "selected" by the enzyme during growth. Given that the Zn^{2+} was the "selected" metal, we tested the Zn^{2+} activation of $FosB^{Bc}$ for both L-cysteine and BSH transferase activity. The results indicate that Zn^{2+} inhibits activity of $FosB^{Bc}$ (Figure 15), which prompted additional kinetic analyses of the $FosB^{Bc}$ enzyme.

Initial analysis of divalent metal activation of $FosB^{Bs}$ nucleophilic addition of L-cysteine to Fos established the activation order as $Ni^{2+} \sim Mg^{2+} > Mn^{2+} > Fe^{2+} > Cu^{2+} > Ca^{2+} \sim Co^{2+} > Zn^{2+}$.[17] However, our access to BSH allowed us to screen several FosB enzymes for BSH transferase activity. The results demonstrate that the four enzymes tested ($FosB^{Sa}$, $FosB^{Bs}$, $FosB^{Ba}$, and $FosB^{Bc}$) have a preference for BSH over L-cysteine as the thiol substrate *in vitro*.[46] The more extensive kinetic analyses of $FosB^{Bc}$ presented in this chapter demonstrates a preference for BSH over L-cysteine and establishes the metal activation of $FosB^{Bc}$ *in vitro* to be $Mn^{2+} > Ni^{2+} > Mg^{2+} > Zn^{2+}$ (Figures 15 and 16). This order is in agreement with the homologous classes of Fos resistance enzymes, FosA and FosX, where both are activated by Mn^{2+} and show only minimal activity with Zn^{2+} in the presence of their respective nucleophiles.[12, 49]

Steady state kinetic analysis of Mn^{2+}-dependent $FosB^{Bc}$ inactivation of Fos by nucleophilic addition of L-cysteine or BSH was completed. This analysis revealed a moderate increase in $FosB^{Bc}$ BSH transferase activity compared to $FosB^{Bc}$ L-cysteine transferase activity (Table 4). There was also a 10-fold increase in $FosB^{Bc}$ L-cysteine transferase activity compared to published data for Mg^{2+}-dependent $FosB^{Bs}$ L-cysteine transferase activity. The catalytic efficiency of Mn^{2+}-dependent $FosB^{Bc}$ BSH transferase activity (k_{cat}/K_m^{thiol} is 1.0 X 10^4 $M^{-1}s^{-1}$) is an order of magnitude lower than the reported Mn^{2+}-dependent FosA GSH transferase activity (k_{cat}/K_m^{thiol} is 1.7 X 10^5 $M^{-1}s^{-1}$).[12] The $FosB^{Bc}$ activity is lower than would be expected to account for the robust *in vivo*

activity of FosB. However, a steady state kinetic analysis of $FosB^{Sa}$ was reported by Roberts et al. in 2013 and our results correlate with their published results.[47]

The preference of $FosB^{Bc}$ for BSH over L-cysteine suggests that the glucosamine-malate domain of the BSH molecule is important for substrate recognition. In the 2013 study completed by Roberts et al., substitution of the malate motif in BSH with either an O-methyl or O-benzyl aglycone group results in a 10- and 18-fold increase for the K_M^{thiol}, respectively, in $FosB^{Sa}$.[47] This indicates that the thermodynamic driving force of the nucleophilic inactivation of Fos is likely the interaction of the glucosamine-malate domain with the surface of the enzyme.

The surface analysis of $FosB^{Bc}$ (Figure 28) revealed a well-defined pocket and access channel that is the correct size and shape to accommodate L-cysteine or BSH. The role of this proposed binding pocket and access channel can be elucidated by either $FosB^{Bc}$•Mn^{2+}•L-cysteine-Fos (PDB 4JH7) or $FosB^{Bc}$•Mn^{2+}•Bs-Fos (PDB 4JH9). In both structures, the nucleophilic addition of the thiolate to carbon-1 of Fos occurs at the end of the channel (Figure 29). The opening of the binding pocket from the access channel begins at the C_α end of the cysteinyl moiety, where the remainder of the BSH domain would be connected through the secondary amine of the Bs-Fos product. Unfortunately, in PDB 4JH9, the complete molecule of Bs-Fos was not observed seated in the binding pocket of the crystal for reasons previously described.

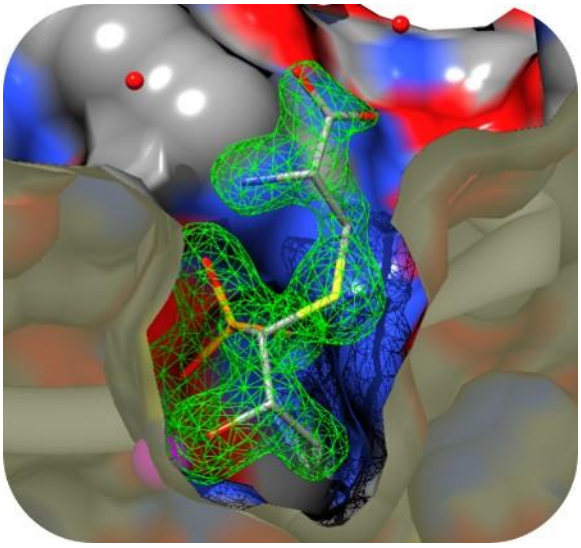

Figure 29. Active site of $FosB^{Bc}$ in complex with Mn^{2+} and L-cysteine-Fos at 1.55 Å resolution (PDB 4JH7). The difference electron density of L-cysteine-Fos is the $2F_o$-$2F_c$ map calculated before the addition of the molecule to the coordinate file and is contoured at 3σ. R_{work} = 13.33% and R_{free} = 18.64%.

Analysis of Fos coordination to the metal in the active site revealed that the molecule is surrounded by a cage of amino acids positioned appropriately to anchor the antibiotic in the orientation necessary for nucleophilic attack, placing the backside of carbon-1 in the center of the solvent access channel (Figure 30). This cage has both polar and nonpolar ends to accommodate Fos. The polar phosphonate group of Fos is coordinated to the metal through one of the phosphonate oxygens and hydrogen bonded to Arg94, Arg124, Tyr64, and Tyr105 through the other two. The triangular cage structure around the phosphonate is maintained by a salt bridge from Arg94 to Asp100 and hydrogen bonds from Arg124 to Tyr39 and Asp100. The oxirane oxygen of Fos is coordinated to the metal such that the methyl group of Fos is held adjacent to Trp46 and carbon-2 of Fos is pointed directly at Ala48. These amino acids that construct the cage structure are conserved throughout the FosB enzymes (Figure 31, green).

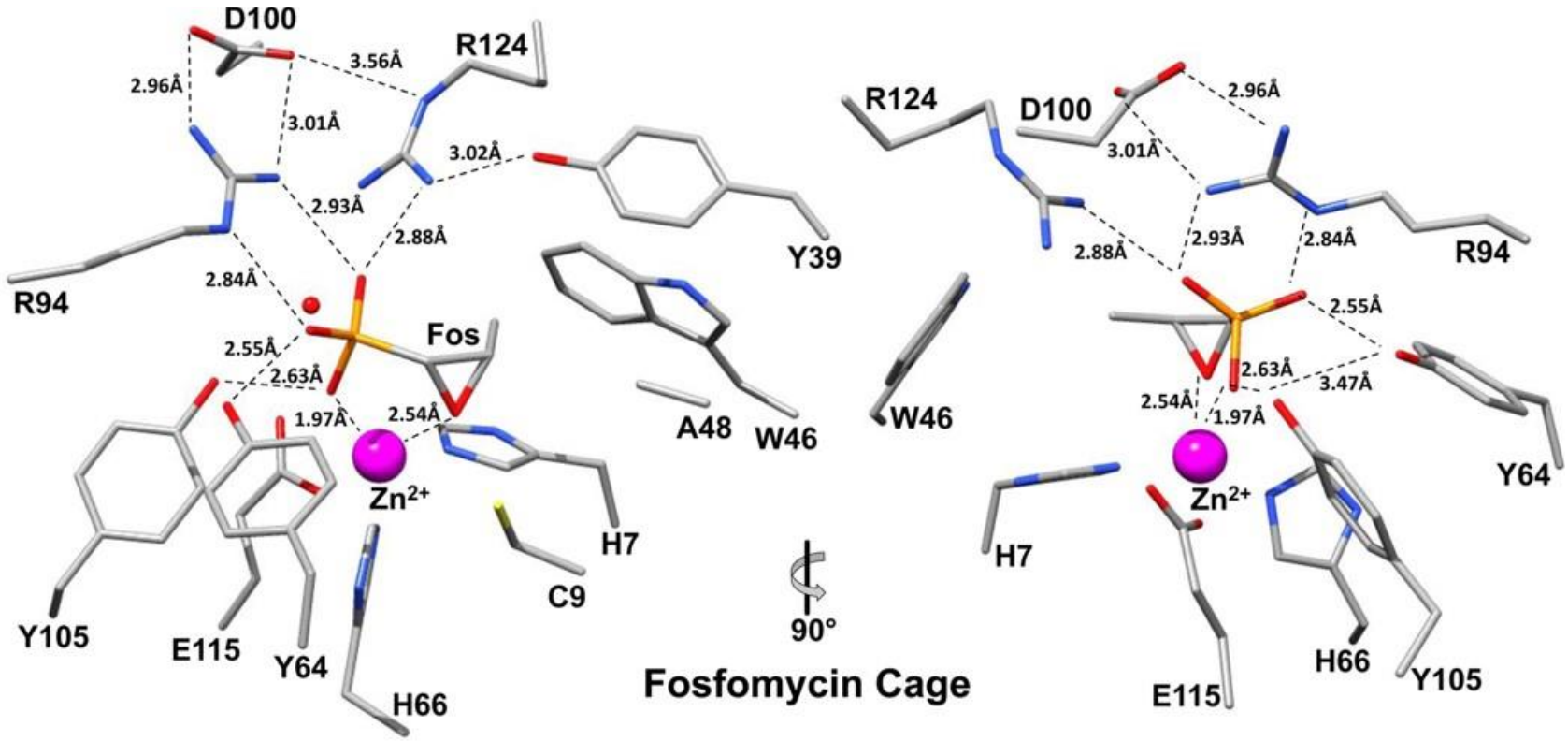

Figure 30. Fos molecule surrounded by a cage of amino acids. The cage consists of a polar and nonpolar end to accommodate Fos. The polar phosphonate group of Fos is coordinated to the metal through one of the phosphonate oxygens and hydrogen bonded to Arg94, Arg124, Tyr64, and Tyr105 through the other two. The oxirane oxygen of Fos is coordinated to the metal such that the hydrophobic methyl group of Fos is held adjacent to Trp46. These amino acids that construct the cage structure are conserved throughout the FosB enzymes.

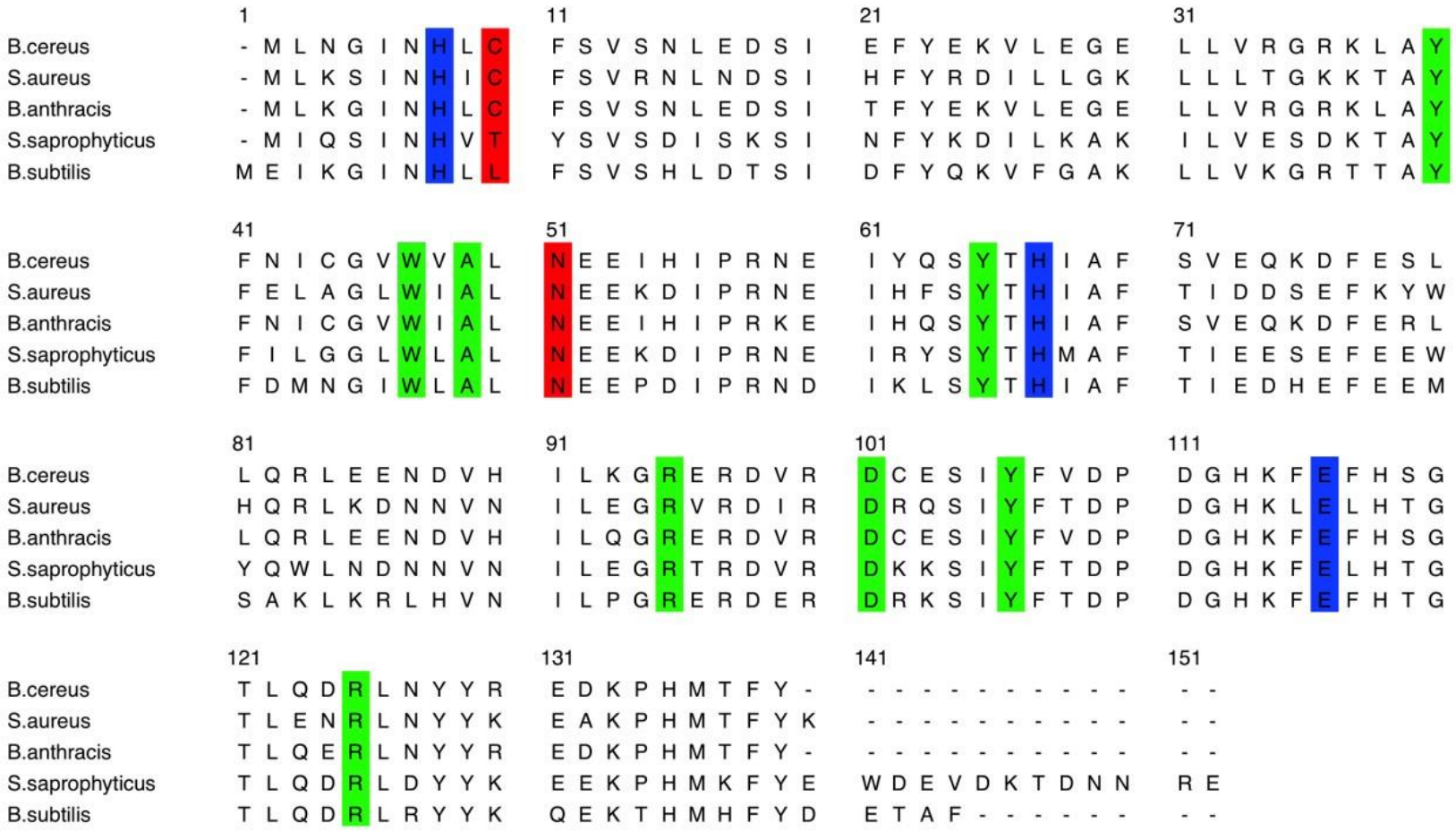

Figure 31. Sequence alignment of current FosB enzymes. Residues highlighted in blue are the metal coordinating amino acids. Residues highlighted in green for the Fos cage. Residues highlighted in red are involved in activation.

The conserved Arg94 and Asp100 residues that form the salt bridge of the loop region in FosB that encloses the Fos phosphonate group are not present in FosA. This region of the FosA enzyme is composed of amino acids that form the K^+ binding loop. This explains why K^+ is required for the optimum activation of FosA, but not for FosB.

Tyr39 is a conserved residue in both the FosA and FosB enzymes. Mutation of this residue to phenylalanine in FosA resulted in a 13-fold reduction in enzymatic turnover and a 50-fold decrease in catalytic efficiency for the thiol substrate (k_{cat}/K_M^{GSH}).[50] Tyr39 was reported to be in a favorable position to ionize GSH in FosA based upon energy-minimized docking. In the $FosB^{Bc}$•Mn^{2+}•L-cysteine-Fos (PDB 4JH7) and $FosB^{Bc}$•Zn^{2+}•Fos•L-cysteine (PDB 4JH8) structures, Tyr39 is approximately 3.31 Å from the L-cysteine sulfur, which is consistent with the docking results for GSH to FosA. Therefore, the function of Tyr39, in FosA or FosB, is likely to abstract a proton from and activate the incoming thiol during the reaction. Hydrogen bonding of Tyr39 to Arg124 would stabilize the tyrosinate anion to facilitate this function (Figure 30).

In summary, the mechanism of FosB catalyzed inactivation of Fos proceeds via direct S_N2 addition of the thiol to the oxirane carbon. This forms the same (1R,2S)-1-(S-L-cysteinyl)-2-hydroxypropylphosphonate (or (1R,2S)-1-(S-bacillithiolyl)-2-hydroxypropylphosphonate) product as that formed by FosA.[15a] Structural analysis also reveals a cage of amino acids that holds Fos in the appropriate position at the bottom of a solvent access channel for nucleophilic attack by a thiol. This indicates that FosB must bind Fos and metal prior to attack by the thiol in a binary binding mechanism. Finally, kinetic analyses reveal that FosB is indeed a Mn^{2+}-dependent BSH transferase.

CHAPTER V

INVESTIGATION OF THE STRUCTURE AND FUNCTION OF FosB FROM *Staphylococcus aureus* CONFIRMS FosB IS INHIBITED BY ZINC AT INTRACELLULAR CONCENTRATIONS AND SUGGESTS A HIGHLY CONSERVED LOOP REGION MUST CHANGE CONFORMATION UPON FOSFOMYCIN BINDING[3]

Results

Time Course Kinetic Analyses of FosB^{Bc} Inactivation of Fosfomycin

Roberts et al. reported a detailed mechanistic investigation of divalent metal activation of FosB^{Sa}.[47] The results indicated that FosB^{Sa} is activated by Zn^{2+} and has the following metal ion activation order: $Zn^{2+} > Ni^{2+} > Mn^{2+} > Mg^{2+} \sim Fe^{2+} \sim Co^{2+} \sim Cu^{2+} \sim Ca^{2+}$. However, these results contradict the metal activation of all other Fos resistance enzymes, including FosA, FosX, FosB^{Bc}, and FosB^{Bs}, in which Zn^{2+} effectively inhibits any transferase activity.[12, 15b, 17, 46, 49, 51] Therefore, we were compelled to confirm the reported results.

Our time course kinetic analyses (Figure 32) indicate that FosB^{Sa} is inhibited for L-cysteine transferase activity and only marginally active for BSH transferase activity at physiological concentration of Zn^{2+} (~100 μM) with an apparent k_{cat}^{thiol} of 0.17 s^{-1}. We also found that 10 μM Mn^{2+} activates FosB^{Sa} BSH transferase activity with an apparent k_{cat}^{thiol} of 5.98 s^{-1}. FosB^{Sa} L-cysteine transferase activity is activated by 10 μM Mn^{2+} with an apparent k_{cat}^{thiol} of 0.05 s^{-1}. These

[3] Reprinted with permission from Thompson, M. K., Mary. E.; Goodman, Michael C.; Hammer, Neal D.; Cook, Paul D.; Jagessar, Kevin L.; Harp, Joel; Skaar, Eric P; Armstrong, Richard N. (2014) Structure and Function of the Genomically Encoded Fosfomycin Resistance Enzyme, FosB, from Staphylococcus aureus, *Biochemistry 53*, 755-765. Copyright 2014 American Chemical Society.

results indicate that FosB has a preference for BSH over L-cysteine and are also consistent with reports of metal activation for all other Fos resistance enzymes, including FosA, FosX, $FosB^{Bc}$, and $FosB^{Bs}$. Finally, we found that 100 µM Zn^{2+} inhibits the reaction even when it is supplemented with 10 µM Mn^{2+} for both L-cysteine and BSH transferase activity. The apparent k_{cat}^{thiol} for this BSH transferase activity is 0.08 s^{-1}, but it could not be determined for L-cysteine transferase activity, which is similar to inhibition by Zn^{2+} alone.

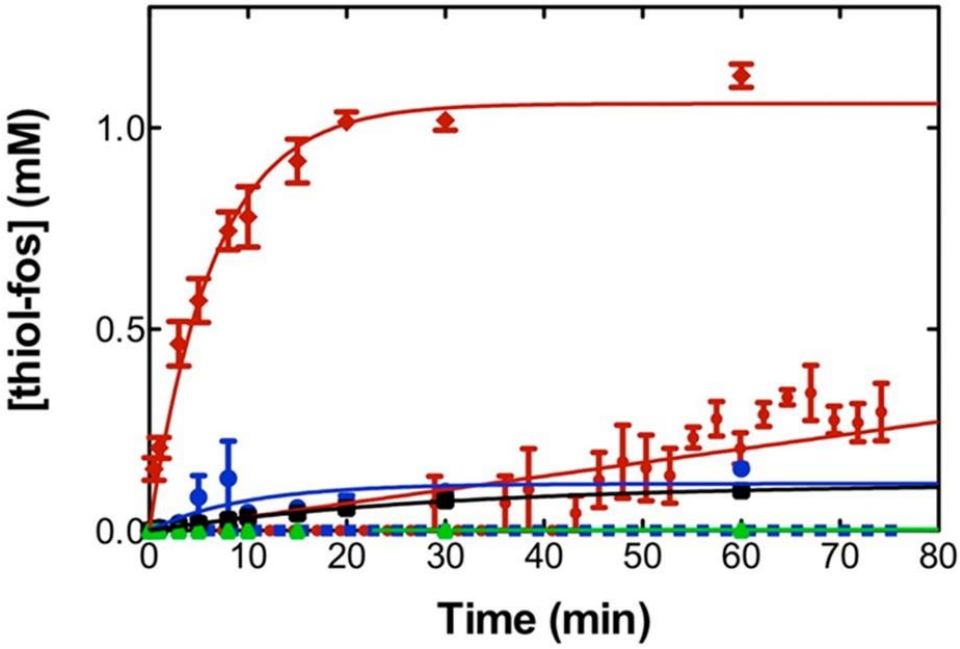

Figure 32. Time course kinetic analysis of $FosB^{Sa}$ catalyzed addition of BSH or L-cysteine to Fos in the presence of Mn^{2+} and/or Zn^{2+}. Reactions were carried out at 25˚ C in 20 mM HEPES, pH 7.0 with 4 mM fosfomycin and 0.50 µM enzyme in the presence of (◆) 1.6 mM BSH and 10 µM Mn^{2+}, (●)1.6 mM BSH and 100 µM Zn^{2+}, (●) 1.6 mM BSH, 10 µM Mn^{2+}, and 100 µM Zn^{2+}, (■) 1.8 mM L-cysteine and 10 µM Mn^{2+} (■) 1.8 mM L-cysteine and 100 µM Zn^{2+}, or (▲) 1.8 mM L-cysteine 10 µM Mn^{2+}, and 100 µM Zn^{2+}.

Disk Diffusion Assays

Kinetic analyses have demonstrated that FosB enzymes prefer BSH over L-cysteine as the thiol substrate for the nucleophilic inactivation of Fos *in vitro*. The detoxification pathway for detoxification of xenobiotics, such as Fos, involving BSH has previously been characterized for *S. aureus in vivo*.[21] BSH null *S. aureus* exhibits an increase in Fos sensitivity for both the Newman and USA300 JE2 strains, but the question of whether FosB null *S. aureus* exhibits a similar increase in sensitivity to Fos remained.[20] In collaboration with Dr. Neal Hammer in the Skaar lab we made an effort to answer this. The Skaar lab conducted Kirby-Bauer disk diffusion assays to test for Fos sensitivity in BSH null and FosB null strains of both Newman and USA300 JE2 *S. aureus*, which were obtained from the Network on Antimicrobial Resistance in *S. aureus*. As anticipated, both of the null strains of USA300 JE2 and Newman show a substantial increase in their sensitivity to Fos as seen by the increased zone of clearing (Figure 33). Furthermore, the zone of clearing for the BshA null mutant is comparable to that of the FosB null mutant (Table 5). This indicates that both BSH and the FosB enzyme are required for optimal survival of *S. aureus* when it is treated with Fos.

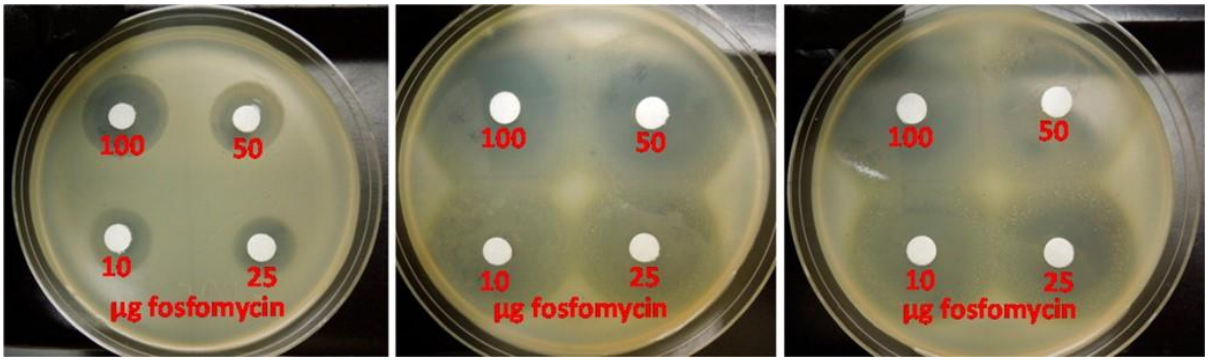

Figure 33. Fos disk diffusion assays for USA300 JE2 (MRSA). The amount of Fos on each disk is shown in red: (left) wild-type MRSA, (center) BshA knockout MRSA, (right) FosB knockout MRSA.

Table 7. Disk diffusion zones of clearing (mm) for MRSA.

Strain	10 µg	25 µg	50 µg	100 µg
WT USA300 JE2	17	18	21	24
BshA KO	34	33	40	40
FosB KO	35	33	37	40
WT Newman	22	24	28	30
BshA KO	35	37	40	40
FosB KO	34	34	39	37

Crystal Structure Determination of FosB^{Sa}

Five high resolution crystal structures of FosB^{Sa} in complex with various combinations of divalent metals and substrates were determined. The crystal structure of FosB^{Sa}•Zn^{2+}•SO_4^{2-} (PDB 4NAY) was refined to 1.42 Å resolutions (Figure 36). An X-ray fluorescence scan of the crystal prior to diffraction data collection confirmed the presence of Zn^{2+} (Figure 34). The diffraction data were collected at the K_α absorption edge of Zn^{2+}, which is a wavelength of 1.28 Å. The initial phases were determined using Zn^{2+} SAD phasing and the final model consists of amino acids 1-91 and 102-138 with a sulfate ion coordinated to the metal. A second crystal of FosB^{Sa}•Zn^{2+}•SO_4^{2-} was used to collect another data set at a wavelength of 1.078 Å to achieve higher resolution. The second data set, determined by molecular replacement using PDB 4NAY, resulted in a 1.15 Å resolution structure of FosB^{Sa} with Zn^{2+} and sulfate in the active site (PDB 4NAZ – Figure 36). The final model also consisted of amino acids 1-91 and 102-139 with a sulfate ion coordinated to the metal.

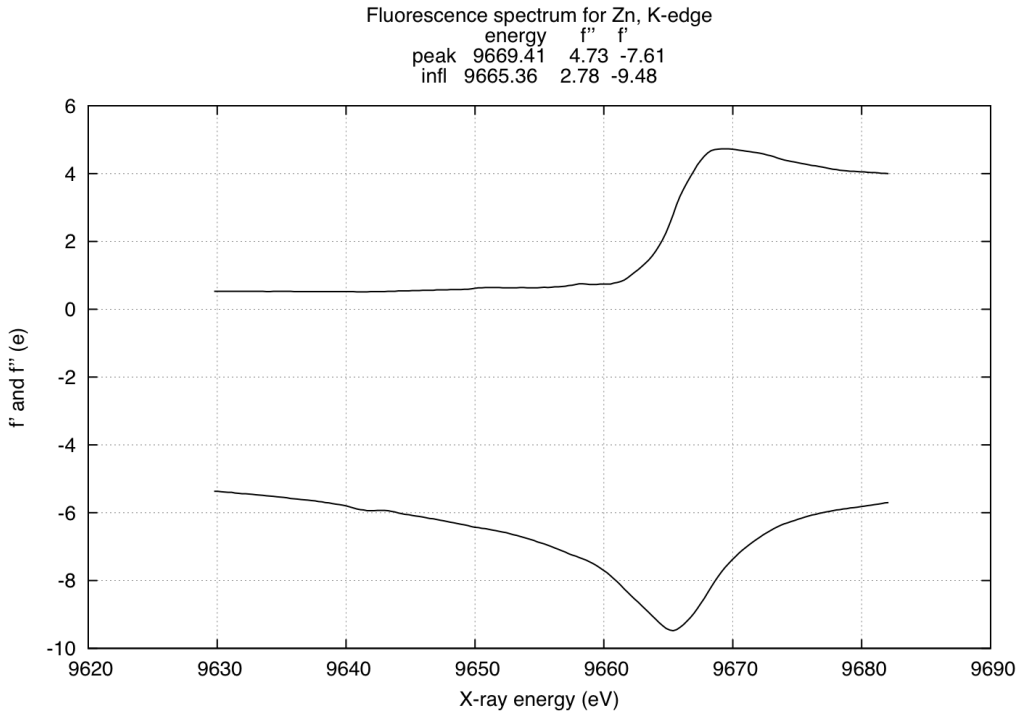

Figure 34. X-ray fluorescence spectrum of the FosB^{Sa}•Zn^{2+}•sulfate crystals.

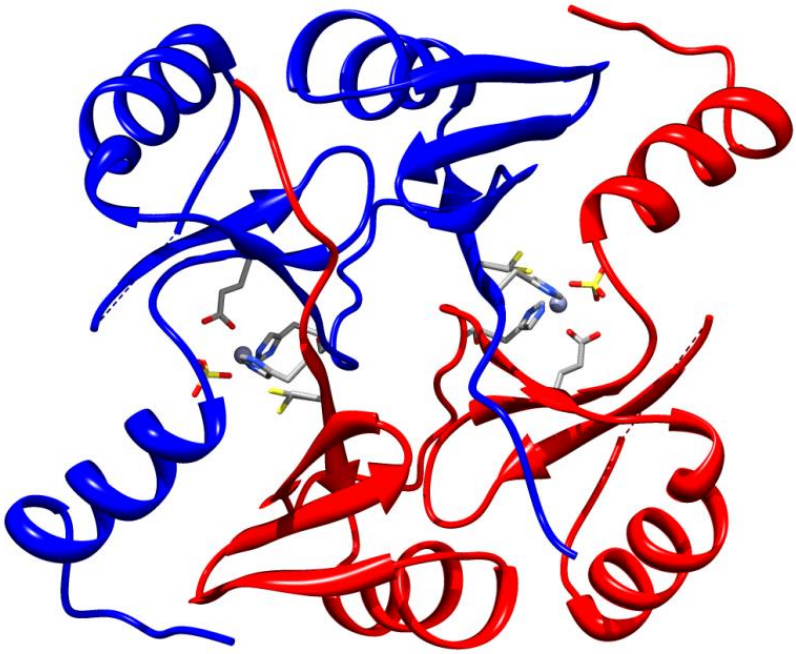

Figure 35. Overall X-ray crystal structure of FosB^{Sa}•Zn^{2+}•sulfate at 1.15 Å resolution (PDB 4NAZ). The structure was solved by molecular replacement using PDB 4NAY. R_{work} = 13.44% and R_{free} = 16.22%.

Co-crystallization of FosB^{Sa} with either BSH or L-cysteine resulted in two structures with a disulfide bond at the Cys9 residue of FosB^{Sa}. These structures were determined by molecular replacement using a homodimer model of the enzyme created from PDB 4NAZ. The structure with a BS-Cys9 disulfide bond was refined to a final resolution of 1.62 Å and the final model consists of amino acids 1-53, 62-91, 102-128, and 133-138 for subunit A and 1-53, 63-129, and 135-138 for subunit B. The structure with an L-cys-Cys9 disulfide bond was refined to a final resolution of 1.62 Å and the final model consists of amino acids 1-52, 61-92, 102-127, and 131-139 for subunit A and 1-53, 64-128, and 134-138 for subunit B.

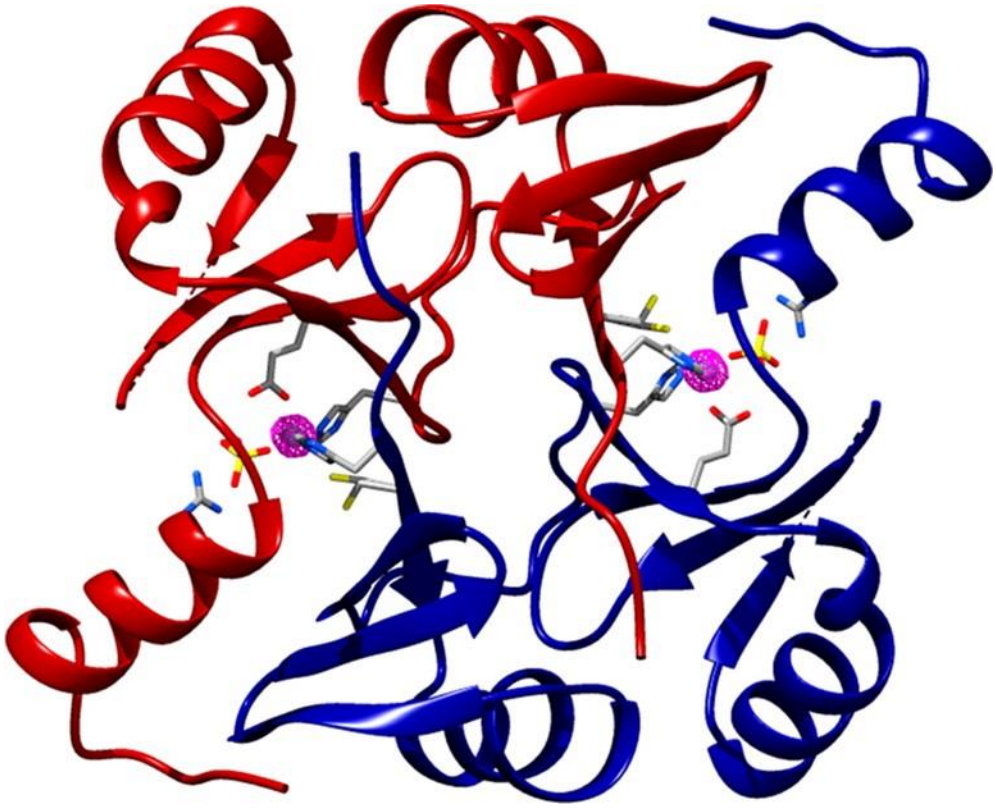

Figure 36. Overall crystal structure of FosB^{Sa} with Zn^{2+} and sulfate in the active site at 1.42 Å. The red and blue color scheme indicates each subunit of the homodimer of the enzyme. The anomalous density map (magenta) around the Zn^{2+} metal ions (purple) is contoured to 5σ and marks the location of the metal within the structure. R_{work} is 12.95% and $\underline{R_{free}}$ is 16.64%.

Co-crystallization of FosB^{Sa} with L-cysteine and TCEP reduced the exogenous disulfide bond and produced an apo structure of the enzyme. The final structure was determined by molecular replacement to a final resolution of 1.62 Å. The final model consists of amino acids 1-56, 62-91, 102-126, and 132-138 for subunit A and 1-53, 63-128, and 135-138 for subunit B.

Structural Characterization of FosB^{Sa}

Similar to the FosB^{Bc} and FosB^{Ba} enzymes, FosB^{Sa} belongs to the VOC superfamily.[51] Although amino acids 92-101 are not observed in PDBs 4NAY or 4NAZ and are observed in only one subunit of PDBs 4NB0, 4NB1, and 4 NB2, the 3D domain-swapped arrangement of sequential βαββββ motifs that define the VOC superfamily is still evident in the overall structure (Figure 36).[3] His7, His66, and Glu115 constitute the metal binding site in FosB^{Sa}, which are the same as those in FosB^{Bc}.[51] In the FosB^{Sa}•Zn^{2+}•SO_4^{2-} structures, the Zn^{2+} is in a tetrahedral coordination geometry with a sulfate oxygen occupying the fourth coordination site of the metal. However, this sulfate molecule is oriented in a position opposite to that observed in FosB^{Bc}, with the second sulfate

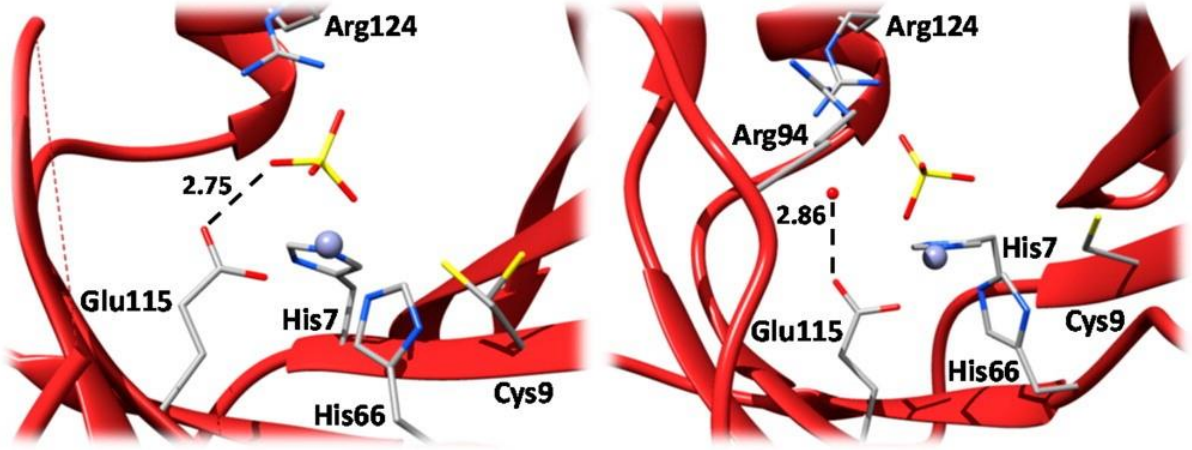

Figure 37. The sulfate molecule of FosB^{Sa} (left) is oriented in a position opposite that observed in FosB^{Bc} (right). In FosB^{Sa}, the second sulfate oxygen is hydrogen bonded to the non-metal-coordinated O_ε atom of Glu115, but in FosBBc this is bonded to a highly conserved water molecule.

oxygen hydrogen bonded to the non-metal-coordinated O_ε atom of Glu115 (Figure 37 left).[51] In $FosB^{Bc}$ (PDB 4JH2), the sulfate is oriented in a position that superimposes the phosphonate moiety of Fos and the non-metal-coordinated O_ε atom of Glu115 is hydrogen bonded to a highly conserved water molecule (Figure 37 right).

In the structures of $FosB^{Sa}$ with BS-Cys9 or L-cys-Cys9 disulfide bonds and the apo structure (PDBs 4NB0, 4NB1, and 4NB2 respectively), amino acids ~90-101 are observed in a conformation different from that found in either $FosB^{Bc}$ or $FosB^{Ba}$ (Figure 38 left). The two different conformations are best described as open, for $FosB^{Sa}$, and closed for both $FosB^{Bc}$ and $FosB^{Ba}$. The difference between the open and closed conformations is the absence and presence of Fos, respectively. In the $FosB^{Sa}$ structure, the open loop region is wrapped around a sulfate molecule (Figure 38 left).

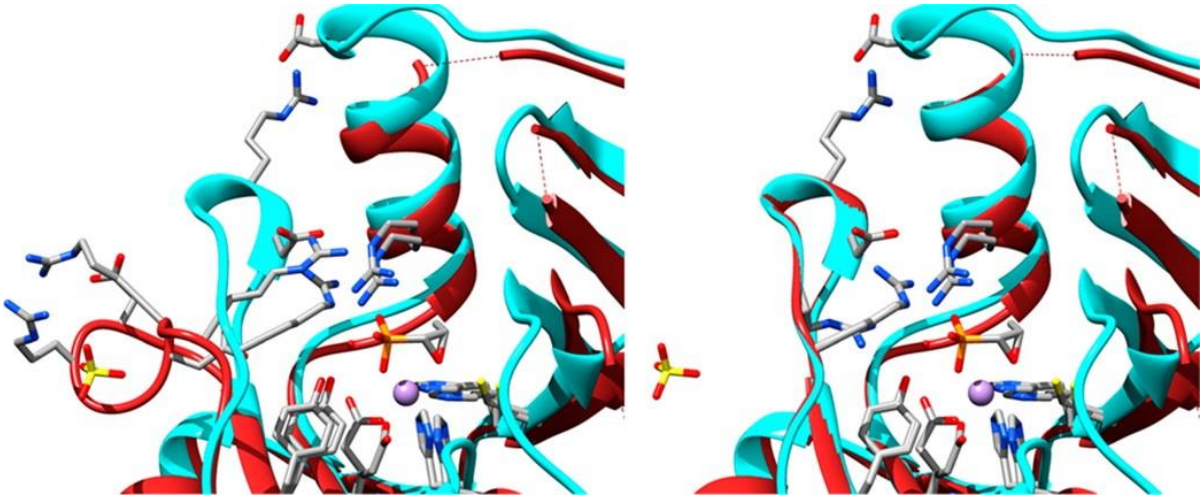

Figure 38. Superposition of $FosB^{Bc}$ (cyan) and $FosB^{Sa}$ (red) (left). In the $FosB^{Bc}$ structure (PDB 4JH6), Mn^{2+} and Fos are bound in the active site and the conserved phosphonate binding loop is observed in the closed conformation. In the $FosB^{Sa}$ structure (PDB 4NB2), there is no metal or Fos bound in the active site and the phosphonate binding loop is observed in the open conformation. Superposition of $FosB^{Bc}$ and $FosB^{Sa}$ with the phosphonate binding loop morphed into the closed conformation (right). The conserved Fos cage residues align after the $FosB^{Sa}$ structure has been morphed into the $FosB^{Bc}$ structure.

Of the approximately 11 residues that compose the loop region, eight are conserved throughout all FosB enzymes (Figure 39). The three nonconserved residues are solvent-exposed in the closed conformation of the loop in $FosB^{Bc}$ (PDB 4JH6) and $FosB^{Ba}$ (PDB 4IR0). The conserved residues of the loop constitute important structural features of FosB. In the closed conformation, they form one side of the Fos binding cage with several hydrogen bonding interactions to the antibiotic. They also form one side of the BSH binding pocket. Additionally, the open residues of $FosB^{Sa}$ can be morphed into the positions of Fos-bound $FosB^{Bc}$ to completely form the important substrate binding structural features (Figure 38 right).

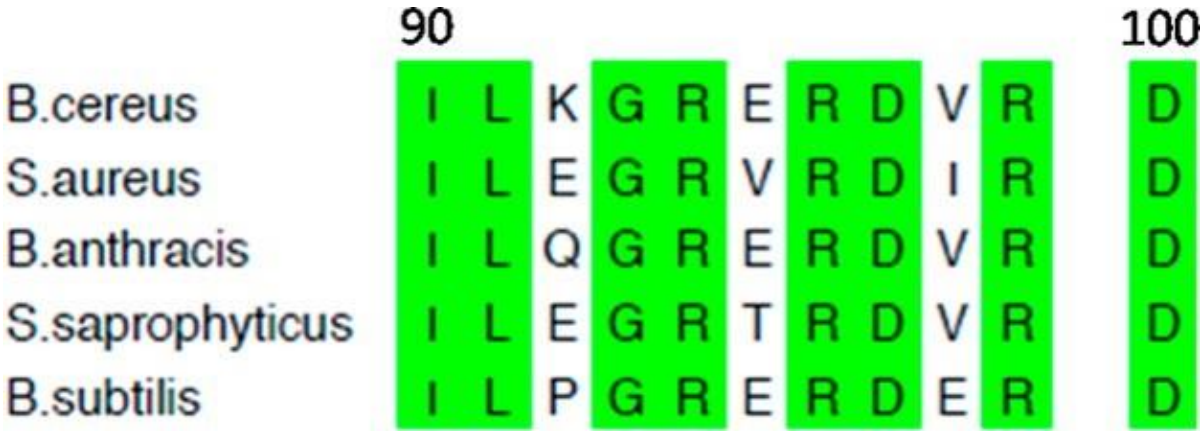

Figure 39. Sequence alignment of the phosphonate binding loop residues. Eight of the eleven residues are conserved throughout the FosB enzymes and the non-conserved residues are all solvent exposed.

Structural dynamic studies of $FosB^{Sa}$ via HDX-MS

Based on the structures determined for $FosB^{Sa}$, $FosB^{Bc}$, and $FosB^{Ba}$, the phosphonate binding loop region appears to move from an open conformation to a closed conformation upon binding Fos. Additionally, we have been unsuccessful in determining a structure of FosB with the entire molecule of BSH present in the active site. In an effort to confirm the possible dynamic

loop movement and the location of BSH binding, HDX-MS analysis was completed. HDX-MS data was collected for $FosB^{Sa}$ in the following states: (1) bound to Mn^{2+}, (2) bound to Mn^{2+} and Fos, and (3) bound to Mn^{2+}, Fos, and BSH.

Prior to collecting HDX-MS data, a peptide map of $FosB^{Sa}$ digested with the acidic protease XVIII was determined using LC-MS/MS analysis. The peptide mapping method was optimized to achieve 97% coverage of the protein (Figure 40) by testing various quench times ranging from 3 to 7 minutes. The coverage map also included multiple peptides for most areas of the protein. This includes the phosphonate loop region, which is 100% covered by 6 different peptides. Based on this peptide map, HDX-MS data was collected for $FosB^{Sa}$ digested by the protease XVIII.

The HDX-MS results of $FosB^{Sa}$ in complex with Mn^{2+}, Mn^{2+} and Fos, or Mn^{2+}, Fos, and BSH showed overall low deuterium incorporation (Figure 41). For the majority of the peptides analyzed, deuterium incorporation remained below 50%. There were also no significant changes in the rate of incorporation between the three various enzyme complex states tested. This indicates that the overall structure of $FosB^{Sa}$ is relatively stable with little overall dynamic movement.

Surprisingly, the signals for all six peptides covering the phosphonate binding loop region were completely lost when collecting HDX-MS data. The exact cause of this loss of signal is unknown. However, it is possible that the flexible regions of the protein could be more readily digested by the protease. This would lead to lower amounts of these particular peptides for analysis. Due to time constraints of the HDX-MS method, it is standard procedure to shorten the gradient used to separate peptides by 50% compared to the gradient utilized for separation during peptide mapping. Taken together, this could explain the loss of signal for the phosphonate binding loop region.

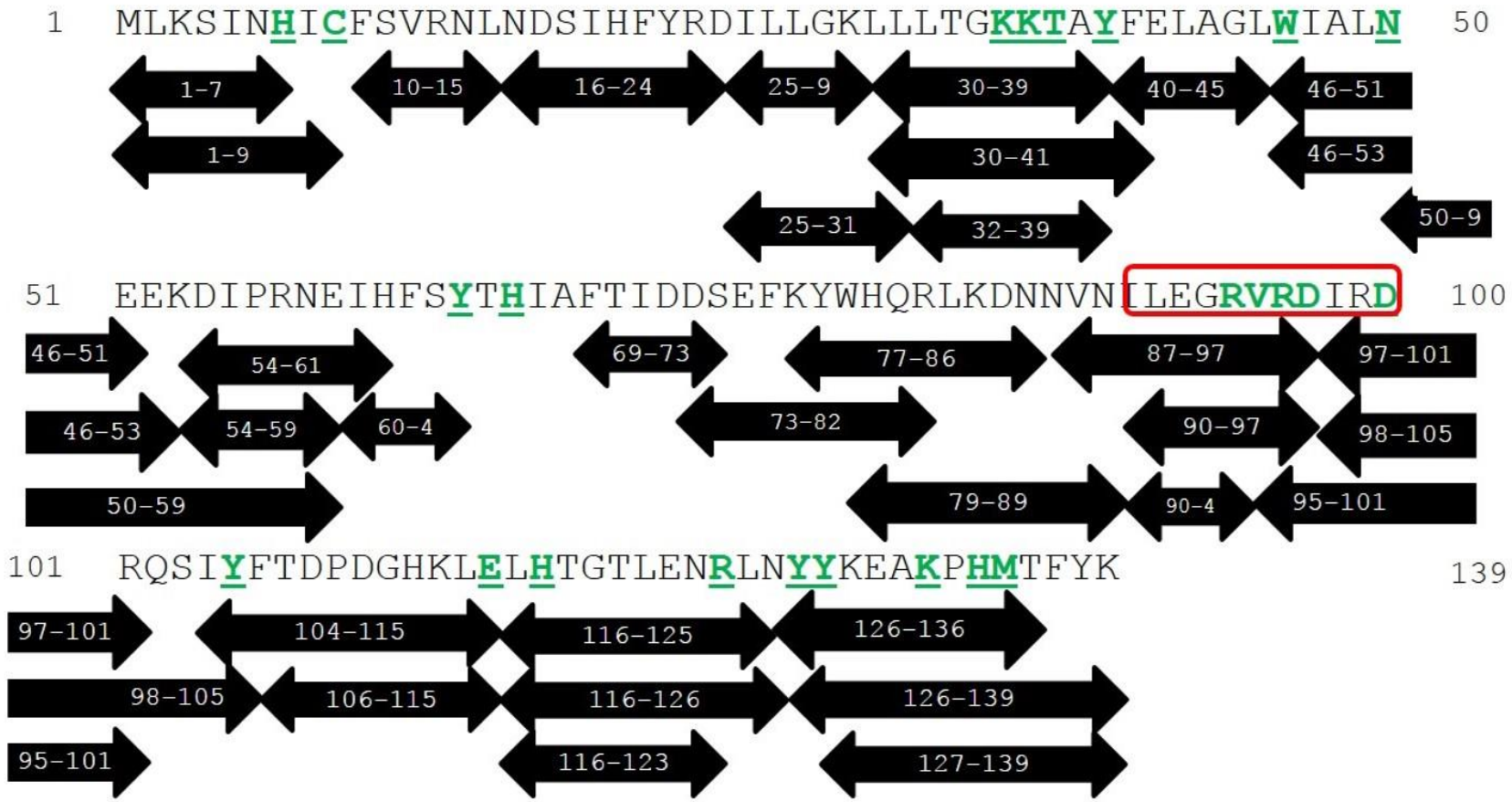

Figure 40. Peptide map of FosB^{Sa}. Peptide mapping of FosB^{Sa} digested with XVIII was optimized to achieve 97% coverage of the protein. The phosphonate binding loop region (boxed in red) was 100% identified by 6 different peptides. Additionally, amino acid residues that help form the BSH binding cavity (shown as green underlined font) are also well covered by multiple peptides.

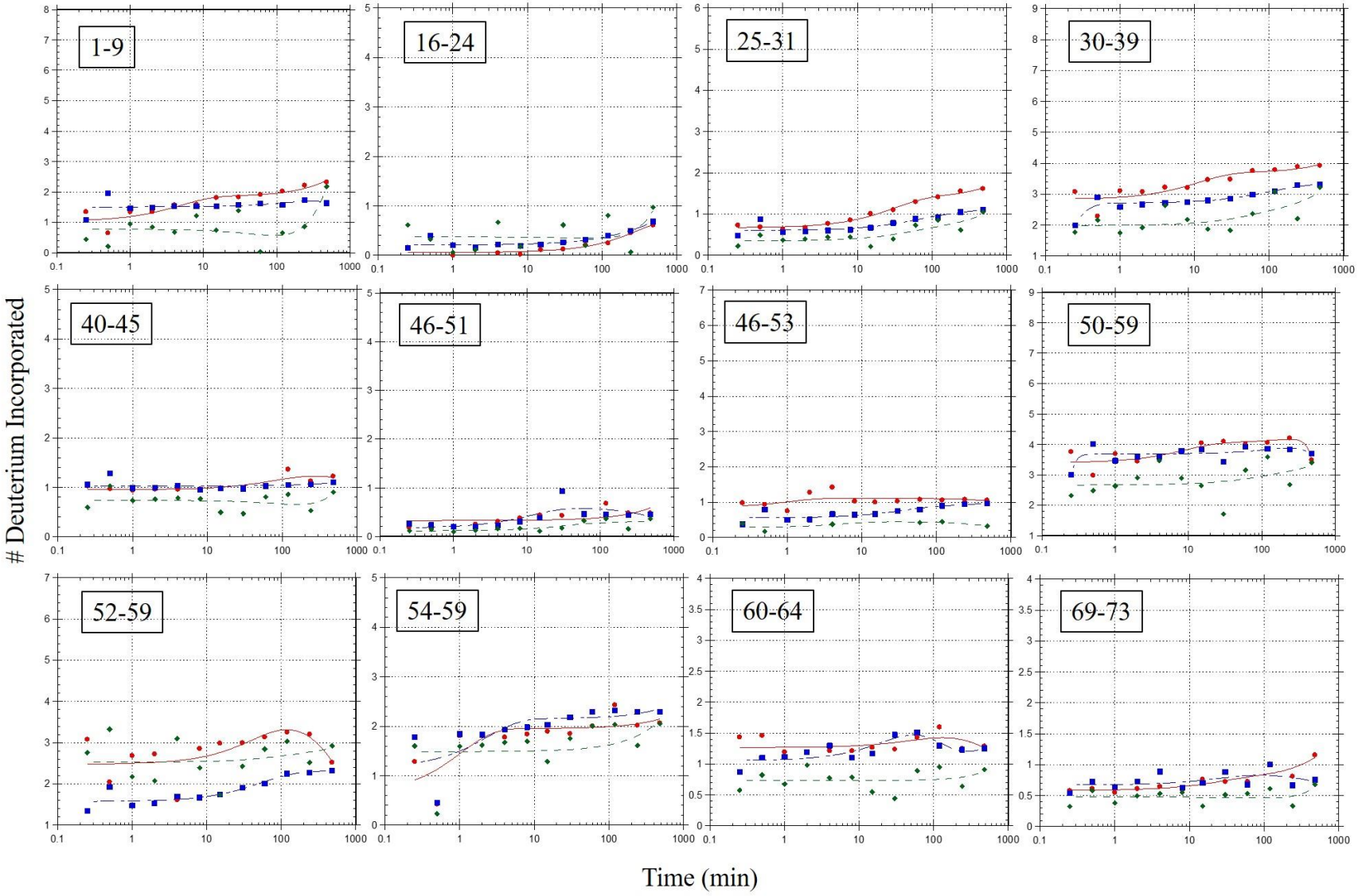

Figure 41. HDX kinetic profiles of representative peptides for the overall structure of $FosB^{Sa}$. Shown are the average kinetic profiles for the deuterium incorporation as a function of time for $FosB^{Sa}$ complexed with either (●) Mn^{2+}, (■) Mn^{2+} and Fos, or (◆) Mn^{2+}, Fos, and BSH. The amino acid residues for each peptide is displayed in the upper left corner of each graph and the number of exchangeable amide protons for each peptide is displayed as the y-max value for each graph.

Discussion

The crystal structures of $FosB^{Sa}$ all contain the 3D domain-swapped arrangement of sequential βαββββ motifs that define the VOC superfamily (Figure 36). Thus, confirming $FosB^{Sa}$ is a member of the VOC superfamily similar to the previously described Fos resistance enzymes. We were also able to crystallize $FosB^{Sa}$ with Zn^{2+} in the active site of the enzyme, similar to our structures of $FosB^{Bc}$, which allowed us to use the metal for SAD phasing of the data.[51] The anomalous scattering density map in Figure 36 establishes the location of the metal within the $FosB^{Sa}$ active site.

The kinetic analyses of $FosB^{Sa}$ reported by Roberts et al. indicated that the enzyme is activated by Zn^{2+} and has the following divalent metal ion activation order: $Zn^{2+} > Ni^{2+} > Mn^{2+} > Mg^{2+} \sim Fe^{2+} \sim Co^{2+} \sim Cu^{2+} \sim Ca^{2+}$.[47] However, the other Fos resistance enzymes, such as FosA, FosX, $FosB^{Bc}$, and $FosB^{Bs}$, are inhibited by Zn^{2+}.[12, 15b, 17, 46, 49, 51] Additionally, several structures of $FosB^{Sa}$ and $FosB^{Bc}$ with Zn^{2+} in the active site were determined. Therefore, we completed time course kinetic analyses to reassess the divalent metal activation and/or inactivation of $FosB^{Sa}$.

While we did not complete full kinetic analyses, we found that $FosB^{Sa}$ is inhibited by Zn^{2+}, which is as we expected given the activation of the other Fos resistance enzymes. $FosB^{Sa}$ is completely inhibited by Zn^{2+} for L-cysteine transferase activity and only marginally active for BSH transferase activity at physiological concentrations of Zn^{2+} (Figure 30). The apparent k_{cat}^{thiol} for Zn^{2+}-dependent BSH transferase activity is 0.17 s^{-1}. By comparison the apparent k_{cat}^{thiol} for Mn^{2+}-dependent BSH transferase activity is 5.98 s^{-1}, which is a > 35-fold increase (Figure 32). Most interestingly, our assays completed at physiological concentrations of both Zn^{2+} and Mn^{2+} demonstrate that $FosB^{Sa}$ is inhibited for either L-cysteine or BSH transferase activity, similar to Zn^{2+} alone.

These results contradict the published result for $FosB^{Sa}$, but are consistent with all other reports for this class of enzymes. The study published by Roberts et al. used concentrations of Zn^{2+} as high as 10 mM in their activation studies, which is physiologically irrelevant.[47] Additionally, an explanation for why this class of enzyme is activated by Mn^{2+} and inhibited by Zn^{2+} has been presented. Lastly, the active site residues for each class of Fos resistance enzymes are conserved. Therefore, we believe that inhibition of $FosB^{Sa}$ by physiological concentrations of Zn^{2+} is correct.

Roberts et al. demonstrated that increasing concentrations of BSH appeared to inhibit activation of $FosB^{Sa}$ by Zn^{2+} until the concentration of Zn^{2+} had eclipsed that of BSH.[47] From their results, they determined that $FosB^{Sa}$ and BSH were competing for complexation with Zn^{2+} and that BSH is therefore a sufficiently strong Zn^{2+} chelator to demetalate the enzyme. While BSH has been suggested to be a M^{2+} chelator based on the nature of its functional substituents, our crystal of $FosB^{Sa}$ with disulfide bonds in the active site suggest an alternate explanation.[19]

The crystallization conditions (100 mM Bis-Tris, pH 6.5; 5 mM Fos; and 5 mM BSH or 100 mM HEPES, pH 7.5; 10 mM Fos; 10 mM L-cysteine) are similar to the kinetic assay conditions used by Roberts et al. (50 mM HEPES, pH 7.0; 25 mM Fos; 0.5-5 mM BSH). Also, the change in the crystallographic space group from C2 to P1 indicates that the disulfide bond formed in solution prior to crystal formation. Therefore, inhibition of $FosB^{Sa}$ by millimolar concentrations of exogenous thiol may actually be due to the formation of the thiol-Cys9 disulfide bond and steric removal of the metal rather than demetalation of the enzyme but the substrate.

Even if BSH were in a strong complex with Zn^{2+}, the thiol would be one of the coordinating ligands, which would mean it would not be able to serve as a nucleophilic substrate for Fos inactivation by FosB. Our kinetic analyses with Zn^{2+} and Mn^{2+} were designed so that even if all

of the Zn^{2+} (100 μM) was in complex with BSH, there is still excess free BSH (1.8 mM) in solution to serve as the nucleophilic substrate for $FosB^{Sa}$ activated by Mn^{2+} (10 μM). Since the reaction does not proceed, we conclude that (1) either Zn^{2+} and Mn^{2+} are in complex with BSH and there is no free metal to activate the enzyme or (2) Zn^{2+} is competing with Mn^{2+} in the active site of $FosB^{Sa}$ and inhibiting the enzyme. Only the second conclusion is plausible because $FosB^{Sa}$ is highly active in the presence of Mn^{2+} and BSH only.

While $FosB^{Bc}$ and $FosB^{Ba}$ were both crystallized with Fos coordinated to the metal, we have been unsuccessful in obtaining a Fos-coordinated structure of $FosB^{Sa}$ even though the antibiotic was present in the crystallization solution at a concentration of 5 mM. This is likely due to the crystallization conditions requiring high concentrations of ammonium sulfate (200 mM), which competes with Fos for binding in the active site of $FosB^{Sa}$. Sulfate is isoelectronic with the phosphonate moiety of Fos and has been observed in the active sites of the classes of Fos resistance enzymes.

A comparison of our apo $FosB^{Sa}$ structure with a Fos and metal coordinated structure of $FosB^{Bc}$ or $FosB^{Ba}$ revealed an interesting loop feature of the FosB enzymes that is composed of amino acids 90-100. In the $FosB^{Bc}$ or $FosB^{Ba}$ structures, the loop is observed in a conformation that encloses the phosphonate end of the polar Fos molecule and represents one side of the Fos cage structure of the enzyme.[51] The cage is composed of residues Tyr39, Trp46, Ala48, Tyr64, Arg94, Asp100, Tyr105, and Arg124, which are all conserved (Figure 30) and is the structural feature that locks the antibiotic in the active site. Fos is held in the proper position with the carbon-1 poised for nucleophilic attack by L-cysteine or BSH. In $FosB^{Sa}$, there is a lack of complete electron density for the region in PDBs 4NAY or 4NAZ, suggesting a high degree of flexibility. In addition, the electron density is observed in PDBs 4NB0, 4NB1, and 4NB2, but the loop is in a

conformation best described as open relative to the $FosB^{Bc}$ or $FosB^{Ba}$ structures (Figure 38). In this open structure, the residues of the loop are wrapped around a sulfate molecule forming five hydrogen bond interactions and demonstrating the propensity of the loop to coordinate sulfate or the possibly the isoelectronic phosphonate end of Fos.

In both the $FosB^{Bc}$ and $FosB^{Ba}$ structures, a narrow access channel leading to carbon-1 of Fos is observed. A cross-sectional area analysis of the access channel at its most narrow point in $FosB^{Bc}$ revealed that it is approximately 15 $Å^2$ (Figure 42). The cross-sectional area of the phosphonate end of Fos is 19 $Å^2$ (Figure 43). This narrow channel is optimized to accommodate the L-cysteinyl domain of BSH and contains several conserved residues involved in the catalytic mechanism of the FosB enzymes. This raises the question of how Fos enters the active site of FosB and we think the opening and closing of the loop region is the answer.

The loop must be open to allow Fos to enter the active site of FosB. The hydrophobic methyl end of Fos would thermodynamically favor the hydrophobic side of the Fos cage in the enzyme. Once bound, the loop would close around the antibiotic holding it in place directly at the end of the access channel poised for nucleophilic attack by the thiol. Loop closure could incorporate the unexplained water molecule, and a combination of hydrogen bonds to the water and to Fos would hold the loop in the closed position forming the final side of the BSH binding pocket (Figure 28 – Chapter IV). This is consistent with the substrate binding studies of FosB, which indicate that Fos must bind first followed by nucleophilic attack of the thiol cosubstrate.[47]

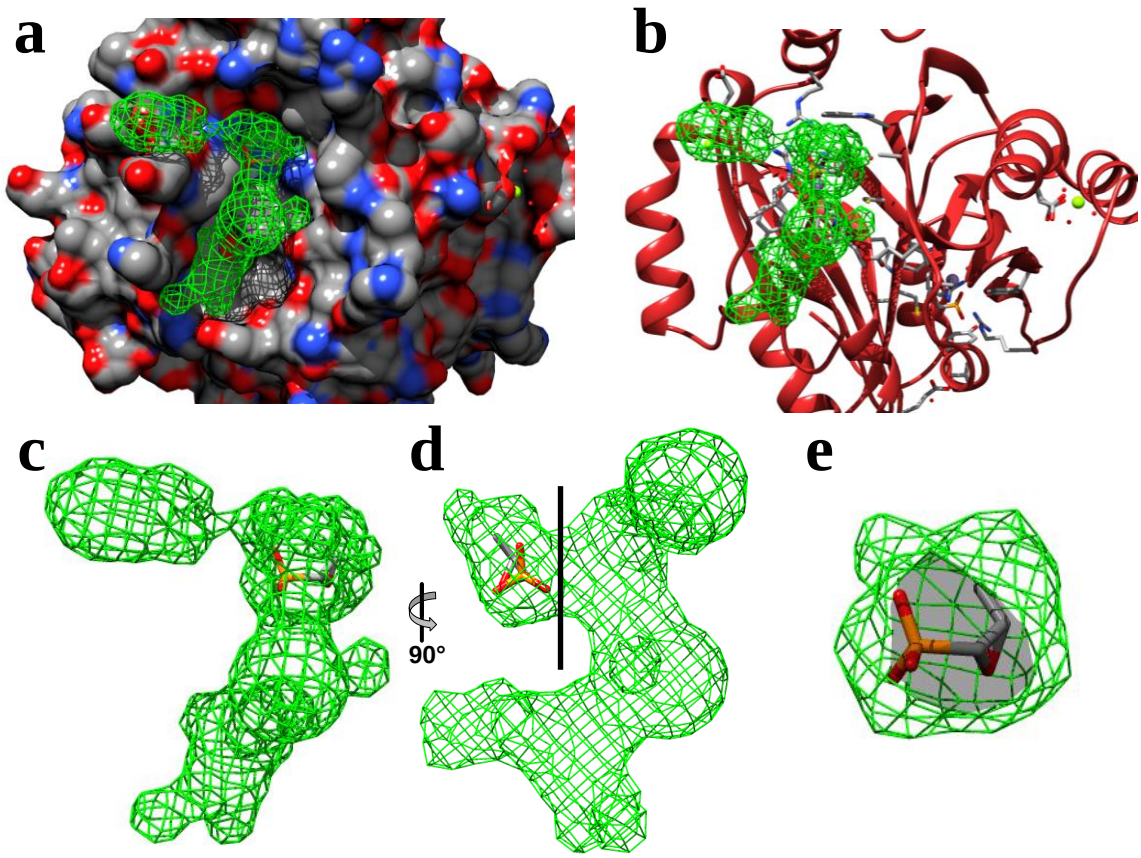

Figure 42. The cross-sectional area of the access channel in FosB^{Bc} at its most narrow point is less than 15 Å^2. The cavity where Fos binds was created using the Surfnet feature of Chimera after removing Fos from the coordinate file (PDB 4JH7). (a) The cavity is shown in the surface model of FosB^{Bc}. The default cutoff distances of the Surfnet feature have connected several nearby cavities and thus resulted in the large cavity structure shown. Fos has been added back to the coordinate file. (b) The cavity is shown in a ribbon model of FosB^{Bc}. (c) The cavity shown alone with Fos. (d) The cavity rotated 90° to the right from c. The black line approximates the clipping plane used to create e. (e) The measured cross-sectional area of the clipped surface varies depending on the angle of the cavity to the clipping plane but is always less than 15 Å^2.

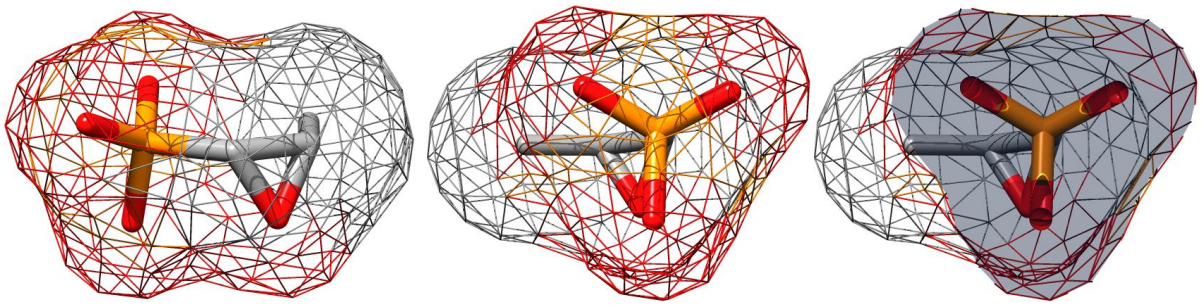

Figure 43. The cross-sectional area of the phosphonate end of Fos is 19 $Å^2$. The surface of Fos was generated using chimera (**Left**). The Fos molecule was oriented (**Center**) such that a clipping plane could be created through the three phosphonate oxygens (**Right**). The cross-sectional area of the clipping plane is 19 $Å^2$.

In order to investigate the dynamic movement of the loop region, HDX-MS analyses of $FosB^{Sa}$ in complex with Mn^{2+}, Mn^{2+} and Fos, or Mn^{2+}, Fos, and BSH were completed. While initial peptide mapping achieved 97% coverage of $FosB^{Sa}$ with multiple peptides covering the loop region, the signals for all of the peptides covering the loop region were lost during HDX-MS analyses. Therefore, we were unable to utilize this method to confirm the dynamic movement of the loop region. However, the results (Figure 41) did indicate that the rest of the structure is relatively stable with little dynamic movement, which was expected based on the multiple crystal structures we have determined. Further investigation of the dynamics of the phosphonate binding loop region are needed to confirm the movement of the loop from open to closed upon binding Fos.

Finally, we completed *in vivo* studies of $FosB^{Sa}$, in collaboration with Dr. Eric Skaar's lab, to further understand the requirements of the enzyme for survival of the pathogen in general. BSH null strains of *B. subtilis* and *S. aureus* have been previously examined for Fos sensitivity. The results demonstrate that BSH is necessary for detoxification of xenobiotics from Gram-positive

organisms and that BSH is required for resistance of the organisms to Fos. Our disk diffusion assays show that FosB knockout *S. aureus* USA300 JE2 and Newman strains demonstrate and increase in Fos sensitivity similar to that of the BSH null cells.

In order to allow for direct comparison of the FosB knockout cells to BSH null cells, we included BshA knockout strains in our studies. The zone of clearing for BSH null USA300 JE2 null cells treated with 100 µg Fos is 40 mm, which is consistent with the published values of 39, 40, and 39 mm for BshA, BshB, and BshC knockouts, respectively, of USA300 JE2 treated with 350 µg Fos. While the published results use an amount of Fos three times greater than ours, we achieved a maximal zone of clearing between 25 to 50 µg Fos and the zone of clearing at 50 µg is the same as that for 100 and 350 µg. Therefore, it appears there is a maximal effectiveness of Fos reached for disk diffusion assays somewhere between 25 and 50 µg of Fos.

Since the zone of clearing for FosB null strains are the same as those for BSH null strains, we conclude that both BSH and the FosB enzymes are equally important for the resistance of MRSA to Fos, which validates FosB as a potential therapeutic drug target. Additionally, the fact that both FosB and BSH null strains of *S. aureus* Newman and USA300 JE2 have an equally increased sensitivity to Fos indicates that the thiol-dependent FosB detoxification pathway for Fos is the primary resistance mechanism of the organism to Fos.

In summary, we have determined the first high resolution crystal structures of $FosB^{Sa}$, which is the enzyme responsible for resistance of the pathogen to Fos. $FosB^{Sa}$ catalyzes the Mn^{2+}-dependent nucleophilic addition of BSH to Fos and represents the sole inactivating pathway of the organism from USA300 JE2 or Newman strains. The new structures revealed a phosphonate binding loop on the enzyme. We believe this loop functions as a door that opens and closes to allow the antibiotic to enter the active site of the enzyme. Once closed, the loop completes

important structural features that bind and secure both cosubstrates. Analysis of $FosB^{Sa}$ via HDX-MS was unsuccessful at probing the dynamics of the loop region, but did reveal that the over structure of $FosB^{Sa}$ is relatively stable with little dynamic movement.

Contrary to published results, we demonstrated that $FosB^{Sa}$ is inhibited by Zn^{2+} similar to other Fos resistance enzymes. Our kinetic results clearly indicate that $FosB^{Sa}$ is a Mn^{2+}-dependent BSH transferase and inhibited by physiologically relevant concentrations of Zn^{2+}. Given the similarity of the susceptibility of the BSH and FosB null strains of MRSA to Fos, we can predict the MIC values of FosB null MRSA to be 10-20 µg/mL based on the reported value for BSH null strains. This is below the reported serum concentration of Fos following the standard 3 g dose. Therefore, targeting $FosB^{Sa}$ therapeutically could serve as a synergistic treatment for pathogens like MRSA.

CHAPTER VI

EFFORTS TOWARD DETERMINING THE SUBSTRATE SELECTIVITY OF BshC, AN ENZYME REQUIRED FOR BACILLITHIOL BIOSYNTHESIS[4]

Results

Crystal Structure Determination of BshC

Dr. Paul Cook's lab at Grand Valley State University determined the first high resolution crystal structure of BshC from *B. subtilis*, which is the putative cysteine ligase in BSH biosynthesis (see Figure 8 – Chapter 1).[20] The overall crystal structure had a final resolution of 1.77 Å and overall R factor of 17.0% (Figure 44). Crystals in this study were grown in the presence of 200 mM citrate and electron density corresponding to a citrate molecule was observed in the canonical Rossmann fold active site. This 5- and 6- carboxylate groups of the citrate molecule likely mimic the 4- and 1-carboxylate groups, respectively, of the malyl moiety of glucosaminyl-malate and BSH, which means this provides clues as to how BshC accommodates that part of the substrate and product.

Additionally, an adenosine diphosphate (ADP) molecule is bound within a pocket distinct from the canonical active site even though no nucleotides were added during the purification, dialysis, or crystallization of BshC. Thus, this ligand came along with the protein when it was expressed in *E. coli* cells. The electron densities of the adenine, ribose, and α-phosphate portions

[4] Reprinted with permission from VanDuinen, A. J., Winchell, K. R., Keithly, M. E., and Cook, P. D. (2015) X-ray crystallographic structure of BshC, a unique enzyme involved in bacillithiol biosynthesis, *Biochemistry* 54 100-103. Copyright 2015 American Chemical Society,

of ADP are well-defined, but the density for the β-phosphoryl group is somewhat ambiguous, which indicates that a group other than phosphate is present at this position (Figure 45). In an effort to identify this substrate, Dr. Cook sent samples of purified protein to our lab for analysis by LC-MS.1

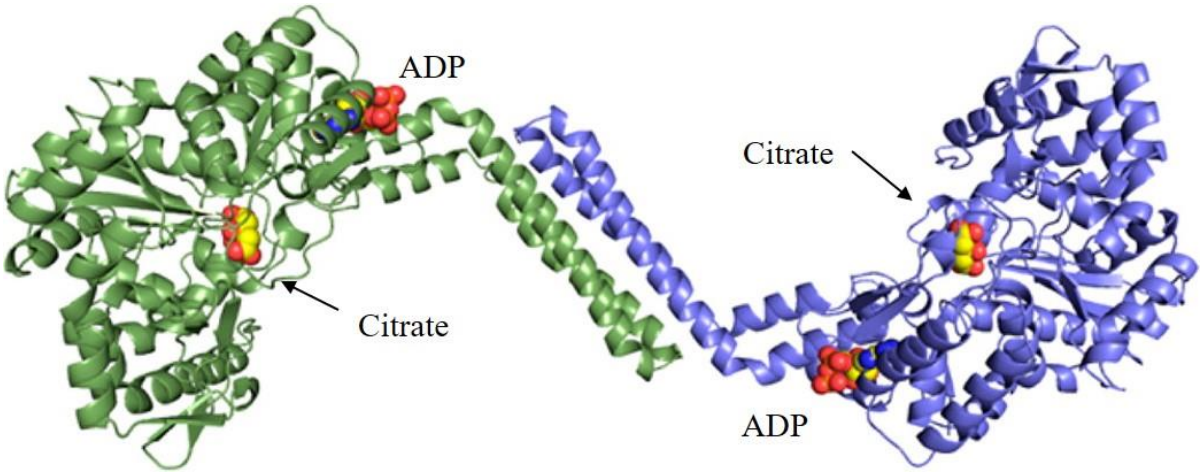

Figure 44. Overall quaternary crystal structure of BshC at 1.77 Å with a citrate and ADP molecule bound to each monomer of the homodimer.

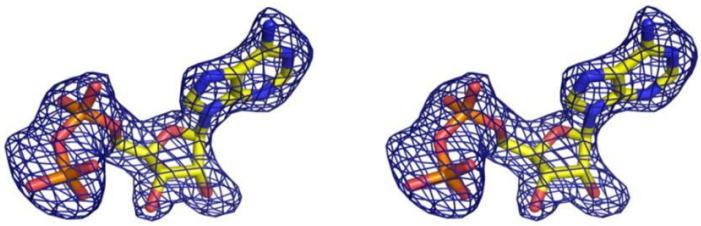

Figure 45. BshC ADP ligand electron density. Stereo view of electron density corresponding to the ADP molecule present in the second binding site. The omit map shown was calculated from F_o-F_c and is contoured at 3σ.

LC-MS Analysis of Purified BshC

The native BshC enzyme was characterized for the presence of tightly-bound ligands using LC-MS analysis. LC-MS of the protein in positive ionization mode was completed to determine

the mass of the overall protein. In order to calculate the mass, the charge state of the protein was determined using Equation 4 and then the mass was calculated from Equation 5.

Equation 4: $$Z_2 = \frac{\frac{m_1}{z_1} - H}{\frac{m_2}{z_2} - \frac{m_1}{z_1}}$$

Equation 5: $$M = Z_2\left(\frac{m_2}{z_2} - H\right)$$

The spectra revealed 2 peaks for each charge state in the centroid envelope of the protein (Figure 46). The mass for each peak set was calculated and two average masses were determined. One mass corresponded to the molecular weight of the purified BshC and the second mass was approximately 200 Da higher. This indicates that we have two distinct protein states, which correlate to the apo protein and substrate bound protein. Additionally, this points to a tightly-bound ligand, which we attempted to identify utilizing LC-MS/MS analysis in negative ionization mode.

Spectra from LC-MS/MS analysis in negative mode revealed four abundant peaks with m/z of 112.72, 156.72, 262.72, and 425.72 (Figure 47). A peak search conducted at MassBank was used to help in identifying these four peaks.[45] The peak at 112.72 is found in adenosine triphosphate (ATP). The peak at 156.72 is found in ADP. The peak at 425.72 correlates to a peak found in ADP and ATP, typically at an m/z of approximately 426.1. The last peak at 262.72 had no match in the database. These data suggest that adenosine nucleosides are present in the sample, but their exact identity could not be confirmed.

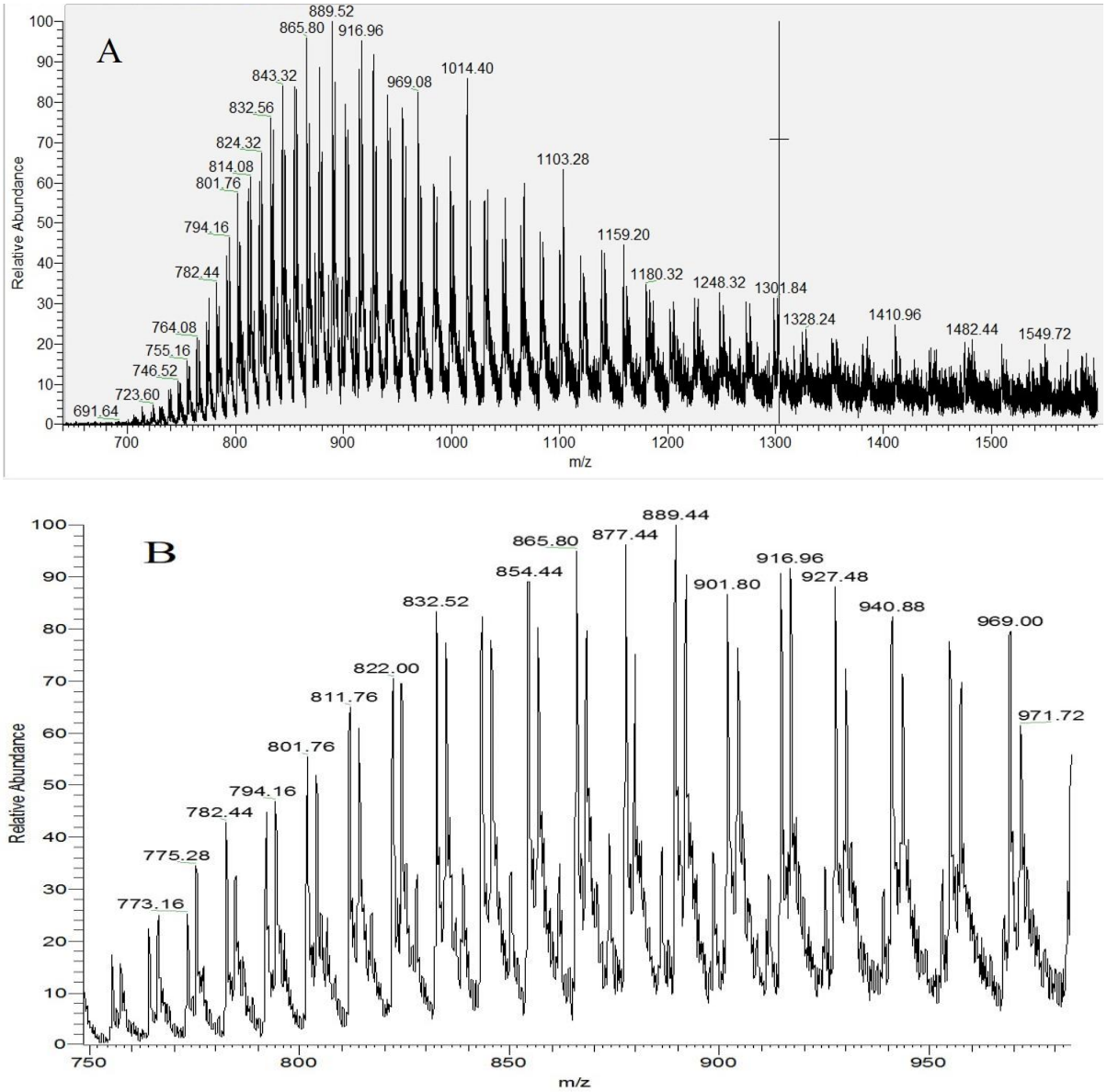

Figure 46. LC-MS analysis of BshC in positive ionization mode. (A) Full spectra of showing the centroid for BshC. (B) Zoom in on the centroid showing the two distinct peaks for the protein.

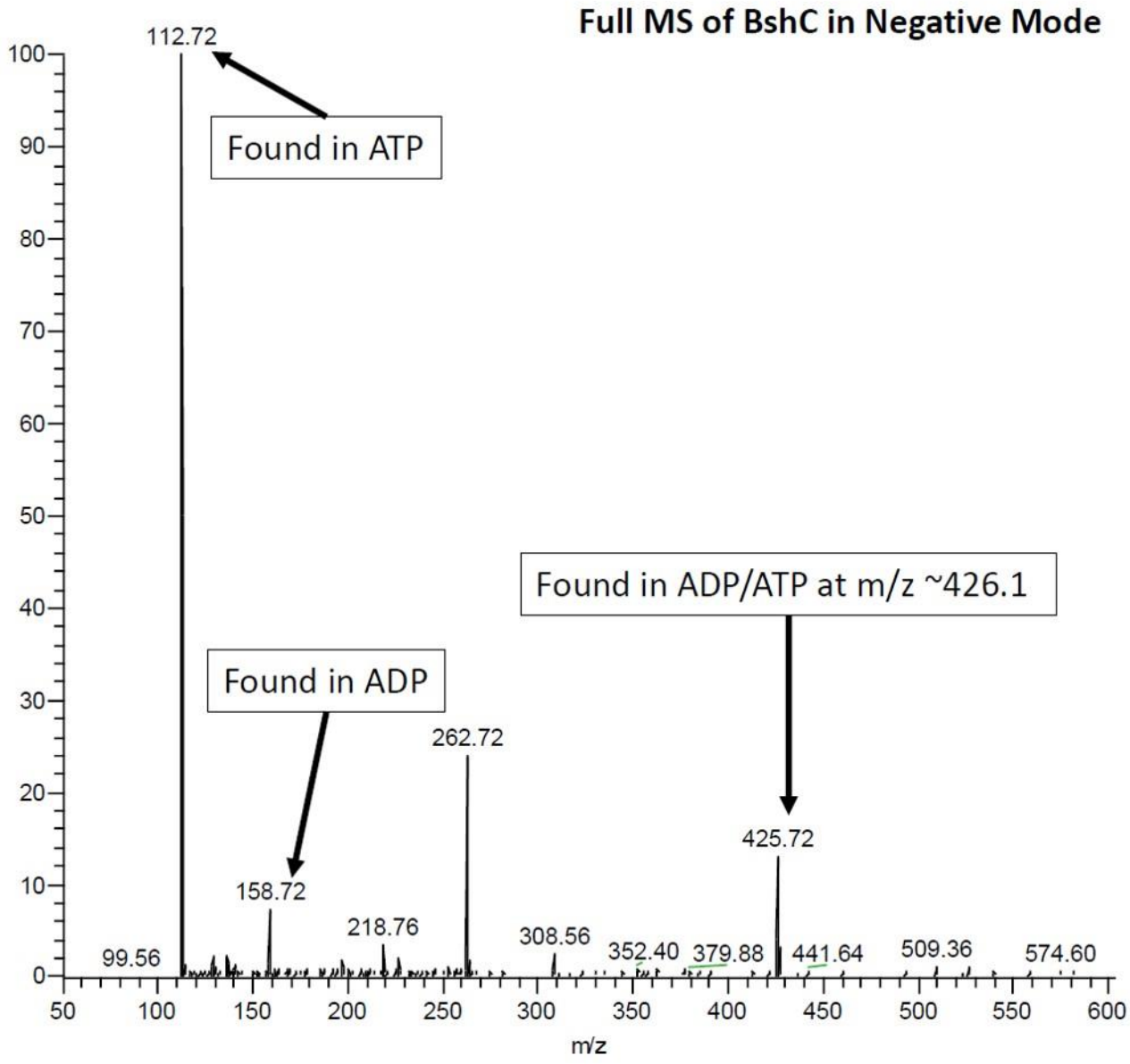

Figure 47. LC-MS spectrum of BshC ligands in negative ionization mode.

Discussion

The proposed biosynthesis of BSH is a three step enzymatic process catalyzed by the glycosyltransferase BshA, the deacetylase BshB, and the putative cysteine ligase BshC.[20] The activities of BshA and BshB have been confirmed via *in vitro* assays, but the activity of BshC has yet to be elucidated. This work represents the first high resolution crystal structure of BshC and has provided insight into possible substrate identification for BshC. The overall crystal structure of BshC (Figure 44) had a citrate bound in the active site, which likely binds to the location for the malyl moiety of the glucosaminyl-malate and BSH substrates. Additionally there is an ADP-like molecule bound in a distinct pocket separate from the active site. Mass spectroscopic analysis of the protein suggests the presence of an adenosine nucleoside, but it could not provide unequivocal identification of the ligand.

Cysteine-tRNA ligases and the MSH cysteine ligase, MshC, add cysteine to an acceptor molecule via a process that requires the activation of cysteine by ATP before attachment of the cysteine to the acceptor molecule.[52] Given the similarities between MSH and BSH, we might expect the putative cysteine ligases to function in a similar matter, which could explain the presence of the ADP-like molecule bound in our crystal structure. However, the ADP-binding pocket of BshC is not present in MshC or cysteine-tRNA ligases. Therefore, the biological significance of the ADP molecule and the binding site that it occupies still remains a mystery. It is possible that the binding pocket functions in regulation or serves as a second catalytic site. Further structural and functional analysis of BshC is warranted to investigate the role of ADP and this binding pocket.

The proliferation of multi-drug resistant pathogens, such as MRSA, represents a growing threat to human health. Investigation of the BSH biosynthesis pathway, including BshC, will

provide insight into new possible therapeutic targets to combat resistance to the antibiotic Fos. The new structure of BshC has provided insight into possible substrates necessary for activity of the enzyme. Furthermore, this work provides a foundation for additional structure and functional studies of BshC.

CHAPTER VII

CONCLUSIONS

Summary

Microbial antibiotic resistance (MAR) was recognized shortly after the introduction of antibiotics to the clinical setting in the 1940's. Over the years, MAR has becoming a global threat that increases each year and has culminated in the emergence of multiple-drug resistant organisms. These infections are invulnerable to treatment with several antimicrobial agents. With the discovery of new antibiotics decreasing each year, new methods of treatment for MAR infections are in dire need.

One method to fight the rising tide of MAR infections is to make old, underutilized antibiotics more effective.[2, 4, 7b, 7c] While the exact mechanism of MAR can vary, antibiotic modifying or destroying enzymes represent one of the most common modes of microbial survival. Combination therapies of administering antibiotics in conjunction with enzyme inhibitors has proven successful. Augmentin combines penicillin, a β-lactam antibiotic, with β-lactamase inhibitors to successfully treat β-lactam resistant bacterial strains.

Fos is a broad-spectrum antibiotic produced by strains of *Streptomyces* that has no significant side effects.[8] It can be administered for the treatment of Gram-positive and Gram-negative bacterial infections in a single three gram dose.[8] Fos functions by inactivating the enzyme MurA, which inhibits bacterial cell wall biosynthesis. MurA catalyzes the first committed step in peptidoglycan biosynthesis, which is a necessary building block for the bacterial cell wall.[9]

However, like all known antibiotics, Fos has known enzymatic antibiotic resistance in both Gram-positive and Gram-negative organisms.

There are three distinct classes of Fos resistance enzymes. FosA is a Mn^{2+}- and K^{+}-dependent GSH-transferase found in Gram-negative organisms that catalyzes the nucleophilic addition of GSH to carbon-1 of Fos.[15] This opens the epoxide ring of Fos and resulting in a modified compound with no bactericidal properties. FosX is a Mn^{2+}-dependent hydrolase that catalyzes the hydration of Fos at carbon-1 forming a vicinal diol and inactivating Fos.[16]

The third class, FosB, is found in Gram-positive organisms, such as *S. aureus*, *B. subtilis*, *B. cereus*, and *B. anthracis*. Initial analysis of $FosB^{Bs}$ categorized this enzyme as a Mg^{2+}-dependent L-cysteine-transferase, which catalyzes the nucleophilic addition of L-cysteine to carbon-1 of Fos in a reaction similar to that of FosA.[17] However, the L-cysteine-transferase activity of $FosB^{Bs}$ is poor (k_{cat}/K_M^{thiol} ~180 $M^{-1}s^{-1}$) compared to the GSH-transferase activity of FosA from *P. aeruginosa* (k_{cat}/K_M^{thiol} ~1.7 X 10^5 $M^{-1}s^{-1}$) and is not sufficient to confer the robust Fos resistance seen *in vivo*.[17]

In 2009, a new LMW-thiol, BSH, was discovered in Gram-positive organisms in concentrations equal to that of L-cysteine.[19] Studies of BSH null strains of *B. subtilis* indicated that these cells had an increased sensitivity to Fos compared to WT cells.[20] Initial time course data completed by Sharma et al. comparing FosB activity with L-cysteine and BSH indicated that FosB prefers BSH over L-cysteine as a thiol substrate.[22] These results prompted the work presented in this dissertation. In an effort to better understand the catalytic mechanism and substrate selectivity of FosB, we completed kinetic analyses, structural studies, and *in vivo* experiments on FosB from multiple strains of Gram-positive bacteria.

The kinetic analyses indicate that FosB has a clear preference for BSH over L-cysteine. A probe of divalent metal activation revealed the order of activation *in vitro* to be Mn^{2+} > Ni^{2+} > Mg^{2+} > Zn^{2+}.[46, 51, 53] Additionally, Zn^{2+} was shown to be a potent inhibitor of FosB BSH-transferase and L-cysteine-transferase activity even when physiological relevant concentrations of Mn^{2+} were present.[51, 53] Lastly, the disk diffusion assays completed in collaboration with Dr. Eric Skaar's lab indicate that both FosB and BSH are necessary for strains of *S. aureus* to be resistant to Fos.[53] Together, these data allowed us to categorize FosB as a Mn^{2+}-dependent BSH-transferase.

We were able to determine a total of 14 high resolution structures of FosB, 9 from $FosB^{Bc}$ and 5 from $FosB^{Sa}$.[51, 53] These structures were determined with FosB in complex with various divalent metals, substrates, and products. The overall structure confirmed that FosB belongs to the VOC superfamily of enzymes, similar to the other Fos resistance enzymes, FosA and FosX. FosB has the three-dimensional domain-swapped arrangement of sequential βαβββ motifs in which both subunits of the homodimer participate in coordination of the metal ion and formation of the active site, which defines the VOC superfamily.

The structures from $FosB^{Bc}$ revealed key structural features of FosB. Analysis of Fos coordination to metal in the active site of $FosB^{Bc}$ revealed a cage of amino acids that orients Fos for nucleophilic attack of the carbon-1 of Fos.[51] The cage has both a polar end, which coordinates to the phosphonate group of Fos, and a non-polar end to coordinate the antibiotic in the active site.

Additionally, surface analysis of the structure revealed a solvent access channel that leads directly to the centered carbon-1 of Fos.[51] This solvent channel is large enough to accommodate either L-cysteine or the cysteine moiety of BSH. At the opening of the solvent access channel, there is a binding pocket that is appropriate in size and shape to bind the glucosamine-malate

moiety of BSH. Since the kinetic analyses indicate FosB has a preference for BSH over L-cysteine, this suggests that the glucosamine-malate moiety of BSH is important for substrate recognition. Therefore, this binding pocket may have a significant role in the achieving maximum catalytic activity of FosB.

A comparison of the $FosB^{Bc}$ structure in complex with Mn^{2+} and Fos (PDB 4JH6) to the apo $FosB^{Sa}$ structure (PDB 4NB2) indicates that movement of the phosphonate binding loop region may be required for Fos binding in the active site of the enzyme.[53] In the $FosB^{Bc}$ complex structure, the loop is observed in the closed confirmation. In contrast, the loop is in an open conformation on the apo $FosB^{Sa}$ structure. The loop, which is conserved in throughout the FosB enzymes, can be morphed from the open conformation into the closed conformation. In addition, the size of the solvent access channel at its most narrow point is not large enough to accommodate Fos. Together these data suggest that the loop region must open to allow Fos to have access to the active site.

In an effort to probe the dynamic movement of the phosphonate binding loop region, HDX-MS analyses were completed with $FosB^{Sa}$. The overall low incorporation of deuterium indicate that FosB is a relatively stable protein with little dynamic movement. While peptide mapping provided 97 % coverage of $FosB^{Sa}$ with multiple overlapping peptides to represent the phosphonate binding loop region, the signal for these peptides was lost when the separation gradient was changed for HDX-MS analysis. Therefore, we were unable to determine any dynamic movement of the phosphonate binding loop using this method.

Finally, we worked in collaboration with Dr. Paul Cook to interrogate the substrate selectivity of BshC, an enzyme necessary for BSH biosynthesis. Since BSH is necessary for maximum FosB activity, the biosynthetic pathway for BSH could also be a therapeutic target for the development of inhibitors to combat Fos resistance. Dr. Cook determined the first high

resolution crystal structure of BshC in complex with an ADP-like molecule and a citrate molecule.[54] Since no nucleosides were introduced during purification or crystallization, we completed LC-MS analysis of the purified protein to probe the identity of the ADP-like ligand. The analysis indicates the presence of an adenosine nucleoside, but unequivocal identification of the ligand was not possible from our data.

Significance and Impact

MAR is a major health threat on the rise and new methods to treat MAR infections must be found. Fos alone and in combination with other antibiotics has recently been used to treat MAR infections in the clinical setting.[11a, 11b, 55] However, the presence of Fos resistance enzymes decreases the efficacy of the antibiotic in the clinical setting. Since Fos is a broad spectrum antibiotic with very few side effects, it would be beneficial to find a way to improve the efficacy of the antibiotic for use in treating MAR infections.

The ability for Fos to treat both Gram-positive and Gram-negative infections make this drug an attractive therapeutic for MAR infections. This work has determined the structure and mechanism of catalytic activity for a variety of FosB enzymes, which are found in Gram-positive bacteria. FosA, found in Gram-negative organisms, has previously been studied. The data from this dissertation combined with the FosA data can be used by drug companies to design inhibitors of the Fos resistance enzymes. The method of combining a resistance enzyme inhibitor with an antibiotic has previously been successful. An inhibitor of Fos resistance enzymes in combination with Fos would increase the efficacy of the antibiotic and make it a more viable treatment for MAR infections.

Future Work

The work presented in this dissertation establishes the *in vitro* substrate selectivity and the order of divalent metal activation for the FosB enzymes. The structural studies provide insight into the catalytic mechanism of FosB. This information could provide crucial details to developing FosB inhibitors that could be given in conjunction with Fos to increase the efficacy of the antibiotic in the clinical setting. However, additional analysis is warranted to confirm *in vivo* activity of FosB and to further probe the structural features identified here.

While we did determine 14 high resolution structures of FosB in complex with various divalent metals, substrates, and/or product, we have not yet been successful in determining a crystal structure with the full molecule of BSH or BS-Fos present, which is necessary for any future structure based inhibitor development. Also, our attempts to probe the dynamic movement of the phosphonate binding loop region using HDX-MS were unsuccessful. Therefore, we have initiated NMR analysis of $FosB^{Sa}$ in order to probe the dynamic movement of the loop region and interrogate the location of BSH binding.

The rapid spread of multi-drug resistant infections, such as MRSA, represents a growing global threat to human health. In order to combat this rising threat, we must continue to develop alternative therapies for treatment. Fos represents a promising antibiotic that could be used to treat these types of infections, but the prevalence of enzymatic resistance to Fos decreases the efficacy of the antibiotic in the clinical setting. Therefore, the development of drugs that can inhibit this resistance pathway can be used in combination with Fos in order to improve the efficacy of the antibiotic. A better understanding of both FosB *in vivo* activity and the BSH biosynthesis pathway can provide the information required for designing these novel inhibitors.

APPENDIX A

STRUCTURE DETERMINATION OF THE BS-Fos PRODUCT FORMED BY THE FosB ENZYME FOUND IN *Staphylococcus saprophyticus*

Preliminary Results

As previously described, a ^{31}P NMR assay can be utilized to determine the time course kinetic profile of the FosB enzymes based upon the amount of product formed over time. This assay requires the use of peak height ratios of Fos and the product with the law of conservation of mass to determine the amount of product formed. FosB^{Sa}, FosB^{Bc}, FosB^{Bs}, and FosB^{Ba} catalyze the nucleophilic addition of both L-cysteine and BSH to Fos producing a unique singlet peak for each product.

During the course of this work, I also assayed the reaction catalyzed by FosB from *Staphylococcus saprophyticus* (FosB^{Ss}). As expected, FosB^{Ss} catalyzed the nucleophilic addition of L-cysteine to Fos producing a singlet peak on the ^{31}P NMR spectra. However, the FosBSs reaction with BSH present, produces two peaks (Figure 48). One possible explanation is that the two peaks represent stereo or region isomers of the BS-Fos product.

I was unsuccessful in isolating these two products from the reaction. However, future work should investigate the identity of these two products. Since BSH is believed to be the *in vivo* substrate for the FosB enzymes, it is imperative to understand why this Gram-positive bacterium produces a different product than other known Gram-positive bacteria. Additionally, insight into the structure of FosB^{Ss} compared to the structures determined for FosBBc and FosBSa will provide further details into the differences between these enzymes. Combined, this information could be

used to better design inhibitors of FosB enzymes from multiple organisms and ultimately increase the efficacy of the antibiotic in the clinical setting.

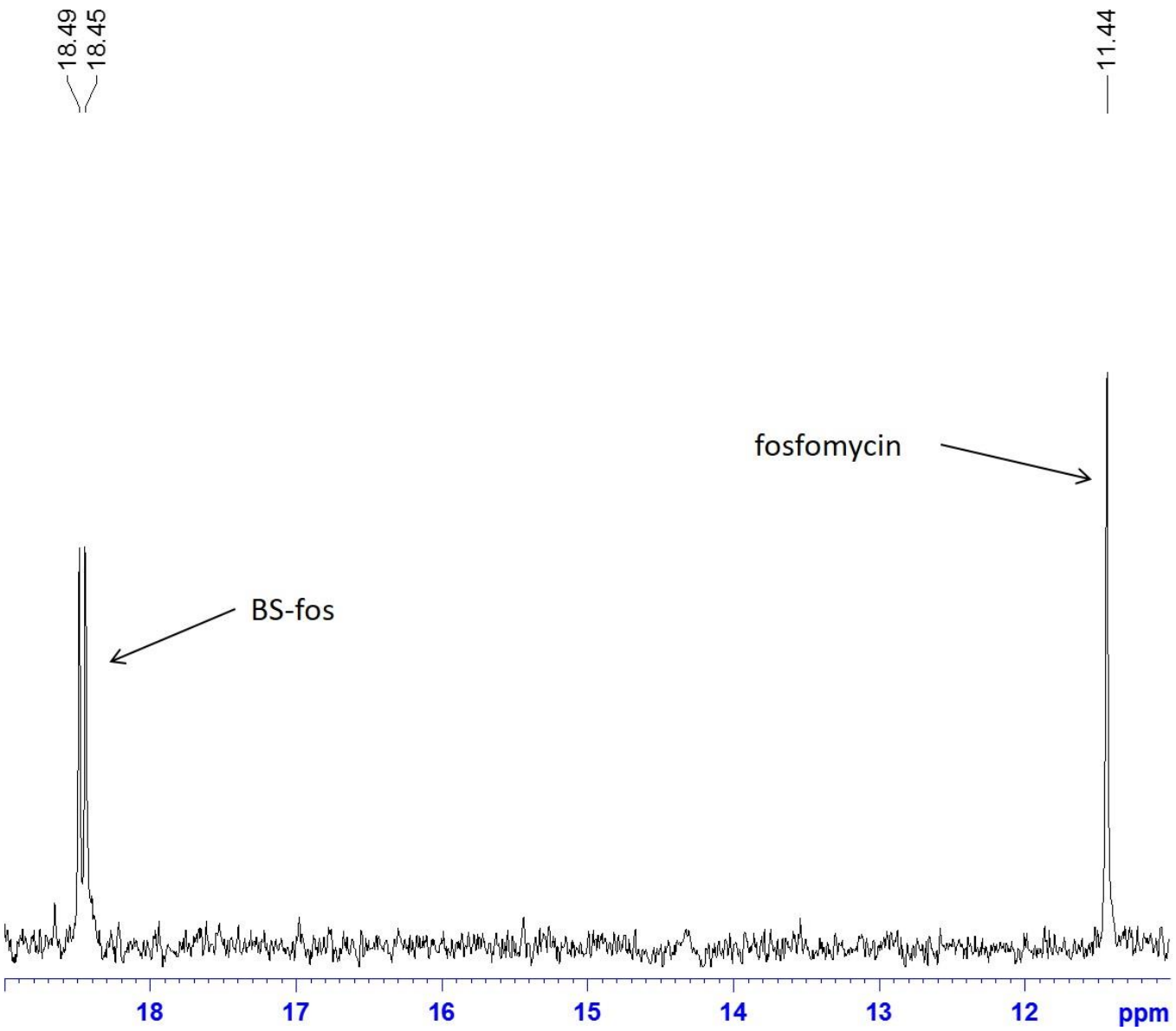

Figure 48. NMR spectrum of the double peak formed by the FosBSs catalyzed nucleophilic addition of bacillithiol to fosfomycin.

APPENDIX B

THE INVESTIGATION OF INHIBITION OF THE FosB ENZYMES BY N-acetylglucosamine-malate, AN INTERMEDIATE OF THE BACILLITHIOL BIOSYNTHESIS PATHWAY

Preliminary Results

FosB enzymes catalyze the nucleophilic addition of BSH to the antibiotic Fos, which modifies Fos making it ineffective. The BSH biosynthesis pathway (see Figure 6 – Chapter 1) produces GlcNAc-Mal as an intermediate. GlcNAc-Mal is a truncated version of BSH that has an acetyl group in place of the cysteine moiety (Figure 49). It cannot perform the nucleophilic attack necessary to inactivate Fos. However, it is possible that it could still bind to the active site of FosB and act as an inhibitor of the enzyme.

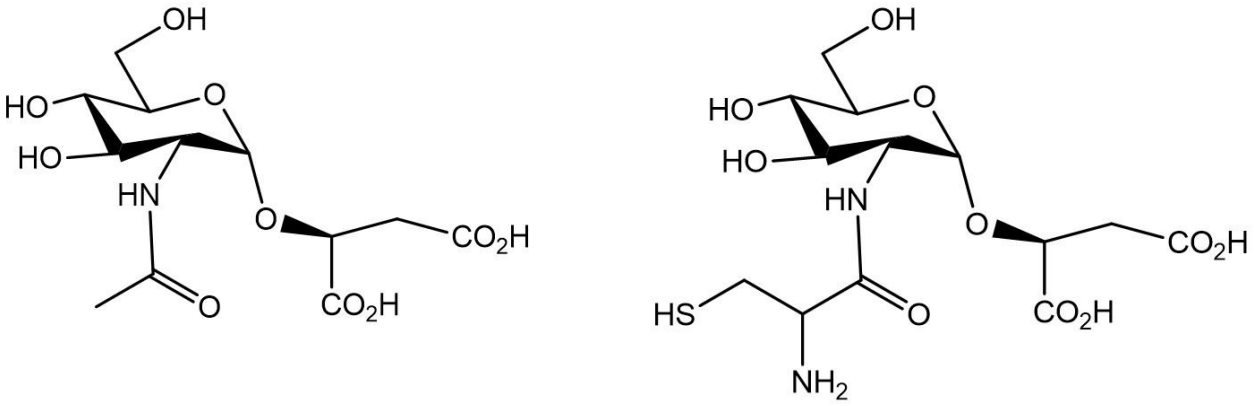

GlcNAc-Mal **BSH**

Figure 49. Comparison of the GlcNAc-Mal and BSH structures. GlcNAc-Mal (left), an intermediate in the BSH biosynthesis pathway, is a truncated version of BSH, which contains an acetyl group in place of the cysteine moiety.

Preliminary NMR assays indicate that GlcNAc-Mal is able to inhibit the $FosB^{Bs}$ catalyzed nucleophilic addition of L-cysteine to Fos (Figure 50). After 10 minutes, the reaction catalyzed in the presence of Glc-NAc-Mal has significantly less product formed than the reaction without Glc-NAc-Mal present. After 30 minutes, additional product formation is seen in the reaction catalyzed in the presence of Glc-NAc-Mal, but the reaction still has not run to completion. This indicates that Glc-NAc-Mal acts as an inhibitor of FosB, but it is not complete inhibition.

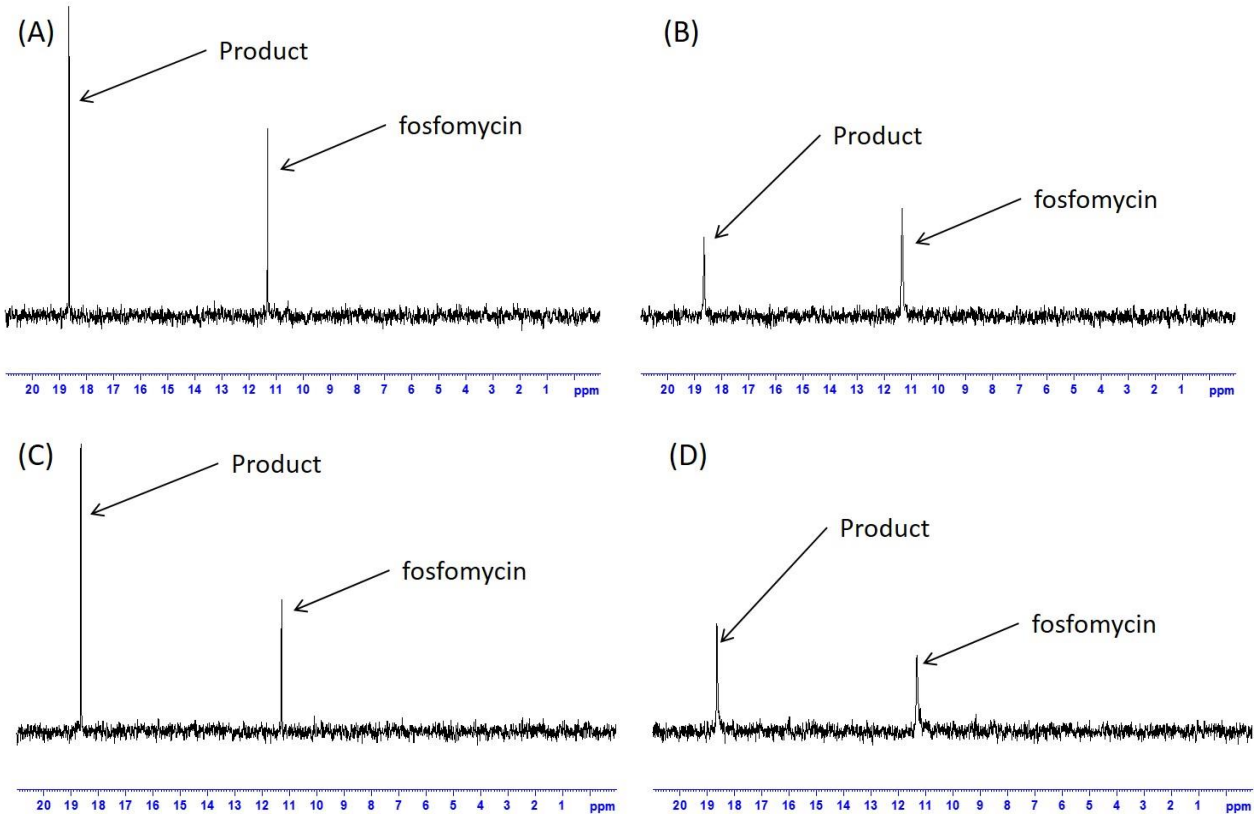

Figure 50. NMR spectra of the FosB catalyzed nucleophilic addition to L-cysteine to Fos at 10 and 30 minutes. Reactions were carried out at 25˚ C in 20 mM HEPES, pH 7.0 with 4.8 mM fosfomycin, 2.4 mM L-cysteine, and 0.8 mM enzyme in the (A) and (C) absence or (B) and (D) presence of 2.22 mM GlcNAc-Mal.

Further analysis, including complete inhibitor kinetic studies, of the FosB catalyzed addition of both L-cysteine and BSH to Fos should be completed. Additionally, crystallography

studies would provide valuable information regarding the mode of inhibition. These data could assist in designing inhibitors of the FosB enzymes to increase the efficacy of Fos. Furthermore, this could indicate that inhibition of BshC increasing Glc-NAc-Mal production would also be a valid pathway to increase Fos efficacy *in vivo*.

APPENDIX C

CV

Mary E. Keithly

17488 E. Hwy 86
Neosho, MO 64850
Cell phone: (615) 428-9487
E-mail: mary.e.keithly@gmail.com

EDUCATION

Ph.D. **Vanderbilt University,** Nashville, TN
August 2016
Department of Chemistry
Advisor: Richard N. Armstrong, Ph.D. (Deceased June 2015)
Charles R. Sanders, Ph.D. and Walter J. Chazin, Ph.D.
Thesis: Structure, substrate selectivity, and catalytic mechanism of the fosfomycin resistance enzyme, FosB, from Gram-positive pathogens

B.S. **University of Missouri – St. Louis,** St. Louis, MO
May 2010
Major in chemistry (*magna cum laude*)

CERTIFICATES

Certificate in College Teaching **Vanderbilt University,** Nashville, TN
May 2015
Center for Teaching

TEACHING EXPERIENCE

Vanderbilt University Center for Science Outreach September 2012- May 2016
Science Teaching Fellow (STF), *7th Grade Science,* Rose Park Middle School
June 2013-May 2016

- Co-taught planned lessons one day per week to ~100 students with a variety of backgrounds and abilities.
- Designed lesson plans and assignments for 7th grade science course in partnership with the teacher.
- Led a presentation and lab activity on my research.

STF, *Interdisciplinary Science Research* , Hillsboro High School September 2012-May 2013

- Assisted with teaching and helping students in 4 ISR courses and 1 Chemistry Course, which includes ~80 students with a variety of backgrounds and abilities.
- Designed lab lesson plans and assignments for Chemistry Course also taught by ISR instructor.
- Graded chemistry assignments that I prepared.

Vanderbilt University Center for Teaching May 2014-December 2015
BOLD Fellow (Teaching as Research Project), *Principles of Genetics*

- Developed 3 web modules for 3 topics to be implemented as a flipped classroom in conjunction with two professors.
- Assisted 2 professors in implementing the flipped classroom for 4 class sessions in genetics.
- Developed and administer pre-/post-tests, satisfaction surveys, and classroom observations to assess the implementation of the flipped classroom.
- Obtain IRB approval for the research project.
- Data showed no specific learning gains when comparing pre-/post-test scores between traditional lecture and a blended class design, but did provide evidence of higher cognitive activity (as categorized by Bloom's Taxonomy) during class time when using a blended classroom approach.
- Student satisfaction surveys indicate that the majority of students like the blended classroom and find it more effective than traditional lecture.
- A description of the project and the results can be found at http://vanderbilt.edu/bold/docs/bsci-2210-principles-of-genetics/

Vanderbilt University Center for Teaching August 2013-May 2015
Graduate Teaching Affiliate

- Attended a two week workshop covering how students learn, leading discussions, effective lecturing and information new teaching assistants (TA's) need in order to prepare for teaching assistant orientation (TAO).
- Led a full day TAO workshop for incoming Chemistry TA's, which included approximately 20 students and for incoming engineering TA's, which included approximately 20 students.
- Prepared and co-led a one hour workshop at GradSTEP (Title: *Interactive Lecturing in Large Classrooms*) for approximately 20 Vanderbilt graduate students, post-docs, or faculty.
- Designed, filmed, and edited videos on what faculty expect of new TA's in the Chemistry and Biological Sciences Department.

Vanderbilt University Department of Biological Sciences April 2015
Guest Lecturer, *Biochemistry*

- Taught 2 lectures on amino acid catabolism.
- Developed a lesson plan with guided worksheets to implement an interactive class lecture.

Vanderbilt University Department of Chemistry August 2010-April 2015
Graduate Teaching Assistant, *Organic Chemistry Stockroom* Spring 2015

- Prepared and setup labs for Organic Chemistry II.
- Maintained inventory of stockroom.
- Cleaned stockroom and labs.

Graduate Teaching Assistant, *General Chemistry Recitation* Fall 2014

- Taught 6 recitation sections to 150 chemistry students of a variety of backgrounds and abilities.
- Created, administered, and graded quizzes.
- Graded exams for General Chemistry lecture.

Graduate Teaching Assistant, *General Chemistry I Laboratory* Fall, Spring 2010-2011

- Taught lab to 48 chemistry students of a variety of backgrounds and abilities.
- Proctored exams for General Chemistry Lecture.
- Graded exams and lab reports.

University of Missouri – St. Louis Disabilities Access Services August 2009-May 2010
Tutor, *Physical Chemistry I and II*

- Tutor one student with disabilities in Physical Chemistry I and II

RESEARCH EXPERIENCE

Vanderbilt University Department of Chemistry June 2010-August 2016
Graduate Research Fellow

Advisor: Richard N. Armstrong, Ph.D. (Deceased June 2015)
Charles R. Sanders, Ph.D. and Walter J. Chazin, Ph.D.
Topic: Structure, substrate selectivity, and catalytic mechanism of the fosfomycin resistance enzyme, FosB, from Gram-positive pathogens.

University of Missouri – St. Louis Department of Chemistry January 2009-May 2010
Undergraduate Researcher

Advisor: Cynthia Dupureur, Ph.D.
Topic: The effect of phosphorylation on the conformation of hormone-sensitive lipase.

ADDITIONAL EXPERIENCE

Vanderbilt University August 2013-May 2014
Conference Organizer, Biomolecular Structure, Dynamic, Function: Membrane Protein

- Student member of organizing committee for the conference.
- Assisted in inviting and choosing speakers.
- Assisted in planning all sessions of the conference.
- Planned the conference dinner for attendees at the Bound'ry restaurant.
- Served as a session chair for one session.

PUBLICATIONS

- Shen J, **Keithly ME**, Armstrong RN, Higgins KA, Edminds KA, Giedroc DP *Staphylococcus aureus CstB is a Novel Multidomain Persulfide Dioxygenase-Sulfurtransferase Involved in Hydrogen Sulfide Detoxification.* Biochemistry. (2015) 54, 4542-54
- Vanduinen AJ, Winchell KR, **Keithly ME,** Cook PD *X-ray crystallographic structure of BshC, a unique enzyme involved in bacillithiol* biosynthesis. Biochemistry. (2015) 54, 100-103
- Thompson MK, **Keithly ME,** Sulikowski GA, Armstrong RN, *Diversity in fosfomycin resistance proteins*. Perspect. Sci. (2015) 4, 17-23.
- Thompson MK, **Keithly ME,** Goodman MC, Hammer ND, Cook PD, Jagessar KL, Harp J, Skaar EP, Armstrong RN, *Structure and Function of the Genomically Encoded Fosfomycin Resistance Enzyme, FosB, from Staphylococcus aureus*. Biochemistry. (2014) 53, 755-765.
  Highlighted in the 58th Annual Biophysical Society National Meeting Press Release.
- Thompson MK, **Keithly ME,** Harp J, Cook PD, Jagessar KL, Sulikowski GA, Armstrong RN, *Structural and Chemical Aspects of Resistance to the Antibiotic Fosfomycin Conferred by FosB from Bacillus cereus.* Biochemistry. (2013) 52, 7350-62.
- Lamers AP, **Keithly ME,** Kim K, Cook PD, Stec DF, Hines KM, Sulikowski GA, Armstrong RN, *Synthesis of Bacillithiol and the Catalytic Selectivity of FosB-type Fosfomycin Resistance Proteins*. Org. Lett. (2012) 14, 5207-9.

PEER REVIEWED PRESENTATIONS

Oral presentation National Science Teacher Association's National Conference April 2016
Music City Center, Nashville, TN
Title: *How To Master Scientists Inside The Classroom With High Results.*

Oral presentation American Chemical Society SERMACS-SWRM Conference November 2015
Memphis-Cook Convention Center, Memphis, TN
Title: *Investigating enzymatic resistance to fosfomycin by FosB in Gram-positive bacteria*

Poster presenter The 35th Midwest Enzyme Chemistry Conference September 2015
Illinois Institute of Technology, Chicago, IL
Title: *Investigating enzymatic resistance to fosfomycin by FosB in Gram-positive bacteria.*

Poster presenter American Chemical Society National Meeting August 2015
Boston Convention & Exhibition Center, Boston, MA
Title: *Investigating enzymatic resistance to fosfomycin by FosB in Gram-positive bacteria.*
Title: *Blending it up: Active learning in a STEM classroom through the use of on-line materials.*

Poster presenter Biomolecular Structure, Dynamic, Function: Membrane Protein May 2014
Vanderbilt University, Nashville, TN
Title: *Interrogation of 5–lipoxygenase activating protein interactions with substrate, inhibitor, and during protein complex formation via Hydrogen-Deuterium exchange mass spectrometry.*

Poster presenter 58th Annual Biophysical Society National Meeting February 2014
Moscone Convention Center, San Francisco, CA
Title: *Substrate and Metal Ion Specificity of Fosfomycin Resistance Protein, FosB.*

Poster presenter 2013 ASBMB Career Symposium September 2013
University of Missouri, Columbia, MO
Title: *Vanderbilt Center for Science Outreach*

Poster presenter VICB Tenth Anniversary Symposium March 2013
Vanderbilt University, Nashville, TN
Title: *Investigation of Substrate and Metal Ion Selectivity of the Fosfomycin Resistance Protein, FosB.*

Poster presenter 23rd Enzyme Mechanisms Conference January 2013
Loews Coronado Bay, San Diego, CA
Title: *Investigation of Substrate and Metal Ion Selectivity of the Fosfomycin Resistance Protein, FosB.*

Poster presenter Vanderbilt Institute of Chemical Biology Student Symposium August 2012
Vanderbilt University, Nashville, TN
Title: *Structural and Functional Investigation of the Fosfomycin Resistance Protein, FosB.*

Poster presenter American Chemical Society National Meeting March 2010
San Francisco, California
Title: *The effect of phosphorylation on the conformation of hormone-sensitive lipase.*

ADDITIONAL PRESENTATIONS

Oral presentation Center in Molecular Toxicology Enzymology Meeting February 2015
Vanderbilt University, Nashville, TN
Title: *Elucidating the Mechanism of the Fosfomycin Resistance Protein, FosB.*

Oral presentation Center in Molecular Toxicology Enzymology Meeting May 2014
Vanderbilt University, Nashville, TN
Title: *Investigation of Substrate and Metal Ion Selectivity of the Fosfomycin Resistance Protein, FosB.*

Oral presentation Center in Molecular Toxicology Enzymology Meeting November 2012
Vanderbilt University, Nashville, TN
Title: *Investigation of Substrate and Metal Ion Selectivity of the Fosfomycin Resistance Protein, FosB and HDX-MS of 5-lipoxygenase Activating Protein.*

Oral presentation Center in Molecular Toxicology Enzymology Meeting December 2011
Vanderbilt University, Nashville, TN
Title: *Functional Study of the Fosfomycin Resistance Enzyme, FosB.*

RESEARCH SKILLS

- Standard molecular biological techniques such as PCR, cloning, western blotting and site-directed mutagenesis
- Recombinant protein expression in *Escherichia coli*
- Protein purification
- Enzymatic synthesis and purification of enzyme substrates
- NMR and HPLC-based enzyme assays
- Mass spectrometry protein sequencing
- Hydrogen-Deuterium Exchange Mass Spectrometry (HDX-MS)
- Molecular graphics including Pymol and Chimera
- Computer Software: HDExaminer, Prism, QualBrowser, PEAKS, MagTran, MassXpert, Kaleidagraph, Microsoft Office Suite

INTERNSHIPS

Summer Intern Research and Development June 2009-August 2009
Covidien, St. Louis, MO

- Analytical testing on Levorphanol for use as a reference standard by Quality Control
- HPLC, GC, Titrations

Volunteer Intern Microbe Inotech Laboratories July 2008-May 2009
Shrewsbury, MO

- Completed accurate daily counts for multiple tests including TPC, TC, SAB, Yeast & Mold counts, Fungi counts.
- Ran tests for strain identification including BioLog and Vytek identification
- Tested for E. Coli, Salmonella, Listeria, and Staph using Vidas and set up tests for plate counts.
- Received samples and maintained files with accurate information for reporting to clients.

AWARDS AND HONORS

Graduate

- Training Program in Environmental Toxicology Trainee (2011-2014)

Undergraduate

- University of Missouri – St. Louis Academic Dean's List (2008-2010)
- Alan F. Berndt Outstanding Senior Award (2010)
- American Chemical Society Award for Analytical Chemistry (2010)
- American Institute of Chemists – Student Award Certificate (2010)
- Certificate of Commendation for Outstanding Service (2010)
- American Chemical Society – St. Louis Section's Outstanding Junior Award (2009)
- The Linda and Michael Finkes Chemistry Scholarship (2009)
- Chemistry Aid to Education Award (2009)

REFERENCES

Charles R. Sanders, Ph.D.
Provisional Advisor (in lieu of Richard N. Armstrong, Ph.D.)
Professor of Biochemistry
Associate Editor of Biochemistry
Aileen M Lange and Annie Mary Lyle Chair of Cardiovascular Research
Vanderbilt University
5110C MRBIII
465 21st Ave S.
Nashville, TN 37232-8725
Phone: (615) 936-3756
Email: chuck.sanders@vanderbilt.edu

Matthew K. Thompson, Ph.D.
Postdoctoral Fellow
Department of Biochemistry
Vanderbilt University
5144E MRBIII
465 21st Ave S.
Nashville, TN 37232-8725
Phone: (919) 455-1775
Email: matthew.k.thompson@vanderbilt.edu

Cynthia J. Brame, Ph.D.
Assistant Director, Center for Teaching
Director, BOLD Fellows program
Senior Lecturer, Biological Sciences
PMB 183
230 Appleton Place
Nashville, TN 37203-5721
Phone: (615) 322-7290
Email: Cynthia.brame@vanderbilt.edu

REFERENCES

1. Levy, S. B.; Marshall, B., Antibacterial resistance worldwide: causes, challenges and responses. *Nat Med* **2004,** *10* (12 Suppl), S122-9.
2. Fischbach, M. A.; Walsh, C. T., Antibiotics for emerging pathogens. *Science* **2009,** *325* (5944), 1089-93.
3. Armstrong, R. N., Mechanistic diversity in a metalloenzyme superfamily. *Biochemistry* **2000,** *39* (45), 13625-32.
4. Taubes, G., The bacteria fight back. *Science* **2008,** *321* (5887), 356-61.
5. (a) Bush, K.; Courvalin, P.; Dantas, G.; Davies, J.; Eisenstein, B.; Huovinen, P.; Jacoby, G. A.; Kishony, R.; Kreiswirth, B. N.; Kutter, E.; Lerner, S. A.; Levy, S.; Lewis, K.; Lomovskaya, O.; Miller, J. H.; Mobashery, S.; Piddock, L. J.; Projan, S.; Thomas, C. M.; Tomasz, A.; Tulkens, P. M.; Walsh, T. R.; Watson, J. D.; Witkowski, J.; Witte, W.; Wright, G.; Yeh, P.; Zgurskaya, H. I., Tackling antibiotic resistance. *Nat Rev Microbiol* **2011,** *9* (12), 894-6; (b) Nathan, C.; Goldberg, F. M., Outlook: the profit problem in antibiotic R&D. *Nat Rev Drug Discov* **2005,** *4* (11), 887-91; (c) Bradley, J. S.; Guidos, R.; Baragona, S.; Bartlett, J. G.; Rubinstein, E.; Zhanel, G. G.; Tino, M. D.; Pompliano, D. L.; Tally, F.; Tipirneni, P.; Tillotson, G. S.; Powers, J. H.; Tillotson, G. S., Anti-infective research and development—problems, challenges, and solutions. *The Lancet Infectious Diseases* **2007,** *7* (1), 68-78; (d) Projan, S. J., Why is big Pharma getting out of antibacterial drug discovery? *Current Opinion in Microbiology* **2003,** *6* (5), 427-430.
6. Prevention, C. f. D. C. a. *Antibiotic Resistance Threats in the United States, 2013*; US Department of Health and Human Services: 2013.
7. (a) Lewis, K., Antibiotics: Recover the lost art of drug discovery. *Nature* **2012,** *485* (7399), 439-40; (b) Bergen, P. J.; Landersdorfer, C. B.; Lee, H. J.; Li, J.; Nation, R. L., 'Old' antibiotics for emerging multidrug-resistant bacteria. *Current opinion in infectious diseases* **2012,** *25* (6), 626-33; (c) Carlet, J. M., J.L., Antibacterial agents: back to the future? Can we live with only colistin, co-trimoxazole and fosfomycin? *Clin Microbiol Infect* **2011,** *18* (1), 1-3.
8. Hendlin, D.; Stapley, E. O.; Jackson, M.; Wallick, H.; Miller, A. K.; Wolf, F. J.; Miller, T. W.; Chaiet, L.; Kahan, F. M.; Foltz, E. L.; Woodruff, H. B.; Mata, J. M.; Hernandez, S.; Mochales, S., Phosphonomycin, a new antibiotic produced by strains of streptomyces. *Science* **1969,** *166* (901), 122-3.
9. Brown, E. D.; Vivas, E. I.; Walsh, C. T.; Kolter, R., MurA (MurZ), the enzyme that catalyzes the first committed step in peptidoglycan biosynthesis, is essential in Escherichia coli. *J Bacteriol* **1995,** *177* (14), 4194-7.
10. Kahan, F. M.; Kahan, J. S.; Cassidy, P. J.; Kropp, H., The mechanism of action of fosfomycin (phosphonomycin). *Ann N Y Acad Sci* **1974,** *235* (0), 364-86.
11. (a) Falagas, M. E.; Giannopoulou, K. P.; Kokolakis, G. N.; Rafailidis, P. I., Fosfomycin: use beyond urinary tract and gastrointestinal infections. *Clin Infect Dis* **2008,** *46* (7), 1069-77; (b) Falagas, M. E.; Kanellopoulou, M. D.; Karageorgopoulos, D. E.; Dimopoulos, G.; Rafailidis, P. I.; Skarmoutsou, N. D.; Papafrangas, E. A., Antimicrobial susceptibility of multidrug-resistant Gram negative bacteria to fosfomycin. *European journal of clinical microbiology & infectious diseases : official publication of the European Society of Clinical Microbiology* **2008,** *27* (6), 439-43; (c) Patel, S. S.; Balfour, J. A.; Bryson, H. M., Fosfomycin tromethamine. A review of its

antibacterial activity, pharmacokinetic properties and therapeutic efficacy as a single-dose oral treatment for acute uncomplicated lower urinary tract infections. *Drugs* **1997,** *53* (4), 637-56.
12. Bernat, B. A.; Laughlin, L. T.; Armstrong, R. N., Fosfomycin resistance protein (FosA) is a manganese metalloglutathione transferase related to glyoxalase I and the extradiol dioxygenases. *Biochemistry* **1997,** *36* (11), 3050-5.
13. García-Lobo, J. M.; Ortiz, J. M., Tn292l, a transposon encoding fosfomycin resistance. *J Bacteriol* **1982,** *151* (1), 477-9.
14. Arca, P.; Rico, M.; Braña, A. F.; Villar, C. J.; Hardisson, C.; Suárez, J. E., Formation of an adduct between fosfomycin and glutathione: a new mechanism of antibiotic resistance in bacteria. *Antimicrob Agents Chemother* **1988,** *32* (10), 1552-6.
15. (a) Bernat, B.; Laughlin, L.; Armstrong, R., Regiochemical and stereochemical course of the reaction catalyzed by the fosfomycin resistance protein, FosA. *Journal of Organic Chemistry* **1998,** *63* (11), 3778-3780; (b) Bernat, B. A.; Laughlin, L. T.; Armstrong, R. N., Elucidation of a monovalent cation dependence and characterization of the divalent cation binding site of the fosfomycin resistance protein (FosA). *Biochemistry* **1999,** *38* (23), 7462-9.
16. Rigsby, R. E.; Fillgrove, K. L.; Beihoffer, L. A.; Armstrong, R. N., Fosfomycin resistance proteins: a nexus of glutathione transferases and epoxide hydrolases in a metalloenzyme superfamily. *Methods Enzymol* **2005,** *401*, 367-79.
17. Cao, M.; Bernat, B. A.; Wang, Z.; Armstrong, R. N.; Helmann, J. D., FosB, a cysteine-dependent fosfomycin resistance protein under the control of sigma(W), an extracytoplasmic-function sigma factor in Bacillus subtilis. *J Bacteriol* **2001,** *183* (7), 2380-3.
18. (a) Rife, C. L.; Pharris, R. E.; Newcomer, M. E.; Armstrong, R. N., Crystal structure of a genomically encoded fosfomycin resistance protein (FosA) at 1.19 A resolution by MAD phasing off the L-III edge of Tl(+). *J Am Chem Soc* **2002,** *124* (37), 11001-3; (b) Fillgrove, K. L.; Pakhomova, S.; Newcomer, M. E.; Armstrong, R. N., Mechanistic diversity of fosfomycin resistance in pathogenic microorganisms. *J Am Chem Soc* **2003,** *125* (51), 15730-1; (c) Pakhomova, S.; Rife, C. L.; Armstrong, R. N.; Newcomer, M. E., Structure of fosfomycin resistance protein FosA from transposon Tn2921. *Protein science : a publication of the Protein Society* **2004,** *13* (5), 1260-5.
19. Newton, G. L.; Rawat, M.; La Clair, J. J.; Jothivasan, V. K.; Budiarto, T.; Hamilton, C. J.; Claiborne, A.; Helmann, J. D.; Fahey, R. C., Bacillithiol is an antioxidant thiol produced in Bacilli. *Nat Chem Biol* **2009,** *5* (9), 625-7.
20. Gaballa, A.; Newton, G. L.; Antelmann, H.; Parsonage, D.; Upton, H.; Rawat, M.; Claiborne, A.; Fahey, R. C.; Helmann, J. D., Biosynthesis and functions of bacillithiol, a major low-molecular-weight thiol in Bacilli. *Proc Natl Acad Sci U S A* **2010,** *107* (14), 6482-6.
21. Newton, G. L.; Fahey, R. C.; Rawat, M., Detoxification of toxins by bacillithiol in Staphylococcus aureus. *Microbiology* **2012,** *158* (Pt 4), 1117-26.
22. Sharma, S. V.; Jothivasan, V. K.; Newton, G. L.; Upton, H.; Wakabayashi, J. I.; Kane, M. G.; Roberts, A. A.; Rawat, M.; La Clair, J. J.; Hamilton, C. J., Chemical and Chemoenzymatic syntheses of bacillithiol: a unique low-molecular-weight thiol amongst low G + C Gram-positive bacteria. *Angew Chem Int Ed Engl* **2011,** *50* (31), 7101-4.
23. (a) Kendrew, J. C.; Bodo, G.; Dintzis, H. M.; Parrish, R. G.; Wyckoff, H.; Phillips, D. C., A three-dimensional model of the myoglobin molecule obtained by x-ray analysis. *Nature* **1958,** *181* (4610), 662-6; (b) Wishart, D. S.; Sykes, B. D.; Richards, F. M., The chemical shift index: a fast and simple method for the assignment of protein secondary structure through NMR spectroscopy. *Biochemistry* **1992,** *31* (6), 1647-51.

24. Ostermeier, C.; Michel, H., Crystallization of membrane proteins. *Current opinion in structural biology* **1997,** *7* (5), 697-701.
25. Wagner, G., Prospects for NMR of large proteins. *Journal of biomolecular NMR* **1993,** *3* (4), 375-85.
26. McPherson, A., *Introduction to Macromolecular Crystallography*. Second ed.; John Wiley & Sons, Inc: Hoboken, New Jersey, 2009.
27. Henzler-Wildman, K.; Kern, D., Dynamic personalities of proteins. *Nature* **2007,** *450* (7172), 964-72.
28. Hvidt, A.; Linderstrom-Lang, K., Exchange of hydrogen atoms in insulin with deuterium atoms in aqueous solutions. *Biochimica et biophysica acta* **1954,** *14* (4), 574-5.
29. Zhang, Z.; Smith, D. L., Determination of amide hydrogen exchange by mass spectrometry: a new tool for protein structure elucidation. *Protein science : a publication of the Protein Society* **1993,** *2* (4), 522-31.
30. Johnson, R. S.; Walsh, K. A., Mass spectrometric measurement of protein amide hydrogen exchange rates of apo- and holo-myoglobin. *Protein science : a publication of the Protein Society* **1994,** *3* (12), 2411-8.
31. Englander, S. W.; Downer, N. W.; Teitelbaum, H., Hydrogen exchange. *Annual review of biochemistry* **1972,** *41*, 903-24.
32. Molday, R. S.; Englander, S. W.; Kallen, R. G., Primary structure effects on peptide group hydrogen exchange. *Biochemistry* **1972,** *11* (2), 150-8.
33. Connelly, G. P.; Bai, Y.; Jeng, M. F.; Englander, S. W., Isotope effects in peptide group hydrogen exchange. *Proteins* **1993,** *17* (1), 87-92.
34. Busenlehner, L. S.; Armstrong, R. N., Insights into enzyme structure and dynamics elucidated by amide H/D exchange mass spectrometry. *Arch Biochem Biophys* **2005,** *433* (1), 34-46.
35. Wuthrich, K.; Wagner, G., Nuclear magnetic resonance of labile protons in the basic pancreatic trypsin inhibitor. *Journal of molecular biology* **1979,** *130* (1), 1-18.
36. Otwinowski, Z. M., W., Processing of x-ray diffraction data collected in oscillation mode. *Methods Enzymol* **1997,** *276*, 307-326.
37. (a) McCoy, A. J.; Grosse-Kunstleve, R. W.; Adams, P. D.; Winn, M. D.; Storoni, L. C.; Read, R. J., Phaser crystallographic software. *Journal of applied crystallography* **2007,** *40* (Pt 4), 658-674; (b) Sheldrick, G. M., A short history of SHELX. *Acta crystallographica. Section A, Foundations of crystallography* **2008,** *64* (Pt 1), 112-22.
38. Langer, G.; Cohen, S. X.; Lamzin, V. S.; Perrakis, A., Automated macromolecular model building for X-ray crystallography using ARP/wARP version 7. *Nature protocols* **2008,** *3* (7), 1171-9.
39. Emsley, P.; Cowtan, K., Coot: model-building tools for molecular graphics. *Acta crystallographica. Section D, Biological crystallography* **2004,** *60* (Pt 12 Pt 1), 2126-32.
40. Murshudov, G. N.; Vagin, A. A.; Dodson, E. J., Refinement of macromolecular structures by the maximum-likelihood method. *Acta crystallographica. Section D, Biological crystallography* **1997,** *53* (Pt 3), 240-55.
41. Pettersen, E. F.; Goddard, T. D.; Huang, C. C.; Couch, G. S.; Greenblatt, D. M.; Meng, E. C.; Ferrin, T. E., UCSF Chimera--a visualization system for exploratory research and analysis. *Journal of computational chemistry* **2004,** *25* (13), 1605-12.
42. Singh, H.; Busenlehner, L. S., Probing backbone dynamics with hydrogen/deuterium exchange mass spectrometry. *Methods in molecular biology* **2014,** *1084*, 81-99.

43. Rusconi, F., massXpert 2: a cross-platform software environment for polymer chemistry modelling and simulation/analysis of mass spectrometric data. *Bioinformatics* **2009,** *25* (20), 2741-2.
44. Clauser, K. R.; Baker, P.; Burlingame, A. L., Role of accurate mass measurement (+/- 10 ppm) in protein identification strategies employing MS or MS/MS and database searching. *Anal Chem* **1999,** *71* (14), 2871-82.
45. Horai, H.; Arita, M.; Kanaya, S.; Nihei, Y.; Ikeda, T.; Suwa, K.; Ojima, Y.; Tanaka, K.; Tanaka, S.; Aoshima, K.; Oda, Y.; Kakazu, Y.; Kusano, M.; Tohge, T.; Matsuda, F.; Sawada, Y.; Hirai, M. Y.; Nakanishi, H.; Ikeda, K.; Akimoto, N.; Maoka, T.; Takahashi, H.; Ara, T.; Sakurai, N.; Suzuki, H.; Shibata, D.; Neumann, S.; Iida, T.; Tanaka, K.; Funatsu, K.; Matsuura, F.; Soga, T.; Taguchi, R.; Saito, K.; Nishioka, T., MassBank: a public repository for sharing mass spectral data for life sciences. *Journal of mass spectrometry : JMS* **2010,** *45* (7), 703-14.
46. Lamers, A. P.; Keithly, M. E.; Kim, K.; Cook, P. D.; Stec, D. F.; Hines, K. M.; Sulikowski, G. A.; Armstrong, R. N., Synthesis of Bacillithiol and the Catalytic Selectivity of FosB-Type Fosfomycin Resistance Proteins. *Org Lett* **2012,** *14* (20), 5207-9.
47. Roberts, A. A.; Sharma, S. V.; Strankman, A. W.; Duran, S. R.; Rawat, M.; Hamilton, C. J., Mechanistic studies of FosB: a divalent metal-dependent bacillithiol-S-transferase that mediates fosfomycin resistance in Staphylococcus aureus. *Biochem J* **2012**.
48. Schuttelkopf, A. W.; van Aalten, D. M., PRODRG: a tool for high-throughput crystallography of protein-ligand complexes. *Acta crystallographica. Section D, Biological crystallography* **2004,** *60* (Pt 8), 1355-63.
49. Fillgrove, K. L.; Pakhomova, S.; Schaab, M. R.; Newcomer, M. E.; Armstrong, R. N., Structure and mechanism of the genomically encoded fosfomycin resistance protein, FosX, from Listeria monocytogenes. *Biochemistry* **2007,** *46* (27), 8110-20.
50. Rigsby, R. E.; Brown, D. W.; Dawson, E.; Lybrand, T. P.; Armstrong, R. N., A model for glutathione binding and activation in the fosfomycin resistance protein, FosA. *Arch Biochem Biophys* **2007,** *464* (2), 277-83.
51. Thompson, M. K. K., Mary. E.; Harp, Joel; Cook, Paul D.; Jagessar, Kevin L.; Sulikowski, Gary A.; Armstrong, Richard N., Structural and Chemical Aspects of Resistance to the Antibiotic Fosfomycin Conferred by FosB from Bacillus cereus. *Biochemistry* **2013,** *52*, 7350-7362.
52. Sareen, D.; Steffek, M.; Newton, G. L.; Fahey, R. C., ATP-dependent L-cysteine:1D-myo-inosityl 2-amino-2-deoxy-alpha-D-glucopyranoside ligase, mycothiol biosynthesis enzyme MshC, is related to class I cysteinyl-tRNA synthetases. *Biochemistry* **2002,** *41* (22), 6885-90.
53. Thompson, M. K. K., Mary. E.; Goodman, Michael C.; Hammer, Neal D.; Cook, Paul D.; Jagessar, Kevin L.; Harp, Joel; Skaar, Eric P; Armstrong, Richard N., Structure and Function of the Genomically Encoded Fosfomycin Resistance Enzyme, FosB, from Staphylococcus aureus. *Biochemistry* **2014,** *53*, 755-765.
54. VanDuinen, A. J.; Winchell, K. R.; Keithly, M. E.; Cook, P. D., X-ray crystallographic structure of BshC, a unique enzyme involved in bacillithiol biosynthesis. *Biochemistry* **2015,** *54* (2), 100-3.
55. MacLeod, D. L.; Velayudhan, J.; Kenney, T. F.; Therrien, J. H.; Sutherland, J. L.; Barker, L. M.; Baker, W. R., Fosfomycin enhances the active transport of tobramycin in Pseudomonas aeruginosa. *Antimicrob Agents Chemother* **2012,** *56* (3), 1529-38.